AN ABSTRACT OF THE THESIS OF

Kathleen M. Fischer for the degree of Doctor of Philosophy in Oceanography presented on 13 June 1983

TITLE: Particle Fluxes in the Eastern Tropical Pacific Ocean - Sources and Processes

Abstract approved: Redacted for privacy
Jack Dymond

Particle fluxes were sampled using sediment traps at two sites in the eastern tropical Pacific Ocean for more than one year (MANOP Site H at 6° 30'N, 93°W; Site M at 8° 50'N,104°W). Sediment traps were positioned on moorings in order to span the water column from ~500 meters depth to within 30 meters of the bottom. The collected samples were analyzed for the following elements and components: carbonate and organic carbon, nitrogen, total and inorganic phosphorus, silicon, aluminum, iron, manganese, nickel, copper, cobalt, barium, strontium, titanium, thorium, lead, uranium, zinc, magnesium, chromium, cadmium, scandium, bromine, and calcium. The yearly average fluxes of most of these elements versus depth indicate that there are added inputs of flux at ~1500 meters and in the bottom ~300 meters at both sites. The fluxes of all elements equal or exceed the accumulation rates at both sites. Near-bottom flux data for manganese indicate that manganese is diffusing from the sediments at Site M and possibly as well at Site H.

Traps at selected levels were equipped with a sample

changing apparatus which allowed for the division of the deployment into three intervals. The flux was greatest for the period from October to the end of January at each site. Organic carbon flux during the season of maximum flux was 2-4 times greater than the rest of the year, and the fluxes of all other components peaked as well during the high flux period. At Site H, the season of maximum flux was the same from 505 m to 3545 m, which indicates the transport of material through 3000 m of water within the four-month sampling period.

The composition of material collected at each of the levels in the water column was partitioned using linear programming into contributions from various defined sources. The results from this partitioning indicate that flux increases in the near-bottom are best accounted for by a combination of resuspension and primary flux. In addition to these two sources of flux, hydrothermal input and/or input from precipitation of Mn recycled in the near-bottom region are required to explain the flux data. Flux increases in the mid-water column include detrital and biogenic components, which suggest that either lateral transport or biological/physical processes must be present to supply additional settling particles.

PARTICLE FLUXES IN THE EASTERN TROPICAL PACIFIC OCEAN - SOURCES AND PROCESSES

by

Kathleen M. Fischer

A THESIS

submitted to

Oregon State University

in partial fulfillment of

the requirements for the

degree of

Doctor of Philosophy

Completed June 13, 1983

Commencement June, 1984

APPROVED

Redacted for privacy

Professor of Oceanography in charge of major

Redacted for privacy

Dean of The School of Oceanography

Redacted for privacy

Dean of The Graduate School

Date thesis is presented 13 June 1983

Typed by Kathleen M. Fischer

ACKNOWLEDGEMENTS

I would like to thank my major professor, Jack Dymond, for his time, interest, patience, and encouragement during the past six years. I appreciate the suggestions and help from my committee members and wish to thank them: Erwin Suess, Julius Dasch, Bernd Simoneit, Robert Becker, and Kenneth Krane. I would like to thank W. D. Loomis for agreeing to substitute for Robert Becker at the defense, especially during a busy time.

Richard Cobler generously shared his inspirations and assistance during my first two years at OSU, and much of the success of the experiment reported herein is the result of his initial work in traps. His help made the transition to graduate school and oceanography much easier for me.

Chris Moser has volunteered so many ideas on trap and mooring design, has worked so hard to meet schedules, and has been a good friend. Thank you, Chris. Thanks also to the OSU trap building crew: Pat Hogan, Ivan Pavlov, Lisa Kaskan, Kathryn Brooksforce, Wayne, Lenny Moeller, and Gary Hewitt.

Thanks to Milo Clauson for numerous designs and technical assistance during the early years, and for many long hours of work. Also, thanks to Mark Brown who helped design the multiple sampling apparatus.

Thanks to Ed Seifert for the initial work in mooring design and deployment.

Lew Hogan and I froze one winter at the Cyclotron designing and building traps, which was beyond the call of duty. Thanks also, Lew, for letting me use your computer to write this thesis and for answering my questions pertaining to physics.

Heidi Powell worked out the nitrogen analytical technique at OSU which was used to analyze these samples. Andy Ungerer has provided chemical and analytical advice which has helped me at various stages of my work. Thanks to Jim Robbins for many AA analyses. Bobbi Conard directed the neutron activation analyses, some of the results of which are reported herein. Bobbi also supplied computer expertise for plotting and developed a data handling scheme which made life easier. Pat Collier spent many hours of tedious sample splitting, acid cleaning, and centrifuging, while Suzanne Miller entered data on the computer. Thanks to both of you.

I would like to thank the following people for their help in understanding computer quirks: Dave Mandell, Dale Mosby, Rand Dow, and Greg Campi. Thanks to Bruce Finney for teaching me how to do linear programming.

Thanks to fellow students and friends whose support has helped me through this long process: Mitch Lyle, Waldo Wakefield (who answered a million questions about plankton), Clare Reimers, Heidi Powell, Karen Weliky, Becky Simpkins (who made an incredible spread of cookies

and cakes for my defense), Bruce "Finhead" Finney, Lisa Luckybeers Kaskan, Anne Matherne, Carlos Lopez, Larry Krissek (the world's best officemate - tied with Kim Murphy), Sarah Hoffman, Bat and Pob Collier, Suzanne Miller (who listened to me while we ran), Herve Dannelongue, Kim Murphy (tied with Larry Krissek for the world's best officemate -- actually, maybe it's just that I'm the world's best officemate), Ian Walsh, Dave Murray, and Tina Emerick.

Not least of all, thanks to Ralph, Trudy, and Chris who put up with me through all of this.

I dedicate this thesis to my family.

TABLE OF CONTENTS

TABLE OF CONTENTS (cont.)

LIST OF FIGURES

LIST OF FIGURES (cont.)

LIST OF FIGURES (cont.)

LIST OF TABLES

LIST OF TABLES (cont.)

PARTICLE FLUXES IN THE EASTERN TROPICAL PACIFIC OCEAN
SOURCES AND PROCESSES

Introduction

In 1975, McCave advanced the idea of rapid transport in the form of large particles as the major mode of material input to the sediments of the ocean. Areas of primary production in the surface waters which are rich in carbonate- or opal-producing species overlie sediments which are also rich in these components. Yet most of these surface-produced plants and animals are too small and light to settle with sufficient velocity to escape dissolution (Brun-Cottan, 1976; Lal and Lerman, 1973). Evidence accumulated which suggested that fecal pellets or marine snow were the particles responsible for the major flux to the sediments. Fecal pellets composed of diatoms were found in surface sediments (Schrader, 1971). High clay contents have also been found in pellets, which would increase settling rates as well as move detrital material to the bottom (Dunbar and Berger, 1981). Direct observation by divers of marine snow indicated the potential for this type of particle mass as a transporting agent (Trent et al., 1978). Filtering of small volumes of water from hydrocasts had been the common technique for sampling oceanic particles prior to the last 10 years. Since this sampling method could not

statistically sample the rare, large particles which were now thought to comprise most of the flux to the sediments, traps and large-volume filtering were developed in order to measure the flux of these particles.

In addition to the transit of surface-produced material, flux increases have been found in the water column at ~1200 m and in the near-bottom suggesting other sources of particles or processes which increase the flux of certain components (Karl and Knauer, 1983; Martin and Knauer, 1982; Honjo et al., 1982c; Brewer et al., 1980; Gardner et al. 1982b).

A main goal of the sediment trap deployments funded through the Manganese Nodule Project (MANOP) was to obtain the best possible measurement of the actual flux to the bottom at the MANOP sites, particularly for those elements involved in manganese nodule formation. This flux data would provide a key factor in describing the chemical environment in which manganese nodules grow. Comparisons of input fluxes to the accumulation rates preserved in the sediments imply reactions which could provide elements for incorporation into nodules or produce a chemical environment necessary for nodule growth. Consequently, trap data from the entire water column below ~500 m at each site was gathered, with particular emphasis on the near-bottom region where recycling of sediments via resuspension was a possibility.

Cone-shaped traps were selected since these provide the greatest mouth opening to collect the most sample, while providing for a low fluid volume in the collection cup located at the apex. The conic shape reduces the sample volume in-situ, simplifying further reduction after recovery. The single, large cone used by Oregon State University (OSU) trap group was designed after the trap developed by Andrew Soutar of Scripps Oceanographic Institution (Soutar et al., 1977).

This thesis is divided into three parts. The first covers the average fluxes obtained over the 13-month deployment. In this first section, the comparisons between the fluxes and accumulation rates at each site are made, as well as the differences in the two sites studied. The second part examines the seasonal data from the OSU traps at each site. Seasonal pulses may temporarily alter conditions at the sediment surface beyond what might be expected from an average flux value for the year. This may be important in nodule genesis. In the third chapter, linear programming is used to partition the sample compositions into contributions from various sources. The sources of flux may provide a key to understanding the processes which control the transport and generation of particles.

Jack Dymond, Andrew Soutar (Scripps), and Susan Rau (Scripps) share authorship on all three papers. Jack

Dymond has been fully involved in the plans and decisions relating to the experiment - from the conceptual models which guided our design choices, to mooring component selection and trap fabrication, sample processing techniques, and data handling - as well as the interpretation of results. Andrew Soutar and Susan Rau provided open and fruitful collaboration, sharing ideas and inspiration in trap and mooring design and conceptual models of oceanic processes. Chris Moser is a coauthor of the second paper which describes seasonal sampling results. Chris played a key role in developing the multiple-sampling apparatus and has provided much input (flux) in the areas of trap fabrication, sample handling, mooring design, deployment, and recovery.

CHAPTER 1

AVERAGE FLUXES FOR ONE YEAR AT MANOP SITES M AND H

Abstract

Sediment traps spanning the water column from ~500 m to within 30 m of the bottom were deployed at MANOP Sites M and H in the eastern tropical North Pacific Ocean from mid-September, 1980 to mid-October, 1981. Flux data were obtained for 23 elements as well as carbonate and organic carbon, opal, and organic and inorganic phosphorus.

At both site, particle flux increases were measured both within the midwater and the near-bottom zones. These flux increases were paralleled by compositional changes in the trapped particles.

Compositional and flux variations from level to level in the water column suggest that the possible sources of flux increases in the upper water column is the lateral transport of particle-rich waters from adjacent areas of higher productivity or biological/ physical particle aggregation processes. Sources of flux increase in the lower 500 m most likely arise from resuspension of bottom sediments and off topographic highs, and introduction of hydrothermal precipitates, particularly at Site M which is near the East Pacific Rise.

Taking the level 300-500 m above bottom as the to-the-bottom flux (free of local resuspension), Site H receives ~2 times as much CaCO3 as Site M, and approximately equal amounts of organic carbon. Site M receives more Mn, Fe, Al, opal, Co, and Ni. Comparison of accumulation rates in the surface sediments show that Site M preserves

more carbonate, organic carbon, nitrogen, and organic phosphorus, as well as Fe and Al. Accumulation rates of Mn, Cu, Co, and Ni are about the same at each site. The preservation of carbonate at Site M may be linked to the fact that it is 500 m shallower than Site H.

Introduction

In recent years, several studies of particulate fluxes through the water column at deep ocean sites have been conducted (for example: Knauer et al., 1979; Honjo, 1980; Honjo et al., 1982a; Brewer et al., 1980; Cobler and Dymond, 1980; Bishop et al., 1980; Deuser et al., 1981). The fluxes of certain major components have been found to remain constant or to decrease with depth at some sites. However, more data is accumulating which indicates that flux increases do occur in the mid-water column and near the bottom.

Increases of in organic carbon and in nitrogen which were linked to increased bacterial activity have been found in traps located from ~900 m to ~1100 m at the base of an oxygen minimum zone (Karl and Knauer, 1983). In this same experiment, increased Al fluxes in this same depth interval were coupled to increased suspended Al concentrations in the water column. Increased fecal pellet numbers indicated that animal activity was greater in this region of the water column. The conclusion from this work was that a zone of high biological activity existed at this depth which resulted in increased flux through biological repackaging and autochemotrophic bacterial production.

Manganese flux increases have also been found in the mid-water region (Martin and Knauer, 1982), and these were attributed to bacterial oxidation of dissolved Mn.

Increasing silicate fluxes with depth have been observed in the Panama Basin (Honjo, 1982) from 3560 m to the 3860 m to bottom. The suggested source of the increased silicate flux was resuspension of sediments off the slope, with subsequent settling due to a biological packaging or scavenging by marine snow.

Near-bottom increases as well have been found in the deep ocean (Gardner, 1982b; Brewer, 1980). The most likely source of these increases is resuspension of bottom sediments. Scavenging of suspended Al onto fluxing materials, such as marine snow, has been proposed for depths in the mid- to lower-water column (Spencer, 1981b). Resuspension of slope sediments and transport in nephloid layers is suggested as the source of the Al.

In this experiment, fluxes from sediment traps were measured in the mid-water column and near-bottom region (from ~500 m to 30 meters above bottom) at two deep ocean sites. Flux variations with depth were measured to monitor the losses or sources of flux in the water column, which might suggest some process, such as decomposition or resuspension. In addition to examining changes in the water column, comparison of flux of an element to accumulation rate in surface sediments is made at each site. The rate of regeneration (loss from the sediments) can be calculated, or, in the case where the estimated

flux is less than the accumulation rate, some additional process is implied. Differences between the sources of particles and processes affecting the fluxes are examined at the two sites, one near the East Pacific Rise crest and both approximately equidistant from land.

Experimental Description

The two sites studied as part of MANOP were located in the eastern tropical Pacific Ocean. Figure I-1 is map of this area showing the position of Site H at 6° 32'N, 92° 50'W and Site M at 8° 50'N, 104° W. Site M is only 25 km from the spreading axis of the East Pacific Rise (EPR) which is a possible source of hydrothermal precipitates and sediments in the region. Site H is ~900 km from the EPR crest, and both sites are ~900 km from the nearest land. Table I-1 lists some of the characteristics of the two sites. They are similar, except Site M is ~500 m shallower and consequently has enhanced carbonate preservation and nearly a factor of two greater rate of sedimentation and accumulation. In addition, the proximity of M to the EPR may provide hydrothermal precipitates to traps located close to the bottom. The much broader oxygen minimum in the water column at M could result in greater precipitation of dissolved Mn by bacteria (Martin and Knauer, 1982), in changes in zooplankton populations in this region of the water column and their effects on particle generation and breakup (Karl and Knauer, 1983), and possibly in reduced decay of organic carbon. The two sites have the same average productivity in the surface waters, and substantial seasonal fluctuations exist at both sites (Chapter 2). About twice as much organic carbon is

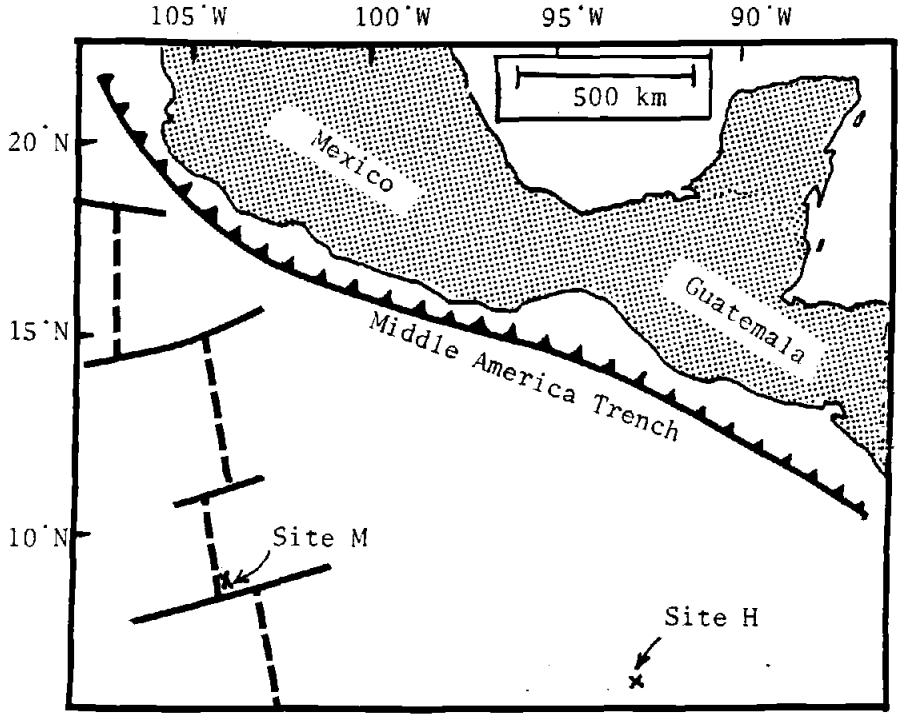

Figure I-1. Map of eastern tropical North Pacific Ocean showing the locations of Sites M and H, the East Pacific Rise submarine spreading center, and the nearest land. (Redrawn from Lonsdale and Spiess, 1980).

Table I-1. Characteristics of Sites H and M.

		Site H	Site M
Location		6°32'N, 92°50'W	8°50'N, 104°W
Water depth		~3600 m	~3100 m
Primary productivity (Owen and Zeitzschel, 1970)		11 mg C/sq-cm/y	10 mg C/sq-cm/y
Season of maximum trap flux		Sept.-Jan.	Sept.-Jan.
Season of maximum measured primary production (Owen and Zeitzschel, 1970)		Feb.-March	Dec.-Jan.
Average molar CaCO3/Opal flux ratios (from trap data in this study):			
	~1500 m	2.0	1.0
	~150 mab	2.1	0.9
Distance to nearest continent		~900 km	~900 km
Distance to East Pacific Rise		~900 km	~25 km
Depth of water column oxygen minimum (J. Edmond, written comm.)		350-450 m	100-600 m
Current speeds, cm/sec: (Appendix 1)	at ~600 m	7-avg., 22-max.	8-avg., 26-max.
	at ~1500 m	4-avg., 12-max.	5-avg., 16-max.
	near bottom	3-avg., 10-max.	4-avg., 13-max.

Table I-1, continued. Characteristics of Sites H and M.

	Site H	Site M
Topography (sea mounts at both sites) (Lonsdale and Spiess, 1980)	+/- 25 m	+/- 100 m
Flux to the sediments (from trap data in this study)	2.1 mg/sq-cm/y	1.6 mg/sq-cm/y
Accumulation rate in sediments (from sediment data of M. Lyle)	0.1 mg/sq-cm/y	0.2 mg/sq-cm/y
Sedimentation rate (D. Kadko, pers. comm.)	0.65 cm/10^3yr	1 cm/10^3yr
Bioturbation coefficient (x 10^9) (J. Kirk Cochran, pers. comm.)	5.1-5.4 sq-cm/sec	0.6-1.9 sq-cm/sec
Nodules present	yes	no

preserved in the sediments at M compared to H, however. Site M has more topographic relief (shown in Figure I-2), which may increase near-bottom particle sources, a significantly lower bioturbation rate which probably affects the chemistry of the sediments, and no manganese nodules. Site H does have nodules, and thus a comparison of the two sites is of interest.

Figure I-3 is a diagram of the two moorings used at each site. Mooring line was made of nylon, and metallic parts were minimal. Hardware within 30 m of a trap mouth was made of 316 stainless steel. Four OSU traps and two Soutar traps were used at Site H. Three OSU traps and two Soutar traps were deployed at Site M. Figures I-4 and I-5 are diagrams of the two traps. Trap materials were selected to minimize metallic contamination. In-situ studies comparing the effects of bactericides on natural substrates have indicated that decomposition of organic materials may be substantial in the absence of some control of bacterial activity (Fischer and Cobler, 1979; Gardner et al., 1982a). Sodium azide (Alfa Chemical) of 99% purity was used as a poison in the OSU trap, and reagent grade formalin buffered with sodium borate to pH 8-9 was the bactericide in the Soutar trap. Sodium azide is commonly used by some investigators (Honjo, 1980; Gardner et al., 1982a) and has been found to preserve the chemical integrity of the sample (Powell and Fischer, 1982). Formalin is also used to reduce bacterial

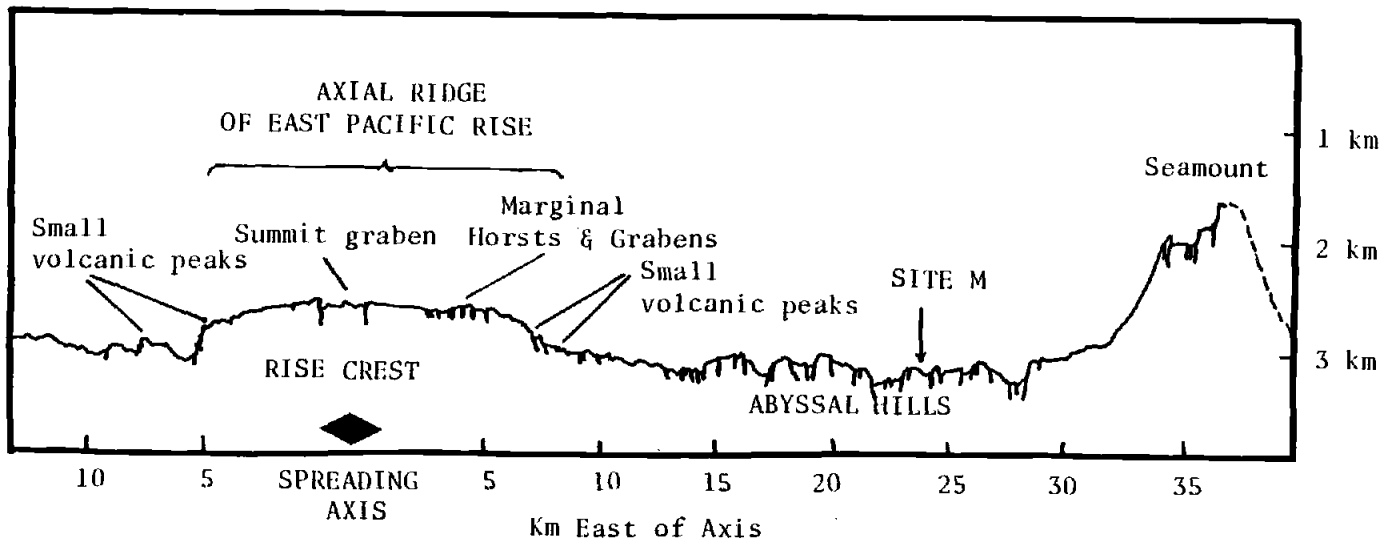

Figure I-2. Cross-section through the East Pacific Rise and Site M showing the vertical relief in the vicinity of Site M. (Redrawn from Lonsdale and Spiess, 1980).

Figure I-3. Schematics of the moorings used at each site with positions of traps and current meters indicated. A long and a short mooring were deployed at each site in order to span the water column, yet provide for easier recovery than a single long and complicated mooring. Mooring lines were nylon, and metal parts within ~50 m of the traps were 316 stainless steel.

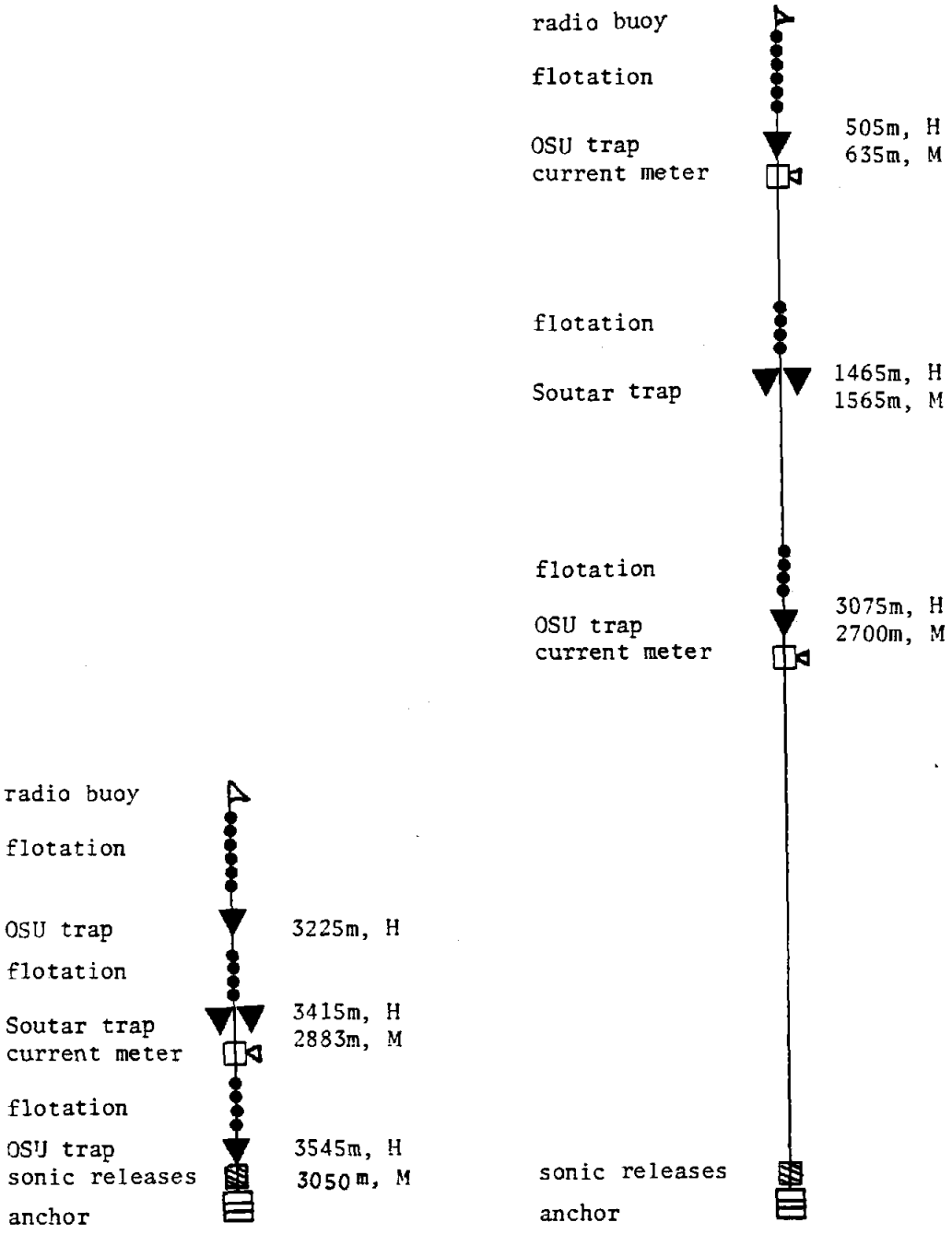
radio buoy
flotation
OSU trap
current meter
505m, H
635m, M
flotation
Soutar trap
1465m, H
1565m, M
flotation
OSU trap
current meter
3075m, H
2700m, M
sonic releases
anchor
radio buoy
flotation
OSU trap
3225m, H
flotation
Soutar trap
current meter
3415m, H
2883m, M
flotation
OSU trap
sonic releases
3545m, H
3050m, M
anchor

Figure I-3

Figure I-4. Diagram of the OSU sediment trap. The mouth area is 0.5 square meters, and the height of the cone is 1.6 meters. The labelled parts of the trap are: (1) epoxy-coated nylon baffles with 1 sq-cm openings which are 5 cm deep; (2) fiberglass cone; (3) fiberglass protective sleeve for the sample cups and sample-changing apparatus; (4) sample-changing apparatus; (5) nylon lines which form a harness connecting the trap to the rest of the mooring; (6) the apex of the cone; (7) upper part of sample cup which holds the sodium azide bactericide; (8) nylon screen and 0.4 um Nucleopore filters which serve as diffusion barriers; (9) PVC sample cup, four per trap; (10) revolving distribution valve which funnels collected sample to the proper collection cup; (11) electronic timer and motor housed in a pressure case which turn the revolving valve at the preset times.

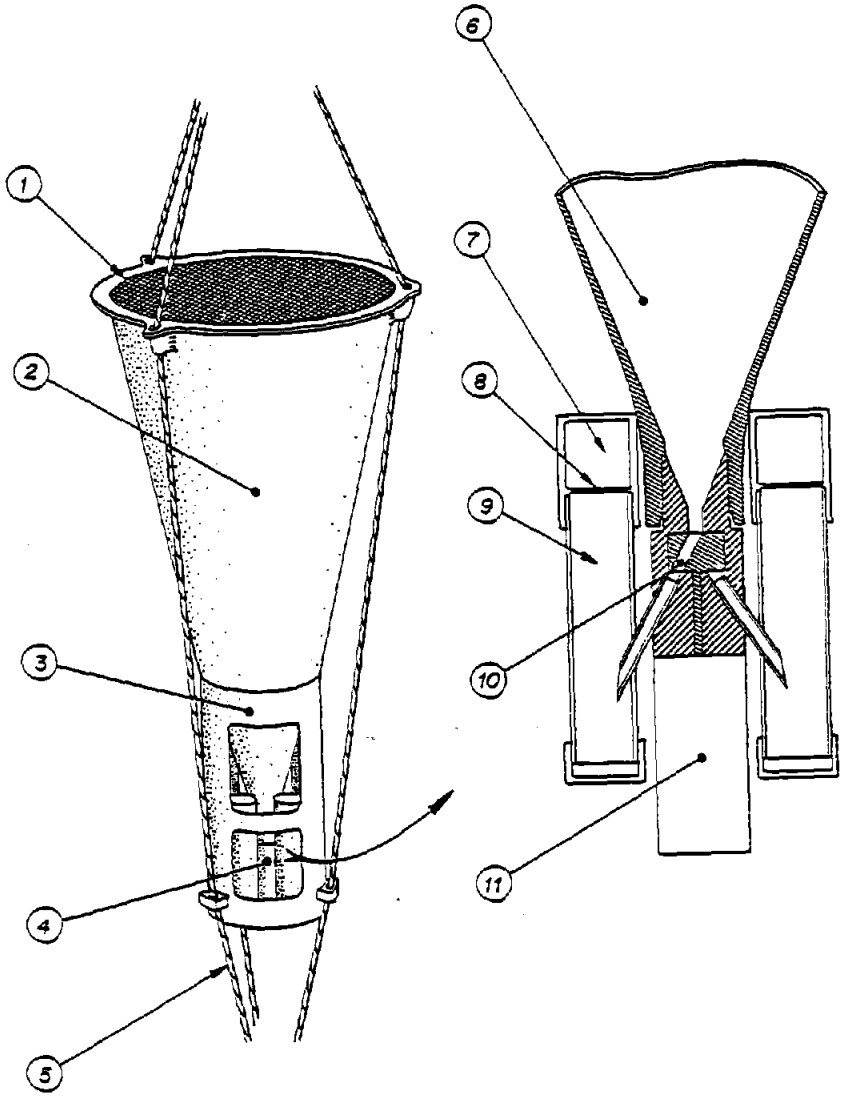

Figure I-4

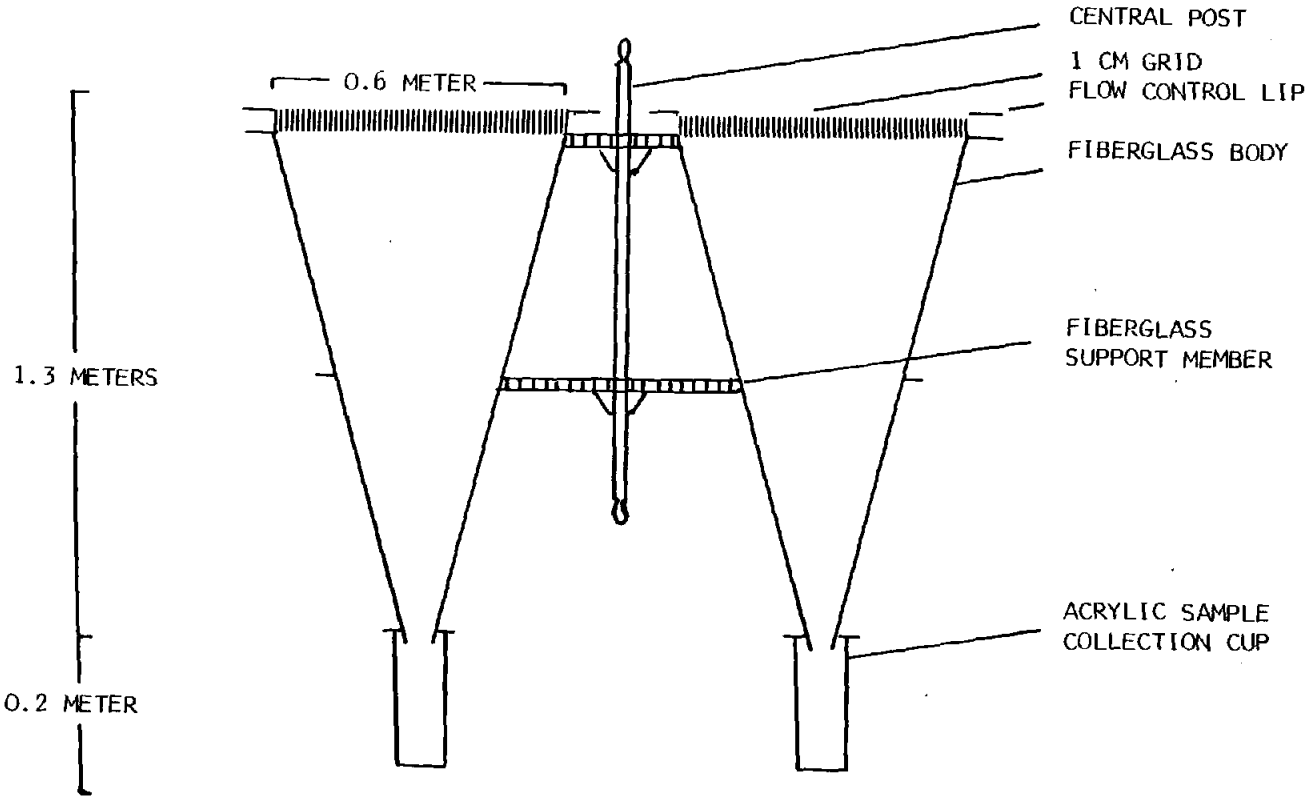

Figure I-5. Soutar trap with labelled parts and dimensions (Soutar et al., 1977). Rudder (not shown), which is fixed to the central post, positions both cones into current.

activity (Martin and Knauer, 1982) and is known to preserve the structure of particles. Since formalin lowers the Eh of the collection cup (Powell and Fischer, 1982) there exists the possibility that some elements, in particular manganese, may be lost from the sample. Recent data from a year-long laboratory study indicate that manganese is not lost from sediments exposed to ~10% formaldehyde (Powell and Fischer, 1982), and dissolved manganese may even be oxidized by certain bacteria in semi-reducing environments (Martin and Knauer, 1982; Emerson et al., 1982).

Table I-2 lists the methods of analysis and estimates of precision from duplicate subsamples. (See Appendix 2 for replicate analyses of C, N, and P.) Table I-3 describes sample processing after trap recovery. Flux data for 28 elements and components are listed in Table I-4 for Site H and Table I-5 for Site M.

Since two different traps were used in this experiment, variability of flux data between the two traps must be estimated. Laboratory, theoretical, and field evaluations of various trap designs have indicated that relative efficiencies may differ (Gardner, 1980a, 1980b, 1982; Hargrave and Burns, 1979). Comparison studies of several different trap designs have been conducted in the Santa Barbara Basin (Dymond et al., 1981) and the Panama

Table I-2. Analytical techniques and precision. Precision is estimated from duplicates, and varies with the concentration of the element determined and with the presence of interfering elements.

Component	precision	method
C-CO3	+/-3%	acid liberation of CO2, thermal conductivity detection
C-organic	+/-3%	chromic acid oxidation to CO2, thermal conductivity detection
N-total	+/-3%	Kjeldahl digestion, titration of NH3
P-organic	+/-6%	calculated as difference between P-total-leachible and P-inorganic
P-total-leach.	+/-3%	high temperature conversion to P-inorganic, acid digestion, spectrophotometric determination by molybdate blue method. (This measurement is for total leachible P.)
P-inorganic	+/-3%	acid digestion, spectrophotometric determination by molybdate blue method
CaCO3	+/-3%	calculated from C-CO3, assumes all carbonate is calcium carbonate
Si-total	+/-4%	air-acetylene Atomic Adsorption analysis - AA
detrital SiO2	+/-5%	detrital Si is calculated at 3 x Al. (Assumes all Al is bound with Si in a fixed ratio, as in clays.)
Opal	+/-9%	calculated at 2.61 x the difference between Si-total and detrital Si. (Reference for 2.61 ratio: van Bennekom and van der Gaast, 1976.)

Table I-2, continued. Analytical techniques and precision.

component	precision	method
Al	+/-5%	Instrumental Neutron Activation Analysis (INAA), also determined by air-acetylene AA
Ba	+/-5%	INAA, also determined by air-acetylene AA
Mg	+/-4%	nitrous oxide-acetylene AA
Br	+/-3%	INAA
Sr	+/-5%	nitrous oxide-acetylene AA
Sc	+/-3%	INAA
Ti	+/-12	graphite furnace AA, instrumental problem experienced
Cr	+/-8%	INAA, also nitrous oxide-acetylene AA
Mn	+/-5%	INAA, air-acetylene AA, average used
Fe	+/-4%	INAA, air-acetylene AA, average used
Co	+/-3%	INAA
Ni	+/-20%	air-acetylene AA
Cu	+/-6%	air-acetylene AA
Zn	+/-11%	air-acetylene AA

Table I-2, continued. Analytical techniques and precision.

component	precision	method
Pb	-	graphite furnace AA
Th	+/-15%	INAA
U	+/-25%	INAA
Cd	-	near detection limit, graphite furnace AA
Ca	+/-4%	nitrous oxide-acetylene AA, (also INAA, +/-5 to 10%)
salt	+/-5%	weight loss, INAA for Cl (All determinations of components were corrected for salt)

INAA - Adapted from Conard, 1976.

AA - HF/HNO3 digestion in polyethylene bottles preceeded all atomic adsorption analyses. Robbins et al., 1983.

Carbon analyses - Weliky et al., 1983.

Phosphate analyses - Aspila et al., 1976.

Nitrogen analysis - Bremner, 1960.

Table I-3. Sample processing description.

Sediment trap samples were processed in the following manner after trap recovery:

1. Pre-processing storage -
   Samples were transfered to acid-cleaned polyethylene bottles and stored refrigerated until processed in a land-based lab.

2. Size Separation -
   The samles were sieved to separate pieces larger than one millimeter. The fraction larger than 1 mm was preserved with $NaCO_3$ buffered (pH 8-9) formalin and retained for microscopic observation. Whole animals, such as copepods, which were capable of swimming into the trap were hand picked and stored in formalin. These animals were not counted as part of the flux. The fraction larger than 1 mm was of negligible mass relative to the fraction less than 1 mm. All analyses covered in this paper refer to the less than 1 mm fraction from each trap.

3. Wet Splitting -
   The less than 1 mm fraction was split into four fractions using a wet splitter developed at OSU. This splitter is made of PVC and consists of a upper chamber which has a bottom that can be released by pulling a plunger. The sample is mixed in the upper chamber, the bottom is released, and the sample rapidly spills into a lower chamber. The lower chamber has four outlets which transfer the liquid into four beakers. In-house tests using sand gave +/-5% precision for splitting on a mass basis.

Table I-3, continued. Sample processing description.

4. Volume Reduction -
Three of the four splits were centrifuged at 10,000 rpm for 15 minutes to concentrate most particles greater than 0.4 um in diameter and having a specific gravity greater than 1.1. As much supernatant sea water as possible was removed, and the separated material was freeze dried. Weight loss of water was recorded to calculate salt retained. Chlorine was also measured by instrumental neutron activation analysis as a check on the salt concentration. The fourth split (the one not centrifuged) was used for microscopic examination.

5. Grinding and Subsampling -
After freeze drying the sample was hand ground in an agate mortar. Subsplits for analysis were taken using a dry splitter. This splitter in made of aluminum and consists of several slots which are interleaved. Each alternate slot leads to an opposite side of the splitter, where a receptacle collects the separated fraction. Thus the sample can be split in two with each pass through the splitter. Our experience with this splitter has shown that it will produce two subsamples that are within +/- 5% by weight. The sample was split as many times as required to reduce the weight to the proper size for a particular analysis.

6. Pre-analysis Drying -
Before analysis, the subsamles were dried in a 60 degree C oven and then cooled and stored in a dessicator until weighing.

Table I-4. Average fluxes of elements and components at Site H for one year. Units are mg/sq-cm/y for total fluxes and ug/sq-cm/y for all other fluxes.

Trap	Depth, m	Total	C-CO3	CaCO3	Si-total	Opal	C-org	N	P-org	P-inorg
OSU	505	1.53	97.3	811.	142.	354.	136.	23.1	1.06	1.97
Soutar	1465	2.54	187.	1560.	238.	570.	189.	27.2	1.43	0.81
OSU	3075	2.09	160.	1340.	181.	419.	112.	19.7	0.72	0.57
OSU	3225	2.54	191.	1590.	241.	541.	141.	22.4	0.86	0.71
Soutar	3415	2.78	204.	1700.	281.	595.	157.	22.0	1.12	0.74
OSU	3545	2.70	190.	1580.	296.	550.	144.	21.8	0.96	1.29

Trap	Depth, m	d-SiO2*	Al	Ti	Th	Sc	U	Ca	Mg	Br
OSU	505	12.5	1.95	0.39	0.00017	0.00070	0.00223	330.	16.1	1.89
Soutar	1465	40.6	6.33	0.59	0.00042	0.00246	0.00171	635.	18.2	2.25
OSU	3075	42.5	6.62	0.70	0.00070	0.00229	0.00215	497.	20.5	1.84
OSU	3225	71.6	11.2	1.21	0.00063	0.00341	0.00237	635.	22.5	2.21
Soutar	3415	114.	17.8	1.19	0.00105	0.00576	0.00206	635.	20.6	1.97
OSU	3545	184.	28.6	1.11	0.00272	0.0102	0.00236	592.	23.4	1.93

* detrital SiO2 (calculated as described in Table I-2)

Table I-4, continued. Average fluxes of elements and components at Site H. Units are ug/sq-cm/y.

Trap	Depth, m	Ba	Sr	Pb	Mn	Fe	Cu	Co	Ni	Zn
OSU	505	1.41	0.97	0.042	0.062	0.83	0.0315	0.00203	0.021	0.307
Soutar	1465	3.55	1.83	0.185	0.279	3.44	0.0719	0.0130	0.096	0.157
OSU	3075	3.31	1.56	0.106	0.466	3.92	0.106	0.00714	0.048	0.286
OSU	3225	4.97	1.86	-	1.46	6.52	0.184	0.0178	0.190	0.405
Soutar	3415	6.09	2.01	0.183	5.69	12.0	0.275	0.0702	0.255	0.241
OSU	3545	7.23	1.87	0.193	14.6	22.8	0.363	0.0470	0.468	0.542

Trap	Depth, m	Cr	Cd
Osu	505	0.0065	0.0053
Soutar	1465	0.0205	0.0047
OSU	3075	0.0168	0.0026
OSU	3225	0.0255	0.0030
Soutar	3415	0.0263	-
OSU	3545	0.0359	0.0021

Table I-5. Average fluxes of elements and components at Site M for one year. Units are mg/sq-cm/y for total fluxes and ug/sq-cm/y for all other fluxes.

Trap	Depth, m	Total	C-CO3	CaCO3	Si-total	Opal	C-org	N	P-org	P-inorg
OSU	635	0.72	45.7	381.	76.6	188.	91.3	13.2	0.55	1.09
Soutar	1565	1.16	60.9	507.	151.	366.	127.	18.4	1.06	0.38
OSU	2700	1.57	74.1	618.	268.	607.	135.	20.5	0.89	0.51
Soutar	2883	2.37	100.	834.	382.	668.	178.	24.9	1.65	1.26
OSU	3050	2.36	93.1	776.	426.	682.	145.	21.5	1.15	1.62

Trap	Depth,m	d-SiO2*	Al	Ti	Th	Sc	U	Ca	Mg	Br
OSU	635	9.6	1.49	0.11	0.00013	0.00042	0.00122	149.	9.92	1.22
Soutar	1565	22.2	3.45	0.44	0.00025	0.00096	0.00078	212.	16.6	1.67
OSU	2700	76.5	11.9	0.74	0.00092	0.00353	0.00222	252.	14.2	1.70
Soutar	2883	270.	42.1	1.76	0.00330	0.0122	0.00298	344.	35.2	2.59
OSU	3050	353.	54.9	3.85	0.00540	0.0190	0.00331	323.	28.8	1.89

Trap	Depth,m	Ba	Sr	Pb	Mn	Fe	Cu	Co	Ni	Zn
OSU	635	0.85	0.34	0.049	0.012	0.62	0.0176	0.00098	0.016	0.319
Soutar	1565	1.92	0.51	0.031	0.088	1.83	0.0450	0.00791	0.042	0.217
OSU	2700	3.02	0.57	-	1.65	12.0	0.138	0.0134	0.105	0.316
Soutar	2883	6.17	0.92	0.067	15.2	51.3	0.319	0.0975	0.385	0.502
OSU	3050	8.33	0.89	0.133	18.2	75.0	0.649	0.0739	0.307	0.523

Trap	Depth, m	Cr	Cd
OSU	635	0.0052	0.0016
Soutar	1565	0.0113	0.0038
OSU	2700	0.0214	0.0016
Soutar	2883	0.0827	0.0027
OSU	3050	0.0899	0.0108

* detrital SiO2

(calculated as described in Table I-2)

Basin (Spencer; 1981a), the results of which suggest that, barring mechanical problems in trap operation and mooring recovery, traps of widely varying design trap within a factor of two of each other. Table I-6 lists the flux of biogenic components for the two OSU traps and one Soutar trap in the bottom 350 m at Site H, and the Soutar trap and OSU trap in the lower 200 m at Site M. The OSU traps at Site H bracket the Soutar trap and provide a check on changes in flux with depth due to resuspension rather than differences in trapping efficiency. Since the biogenic components constitute only a small fraction of the sediments at each site (see Table I-13), resuspension would not be expected to contribute greatly to the flux of these components. (Some resuspension of relatively fresh biogenic material may occur, as discussed in Walsh et al., 1983 and Gardner et al., 1982c. Hydrothermal input from the EPR has negligible amounts of these components (Dymond, 1981). Transport of particle-rich waters may be a possible source of additional flux at depth; however, dramatic changes would not be expected within a few 100 meters. Thus, the bottom three traps at Site H should collect similar amounts of these components. Sr is also included in Table I-6 since this element is found in association with carbonate and it is depleted in the bottom sediments. Consequently, resuspension will not contribute additional Sr. The traps collect +/- 10% of each other with the

Table I-6. Comparison of fluxes of selected components from the Soutar and OSU traps. Units are ug/sq-cm/y.

Site H:

Trap	depth, m	C-org	Opal	CaCO3	N	Sr	P-org
OSU	3225	141.	541.	1590.	22.4	1.86	0.86
Soutar	3415	157.	595.	1700.	22.0	2.01	1.12
OSU	3545	144.	550.	1580.	21.8	1.87	0.96
Average of two OSU traps		143.	546.	1585.	22.1	1.87	0.91
%, Soutar/OSU *		+10%	+9%	+7%	0%	+7%	+23%

Site M:

Trap	depth	C-org	Opal	CaCO3	N	Sr	P-org
Soutar	2883	178.	668.	834.	24.9	0.92	1.65
OSU	3050	145.	682.	776.	21.5	0.89	1.15
%, Soutar/OSU *		+23%	-2%	+7%	+16%	+3%	+43%

* 100 x (1 - Soutar/OSU)

exception of organic phosphorus, for which the Soutar trap collected 23% more than the average of the OSU traps. Since the analysis for phosphorus measures the leachible fraction of this element, the difference in collected organic phosphorus may reflect greater preservation of leachible phosphorus by the formalin used in Soutar trap. The validity of the assumption of almost constant flux of biogenic components with depth in the lower 350 meters can be checked by comparing the two lowest OSU traps which collect almost identical fluxes for all components listed.

For Site M, where there is significant near-bottom input of flux, most likely from topographic highs in the region (Figure I-2), only the bottom Soutar and OSU traps are compared since they are within 170 m of each other. Agreement is within +/- 23% for all components but organic phosphorus. Table I-7 shows flux data for the comparison of the Soutar trap and the Honjo trap during the Sediment Trap Intercomparison Experiment (Spencer, 1981a). The traps collected within 31% of each other. Th-230 was measured in another deployment of Honjo traps in the Atlantic (Brewer et al., 1980). The calculated absolute efficiencies ranged from 70-80% of that expected from the model for the behavior of Th in seawater.

Since the Soutar trap is a double cone, comparison of the fluxes collected by each cone can be compared,

Table I-7. Comparison of fluxes of selected components from Soutar and Honjo traps. Data from the Sediment Trap Intercomparison Experiment in the Panama Basin (Spencer, 1981a). Units are mg/sq-m/d.

Trap	depth, m	total flux	> 1 mm	1 mm - 62 um	<62 um
Soutar	2288	152.3	4.6	42.7	105.
Honjo	2265	126.3	3.5	39.7	83.
%, Soutar/Honjo *		+21%	+31%	+8%	+27%

Trap	depth, m	carbonate	non-combustible	combustible	carbon
Soutar	2288	49.7	74.1	25.2	61.0
Honjo	2265	45.4	59.5	21.5	53.8
%, Soutar/Honjo *		+9%	+25%	+17%	+13%

* 100 x (1 - Soutar/OSU)

providing a duplicate measurement at a level. In most cases, the two cones trapped within 5% of each other. Average values for each pair of double cones are given in the data tables shown here.

On the basis of the comparisons discussed above, the OSU and Soutar trap data may be considered comparable. Suspected deviations (Zn and Co) from this conclusions are noted in the data interpretation section.

The validity of the collection efficiency of the Site H 3075 m trap might be called into question on the basis of most of the flux data in general. Relative to the 3225 m trap, the CaCO3 flux is 15% low, the opal flux is 25% low, the C-organic flux is 25% low, and the N flux is 15% low. One arguement against the assignment of a lower collection efficiency for this trap is that the Al flux is the same (as might be expected from our notions of this element as discussed below) from 1465 m to 3075 m, and matches the Al accumulation rate in the sediments. Figure I-6 is a hypothetical and simplified version of water column processes affecting flux. Water column inputs due to lateral transport and large particle generation are not shown. Hydrothermal input is also not shown.

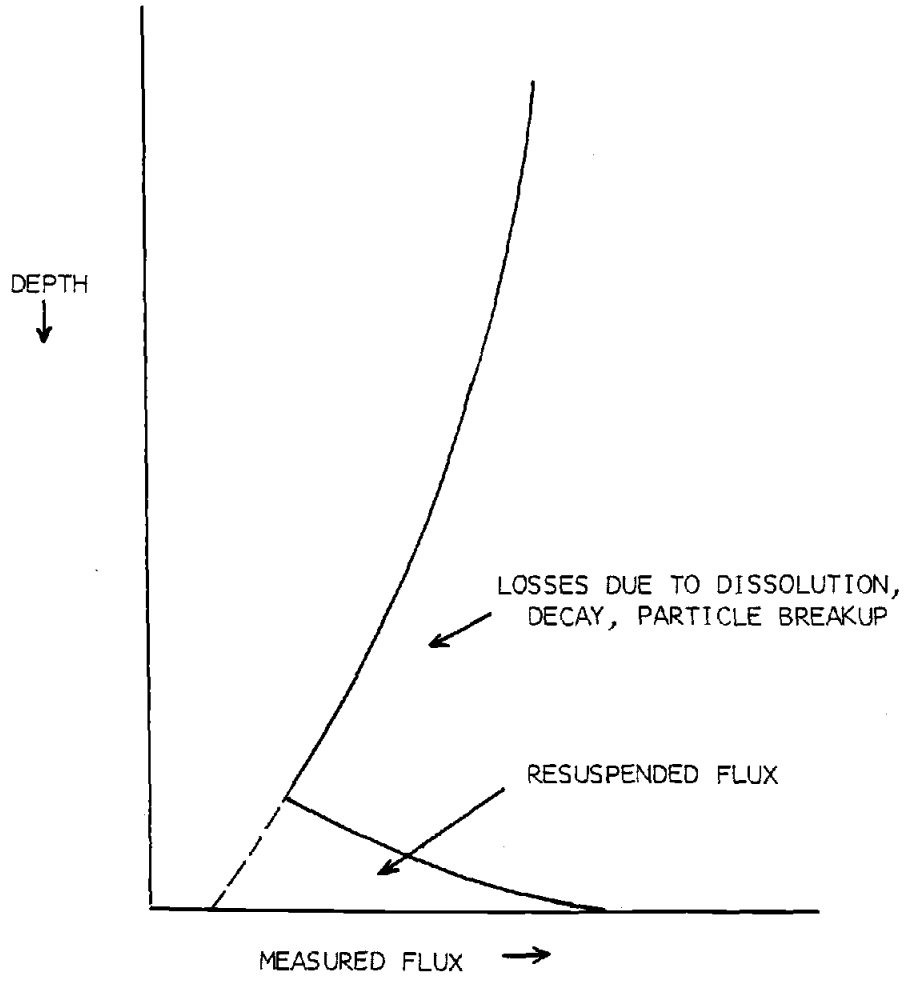

Figure I-6. Hypothetical flux versus depth profile showing flux losses in the water column due to dissolution and other processes, as well as near-bottom increases due to resuspension. (The x-axis represents the sediment surface.)

Flux Data and Interpretation

An increase in total flux versus depth at both sites (Figure I-7) is apparent. The top traps at each site, which are located in the oxygen minimum, collected the lowest flux. Flux increases at midwater level (~1500 m) and again near the bottom, particularly at M. It is unlikely that differences in current speeds could cause the variations in flux since the speeds throughout the water column averaged ~10 cm/sec. Differences in trapping efficiency are not expected at these speeds (Gardner, 1980a). The flux at both sites is composed primarily of carbonate, opal, and organic carbon, and the mid-water and near-bottom increases in flux for these components (Figures I-8 through I-10) is most surprising since these biogenic components are produced dominantly in the photic zone. Previous studies have noted flux increases of several components in the mid-water column (Honjo, 1980; Brewer et al., 1980; Honjo et al., 1982c; Martin and Knauer, 1982; Karl and Knauer, 1983). Flux increases in the lower 500 m of the water column have also been observed (Gardner et al., 1982b; 1982c) and have been attributed to resuspension of bottom sediments. At Sites H and M, flux increases in the lower 500 m are greatest for elements with high abundances in the sediments: Al, Fe, detrital silica, Ti, Th, Sc, Ba, Mn, Cu, Co, Ni, Zn, and Cr. As discussed in Chapter 3 and Walsh et al., 1983, however, biogenic component fluxes

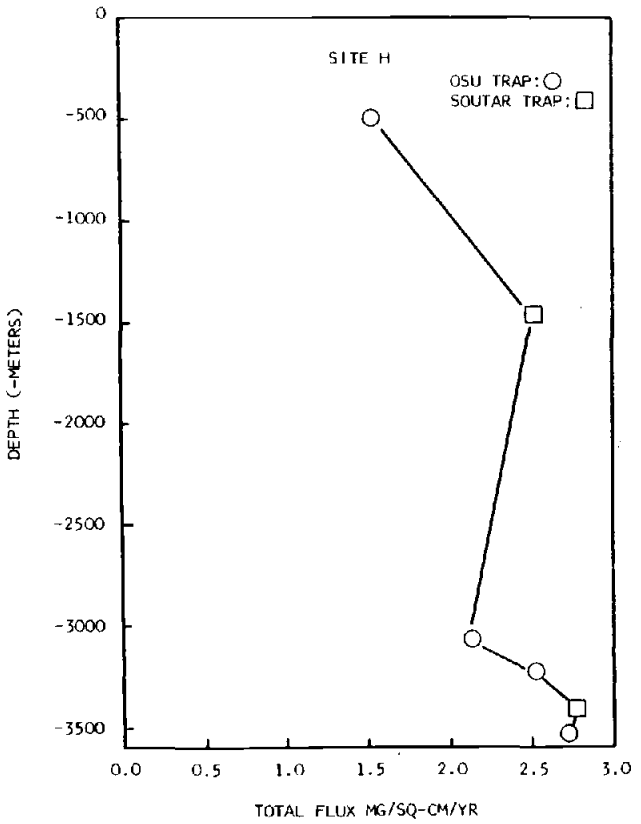

Figure I-7a

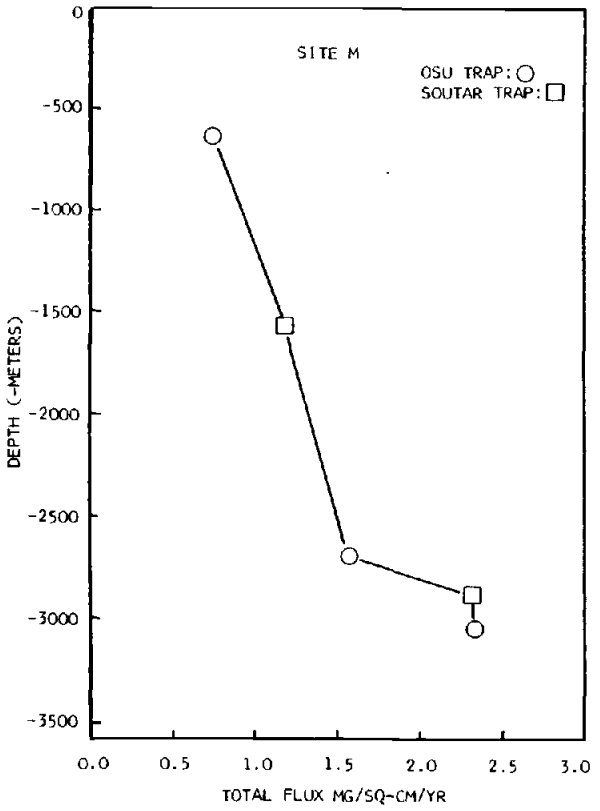

Figure I-7b

Figures I-7a and I-7b. Total flux for 13-month deployment period versus depth at Sites H and M. Bottom at Site H is 3575 m. Bottom at Site M is 3080 m.

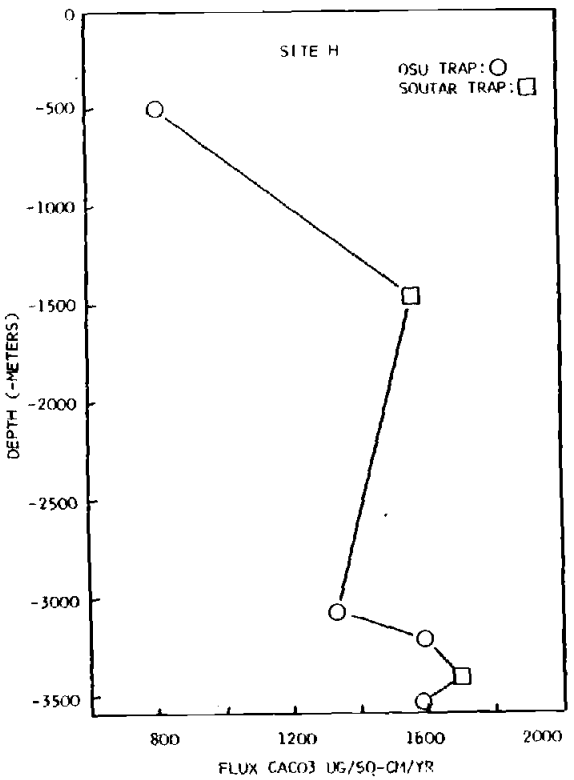

Figure I-8a

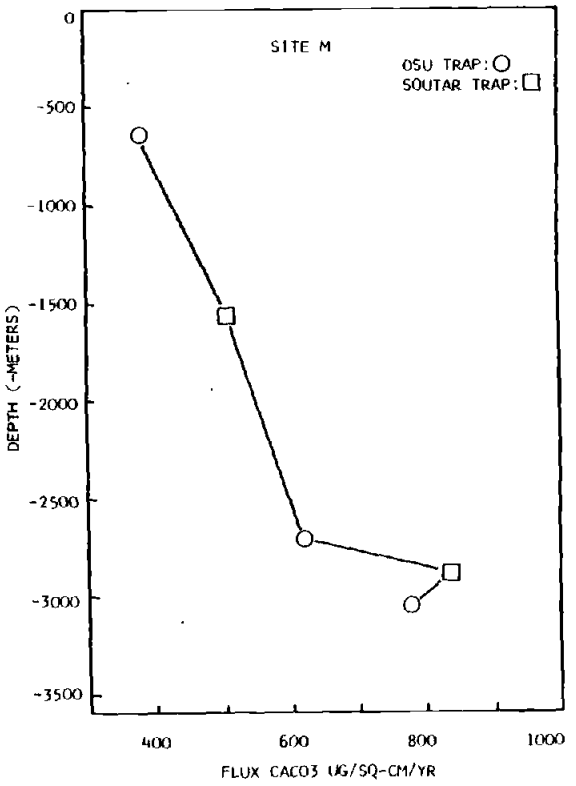

Figure I-8b

Figures I-8a and I-8b. CaCO3 flux for 13-month deployment period versus depth at Sites H and M. Bottom at Site H is 3575 m. Bottom at Site M is 3080 m.

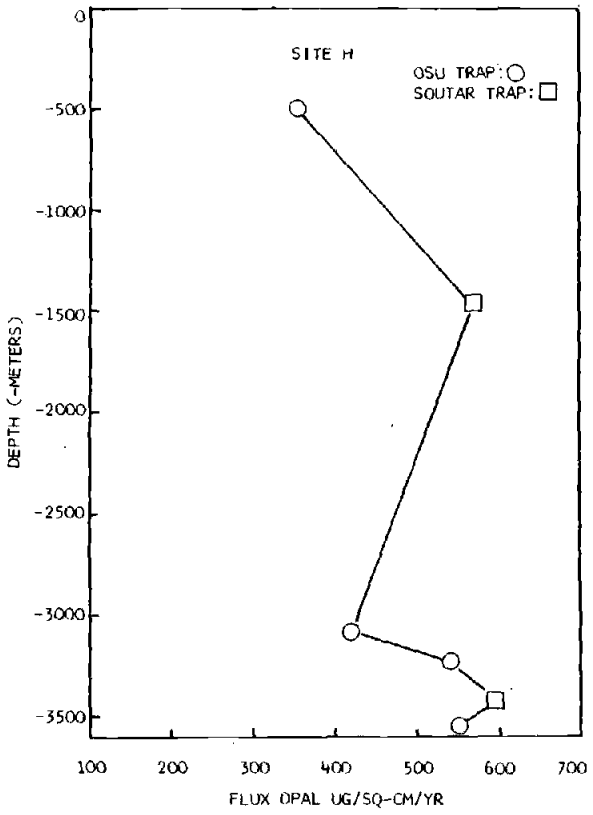

Figure I-9a

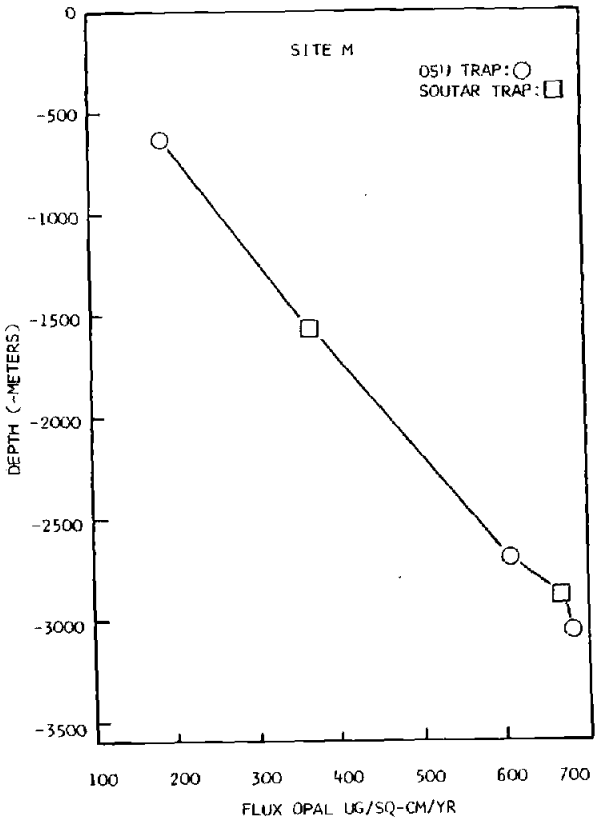

Figure I-9b

Figures I-9a and I-9b. Opal flux for 13-month deployment period versus depth at Sites H and M. Bottom at Site H is 3575 m. Bottom at Site M is 3080 m.

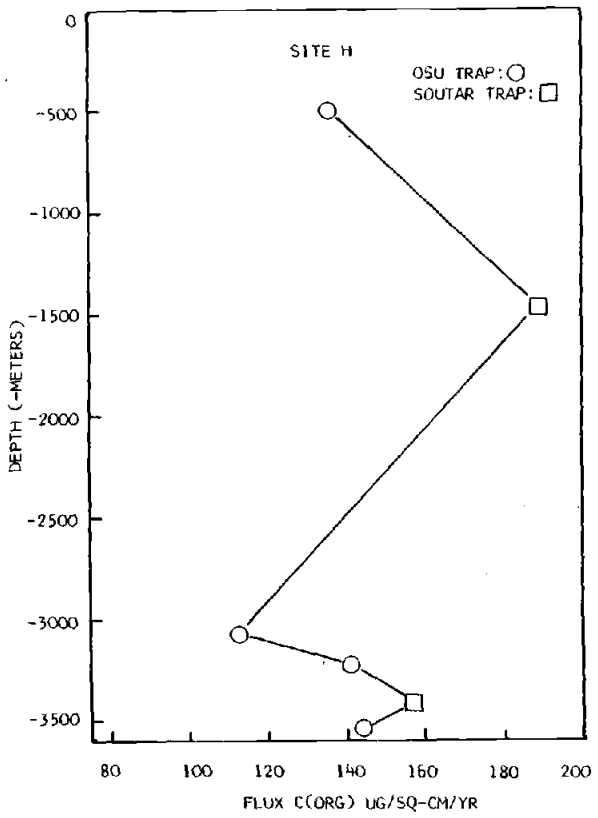

Figure I-10a

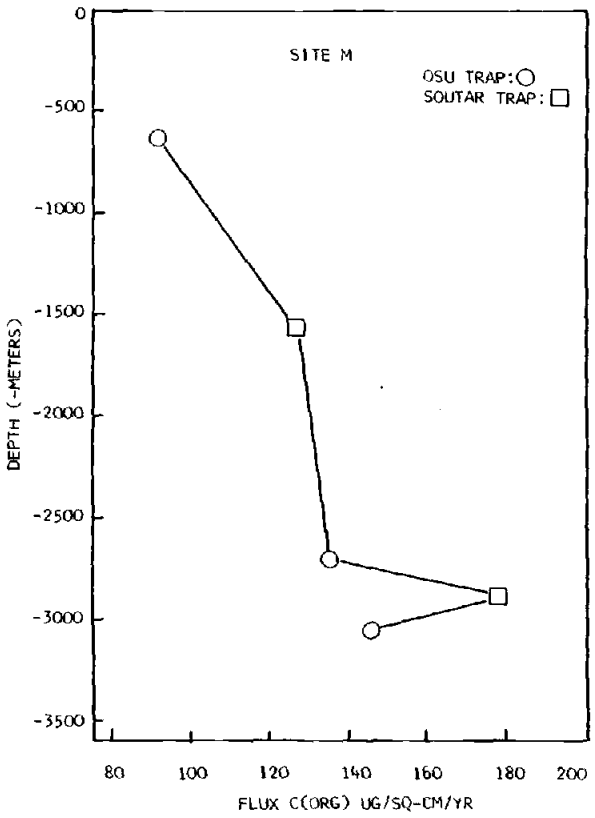

Figure I-10b

Figures I-10a and I-10b. Organic carbon flux for 13-month deployment period verus depth at Sites H and M. Bottom at Site H is 3575 m. Bottom at Site M is 3080 m.

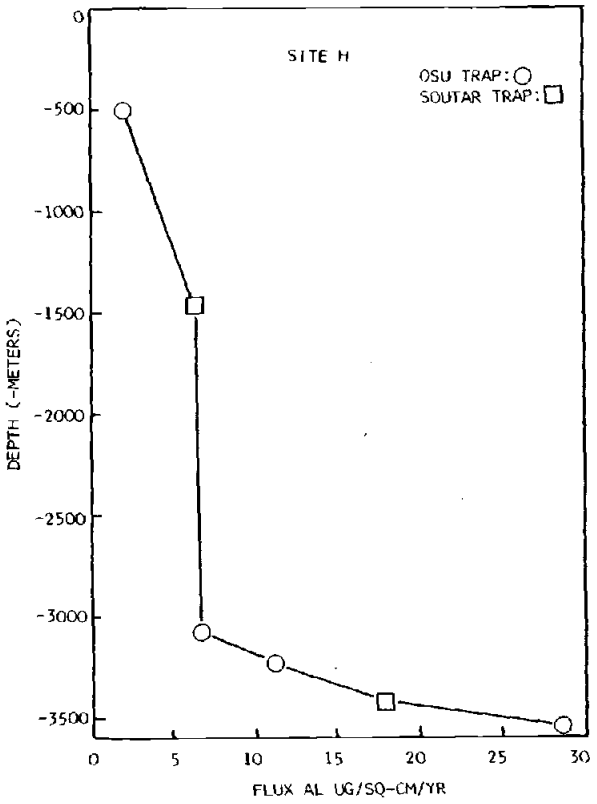

Figure I-11a

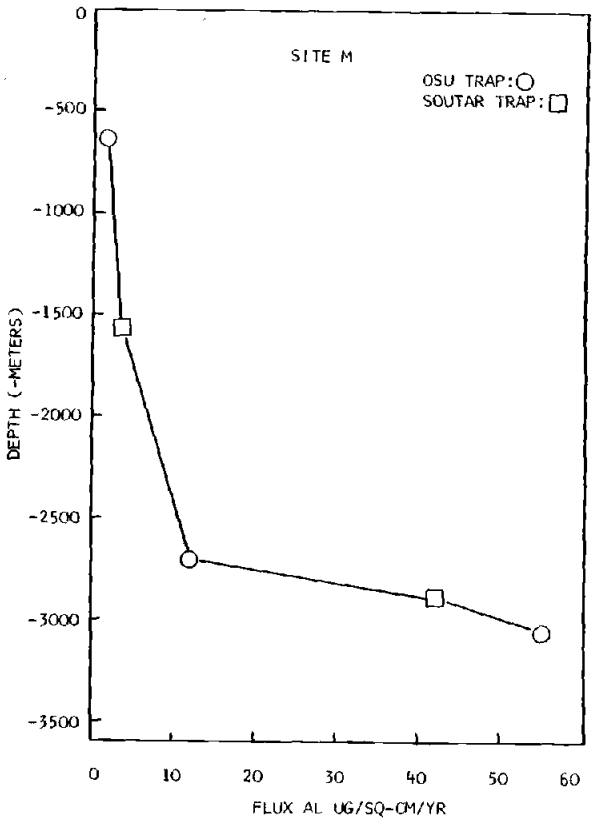

Figure I-11b

Figures I-11a and I-11b. Aluminum flux for 13-month deployment period versus depth at Sites H and M. Bottom at Site H is 3575 m. Bottom at Site M is 3080 m.

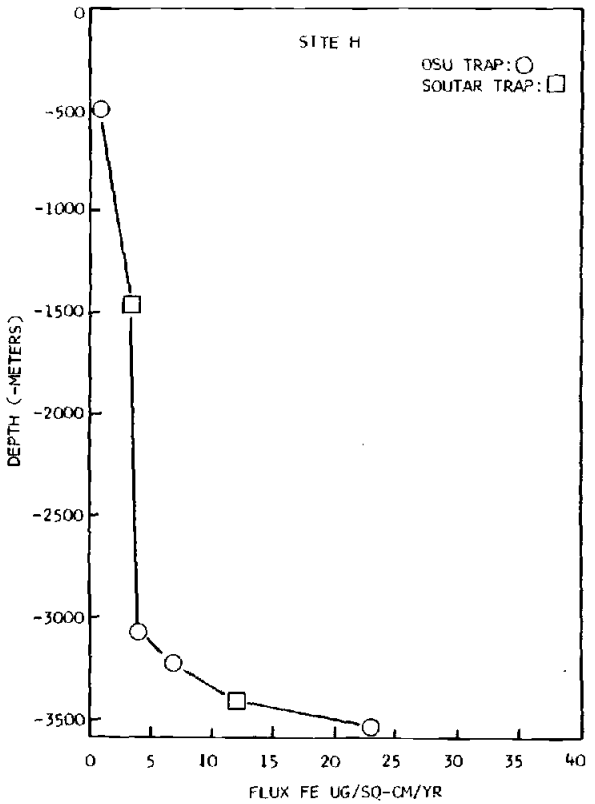

Figure I-12a

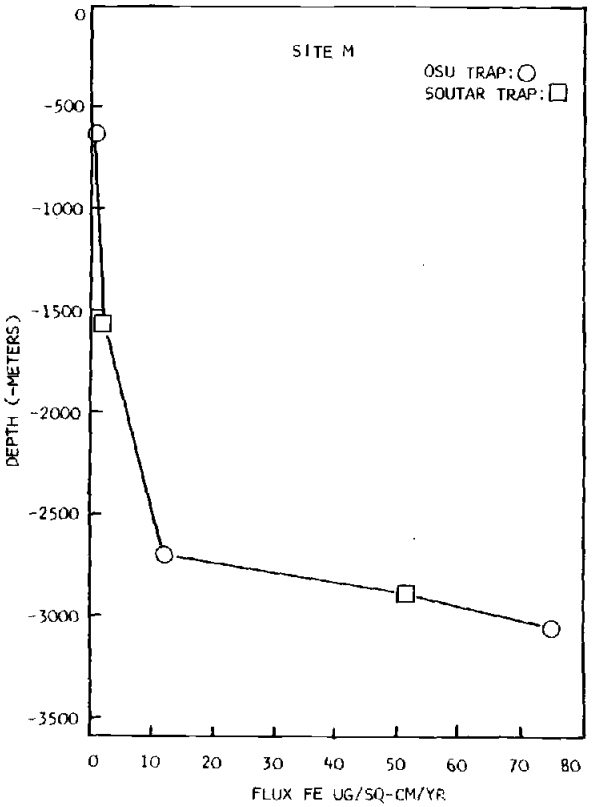

Figure I-12b

Figures I-12a and I-12b. Iron flux for 13-month deployment period versus depth at Sites H and M. Bottom at Site H is 3575 m. Bottom at Site M is 3080 m.

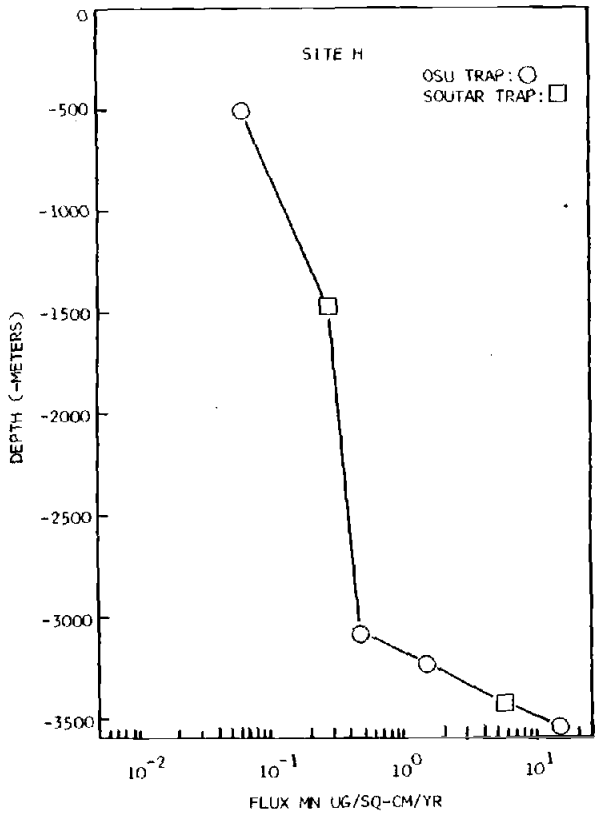

Figure I-13a

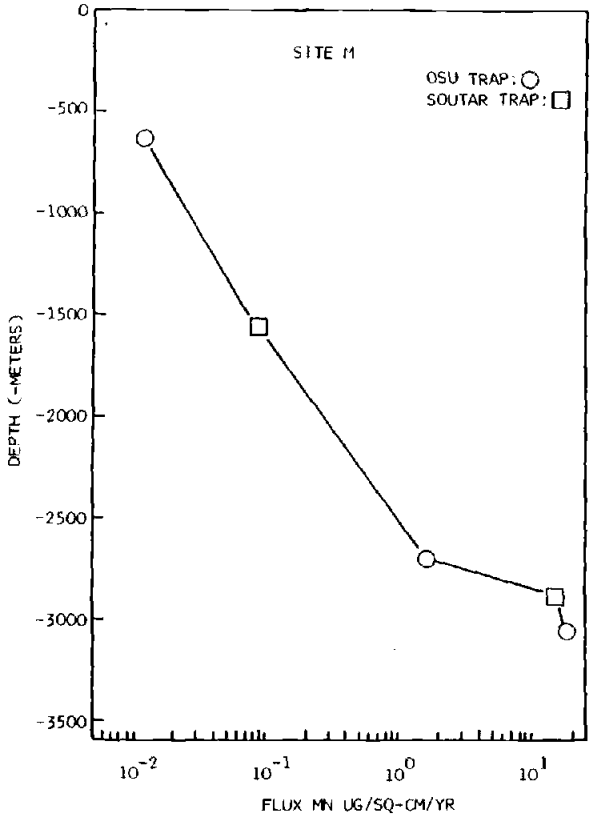

Figure I-13b

Figures I-13a and I-13b. Manganese flux for 13-month deployment period versus depth at Sites H and M. Bottom at Site H is 3575 m. Bottom at Site M is 3080 m.

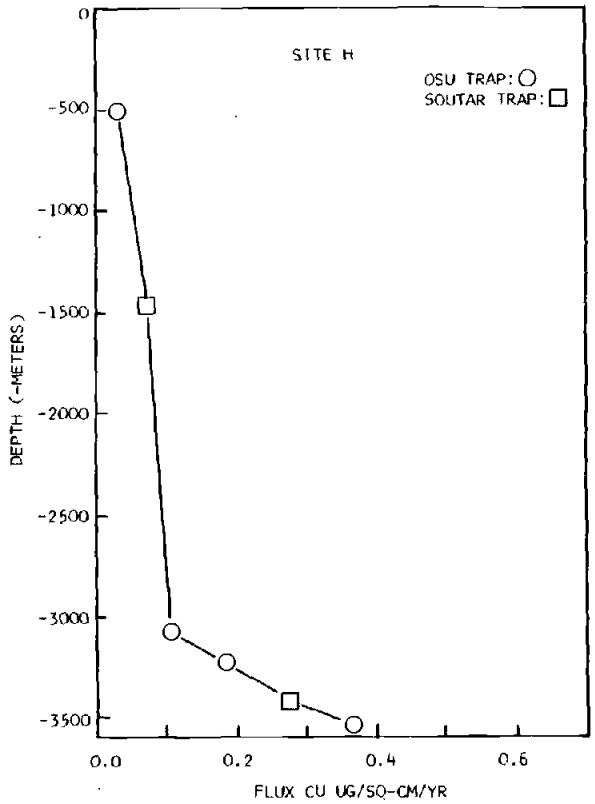

Figure I-14a

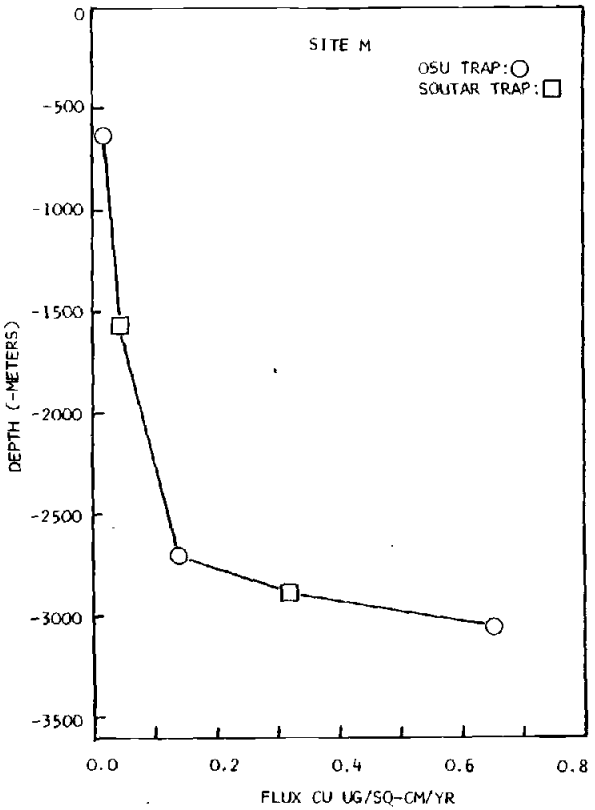

Figure I-14b

Figures I-14a and I-14b. Copper flux for 13-month deployment period versus depth at Sites H and M. Bottom at Site H is 3575 m. Bottom at Site M is 3080 m.

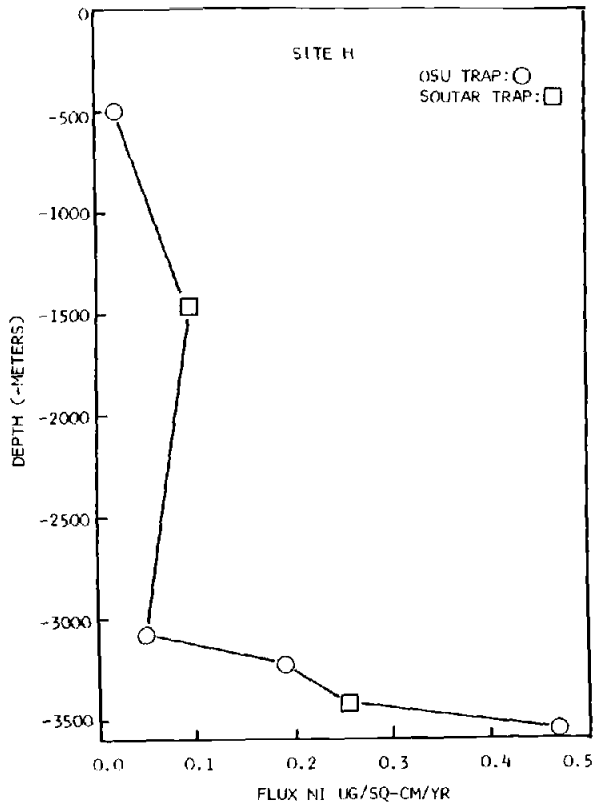

Figure I-15a

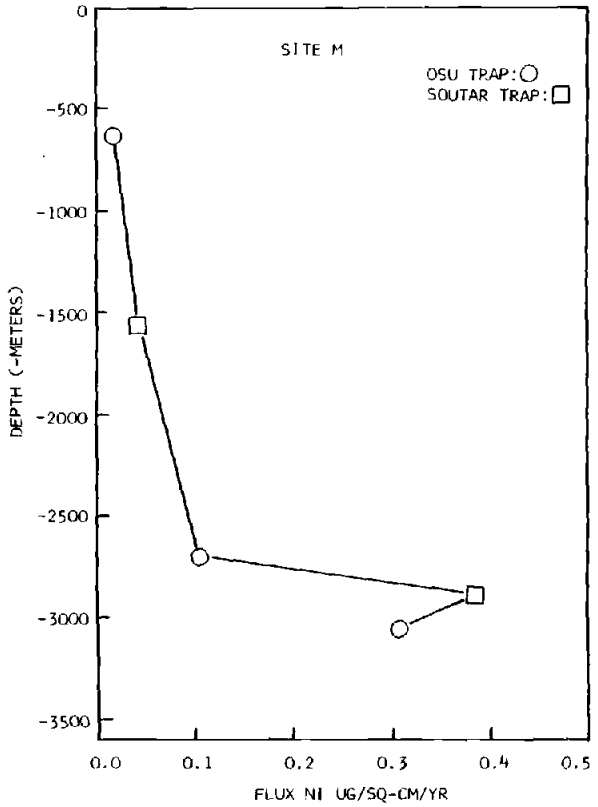

Figure I-15b

Figures I-15a and I-15b. Nickel flux for 13-month deployment period versus depth at Sites H and M. Bottom at Site H is 3575 m. Bottom at Site M is 3080 m.

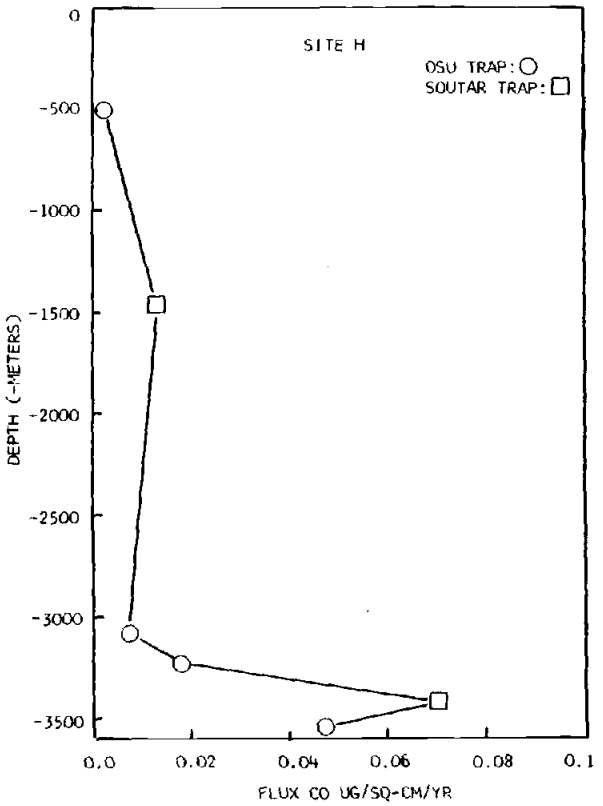

Figure I-16a

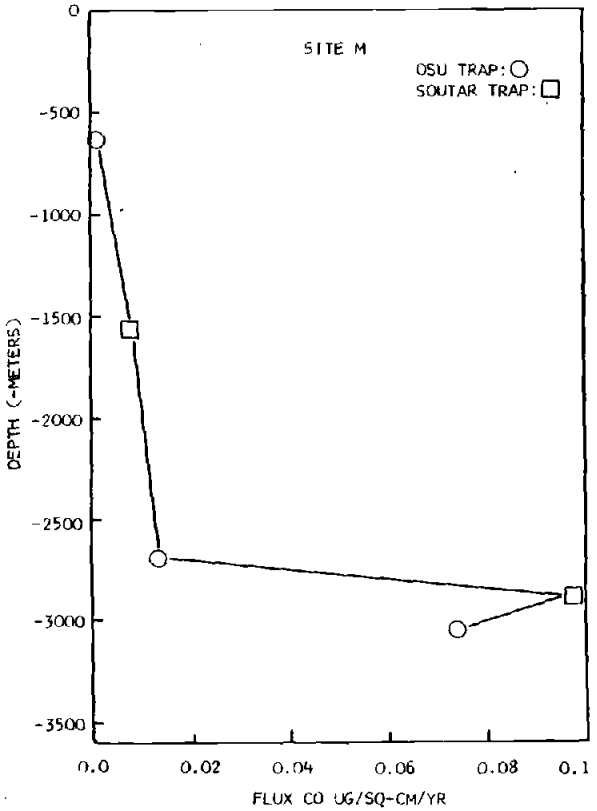

Figure I-16b

Figures I-16a and I-16b. Cobalt flux for 13-month deployment period versus depth at Sites H and M. Bottom at Site H is 3575 m. Bottom at Site M is 3080 m.

also increase in the bottom 500 m, and this observation cannot be explained by simple resuspension of local sediment since the sediments are impoverished in the biogenic components.

Aluminum in suspended particles is generally believed to be bound in unreactive silicate phases, and its principal source in regions away from spreading centers is continental detritus. If there are no additional sources of Al particulates at depth and particles transporting Al to the bottom remain intact, the Al flux should be constant with depth. As can be seen in Figures I-11a and b, the Al flux is constant from 1465 m to 3075 m at Site H but increases exponentially with depth in the near-bottom zone, due most likely to the collection of resuspended sediments in the traps. At Site M, the Al flux increases gradually throughout the water column and more rapidly within 300 m of the bottom. The rate of flux increase with depth lessens between the 1565 m and the 2700 m depths (Figure I-11b), and there may exist a depth interval, similar to Site H, over which the Al flux changes little. Aluminum is relatively abundant in the sediments at both sites (5-6%). Calculating on the basis of increased aluminum flux relative to the 3075 m trap, the deepest trap at Site H would consist of 14% by weight resuspended sediments. At Site M, the resuspended component would have to be 31% by weight of the material collected in the lowest trap (calculating relative to the 2700 m trap).

The Fe flux profiles (Figures I-12a and b) show very similar trends to the Al profiles. The Fe/Al ratios for the upper water column traps (~500 m and ~1500 m are ~0.5 at both sites, which is similar to that observed in intermediate to siliceous igneous rocks and sedimentary rocks from continents (Wedepohl, 1969a, 1969b). Consequently, the major portions of the Fe and Al seen at these levels of the water column is carried in continentally derived aluminosilicates. Near the bottom at both sites the Fe/Al ratio increases, and this indicates the need for an additional source of particles with a higher Fe/Al ratio. If the source were the bottom sediments, almost all of the flux in lower two traps would have to be resuspended material (60% at H and 81-92% at M, depending if the 1565 m or 2700 m trap is used for calculation). The flux inputs at the 3075 m level at H and the 2700 m level at M may be assumed to have small contributions from resuspension, since these traps are 500 m and 380 m above bottom, respectively. The flux from the 3075 m level at H is 77% of the flux at 3545 m, substantially less than 40%. Similarly, the flux from the 2700 m trap at M is 67% of the 3050 m trap flux, much less than 8%. This reasoning assumes that the dissolution and decomposition in the lower 500 m of the water column at each site is small. Resuspension of unfractionated sediments will not account for the change in the Fe/Al ratios seen in the lower traps. Hydrothermal

Table I-8. Metal to aluminum ratios from traps and surface sediments at Sites H and M.

Site H:

Depth, m	Fe/Al	Mn/Al	Ni/Al	Cu/Al	Co/Al
505	0.43	0.032	0.011	0.016	0.0010
1465	0.54	0.044	0.015	0.011	0.0021
3075	0.59	0.070	0.007	0.016	0.0011
3225	0.58	0.13	0.017	0.016	0.0016
3415	0.67	0.32	0.014	0.015	0.0039
3545	0.68	0.51	0.016	0.013	0.0016
3575 - sediment	0.83	0.65	0.018	0.011	0.0014
hydrothermal source*	166.	3.45	0.15	0.70	-

Site M:

Depth, m	Fe/Al	Mn/Al	Ni/Al	Cu/Al	Co/Al
635	0.42	0.008	0.011	0.012	0.0007
1565	0.53	0.026	0.012	0.013	0.0023
2700	1.01	0.14	0.009	0.012	0.0011
2883	1.22	0.36	0.009	0.008	0.0023
3050	1.37	0.33	0.006	0.012	0.0013
3080 - sediment	1.44	0.34	0.006	0.005	0.0009
hydrothermal source*	166.	3.45	0.15	0.70	-

*From Dymond, 1981. See Chapter 3, Table III-1.

precipitates from the rise crest (see Chapter 3) or sorption onto particles of dissolved Fe may provide the additional Fe. Only a small input of hydrothermal material is needed to account for the Fe/Al of the lower traps. At Site H, 0.06% of the lowest trap flux would need to come from a hydrothermal source. At Site M, a hydrothermal input equalling 2.2% of the flux of the lowest trap would be necessary.

Mn/Al ratios also increase in this near-bottom zone. It is even more difficult to account for the observed Mn/Al ratio by resuspension. If sufficient hydrothermal material is added to account for all the needed Mn, far too much Fe results. Since Mn is more readily reduced than Fe to a soluble form, bottom sediments might strongly enrich bottom waters in Mn. The uppermost 10 cm of sediment at Site H are oxidizing with respect to Mn(IV), and contain very low levels of dissolved Mn (Heggie and Bender, 1983). However, Site H is less than 100 km from areas of the seafloor where the surface sediments are sufficiently reducing (Lyle, 1983) to mobilize Mn in bottom waters. At Site M, the maximum in Mn concentration is at the surface of the sediments, and reduced Mn species have been found in the surface sediments (Kalhorn et al., 1983). Mn appears to be fluxing out of the sediments (Heath and Lyle, 1982). Precipitation of Mn diffusing from the sediments and sorption of Mn on settling particles in the

bottom waters could account for the high Mn flux in the lower water column (Figures I-13a and b). The Mn flux, however, increases throughout the water column to a degree exceeding any other element, and this mechanism alone may not account for all of the increase. Bacterial oxidation of Mn onto particles is believed to be the source of additional Mn in the oxygen minimum region (Martin and Knauer, 1982).

Ni/Al increases with depth at Site H, and Ni/Al of the sediments is slightly higher than the lowest trap. Although the Ni/Al in hydrothermal precipitates is relatively high (Dymond, 1981), the fraction of hydrothermal particles in near-bottom traps determined by normative analysis (Chapter 3) is too low to account for the Ni/Al increase observed in near-bottom traps from at Site H. Possibly, Ni tracks Mn and mobilization of and reprecipitation of Mn results in scavenging of Ni. At Site M, the Ni/Al decreases throughout the water column, and the lowest trap has a ratio equal to that of the surface sediments (Table I-8). Since the hydrothermal ratio is much higher (0.15, Dymond, 1981), hydrothermal particles would tend to raise the ratio. Therefore, the reason for the decreasing Ni/Al at M is uncertain; however, some Ni is probably regenerated from biogenic particles and is returned to bottom water whereas most of the Al remains in refractory aluminosilicates. Resuspension of sediments with relatively high Ni/Al could contribute to the lower

Ni/Al observed in the three deepest traps from Site M.

Cu/Al at both sites is almost constant throughout the water column, but decreases in the sediments (Table I-8). Co flux is consistently higher in the Soutar trap (Tables I-4 and I-5), and the Co/Al ratios are higher as well. Possibly the difference in bactericide used in the two traps is related to the difference in Co flux. Co/Al ratios increase with depth at both sites, although the sediments have a lower Co/Al ratio than the traps.

From the discussion above, it would seem that resuspension of bottom sediments is consistent with the transition metal flux increases in the bottom traps at both sites. Additional sources of Fe and Mn flux are required apart from resuspension. Input of a small amount of hydrothermal material will account for the increased Fe flux. A source richer in Mn than hydrothermal precipitate is needed, however, to account for the Mn flux increase. Input of dissolved Mn from reducing bottom sediments followed by precipitation or sorption on particles may supply Mn to the lower traps.

Flux Ratio Variations with Depth

Tables I-9 and I-10 list the flux ratios between traps at successive depths in the water column. Most components show an increase at the ~1500 m level over the ~500 m level. While the $CaCO_3$, opal, organic carbon, N, and organic phosphorus increase in this upper region by a factor less than two, Al, Sc, Mn, Fe, Ni, and Cr increase by more than a factor of 3. This indicates that the flux increase at the ~1500 m level is enriched in these metals relative to the biogenic constituents. The mid-water increases in shell material along with organic matter might arise through lateral transport of particle-rich waters from adjacent areas of higher productivity, such as would be found in the upwelling region to the east. However, currents at this depth are generally to the east at this depth (Appendix 1). They are to the west at the ~600 m level, and possibly material is moving in from the east above the 1500 m trap. Biological repackaging of small particles into faster settling units may occur as well. Advection of small particles into the mid-water column by currents is still required to maintain mass balance, however.

Similarly, in the near-bottom region the ratios for the biogenics are ~1, whereas the ratios for Mn, Fe, Al, Th, Sc, Cu, Ni, and Cr are greater than 1.5. Increases in these components is probably from resupension. Mn ratios are greater than any other element, suggesting

Table I-9. Site H - Flux Ratios for traps at successive depths.

Depth/Depth	CaCO3	Opal	C-org	N	P-org	P-inorg	Al	Ti	Th
1465/505	1.92	1.61	1.39	1.18	1.35	0.41	3.25	1.51	2.47
3075/1465	0.86	0.74	0.59	0.72	0.50	0.70	1.05	1.19	1.67
3225/3075	1.19	1.29	1.26	1.14	1.19	1.25	1.69	1.73	0.90
3415/3225	1.07	1.10	1.11	0.98	1.30	1.04	1.59	0.98	1.67
3545/3415	0.93	0.92	0.92	0.99	0.86	1.74	1.61	0.93	2.59

Depth/Depth	Sc	U	Mg	Br	Ba	Sr	Pb	Mn	Fe
1465/505	3.51	0.77	1.13	1.19	2.52	1.89	4.04	4.50	4.14
3075/1465	0.93	1.26	1.13	0.82	0.93	0.85	0.57	1.67	1.14
3225/3075	1.49	1.10	1.10	1.20	1.50	1.19	-	3.13	1.66
3415/3225	1.69	0.87	0.92	0.89	1.23	1.08	-	3.90	1.84
3545/3415	1.77	1.15	1.14	0.98	1.19	0.93	1.05	2.57	1.90

Depth/Depth	Cu	Co	Ni	Zn	Cr	Cd	Total
1465/505	2.28	6.40	4.57	0.51	3.15	0.89	1.66
3075/1465	1.47	0.55	0.50	1.82	0.82	0.55	0.82
3225/3075	1.74	2.49	3.96	1.42	1.52	1.15	1.22
3415/3225	1.49	3.94	1.34	0.60	1.03	-	1.09
3545/3415	1.32	0.67	1.84	2.25	1.37	-	0.97

Table I-10. Site M - Flux Ratios for traps at successive depths.

Depth/Depth	CaCO3	Opal	C-org	N	P-org	P-inorg	Al	Ti	Th
1565/635	1.33	1.95	1.39	1.39	1.93	0.35	2.32	4.00	1.92
2700/1565	1.22	1.66	1.06	1.11	0.84	1.34	3.45	1.68	3.68
2883/2700	1.35	1.10	1.32	1.21	1.85	2.47	3.54	2.38	3.59
3050/2883	0.93	1.02	0.81	0.86	0.70	1.29	1.30	2.19	1.64

Depth/Depth	Sc	U	Mg	Br	Ba	Sr	Pb	Mn	Fe
1565/635	2.29	0.64	1.67	1.37	2.26	1.50	0.63	7.33	2.95
2700/1565	3.68	2.85	0.86	1.02	1.57	1.12	-	18.8	6.56
2883/2700	3.46	1.34	2.48	1.52	2.04	1.61	-	9.21	4.28
3050/2883	1.56	1.11	0.82	0.73	1.35	0.97	1.99	1.20	1.46

Depth/Depth	Cu	Co	Ni	Zn	Cr	Cd	Total
1565/635	2.56	8.07	2.63	0.68	2.17	2.38	1.61
2700/1565	3.07	1.69	2.50	1.46	1.89	0.42	1.35
2883/2700	2.32	7.27	3.67	1.59	3.86	1.69	1.51
3050/2883	2.03	0.76	0.80	1.04	1.09	4.00	1.00

that the dominant flux changes for this element is decoupled from the others.

Tables I-11 and 12 show the compositional and flux ratios for comparable depths at the two sites. Compositional differences are less than a factor of two, atesting to the similarity of the material fluxing to the sites. Mn and Fe are exceptions and are generally greater at M in near-bottom region. This is probably the result of greater hydrothermal input at M, as well as more recycling of Mn. Flux ratios between the two sites show that fluxes for all components at M are less than at H in the upper water column, but are approximately equal or larger in the lower water column.

Table I-11. Site M / Site H - Compositional ratios for traps at similar depths at each site.

Depth/Depth	CaCO3	Opal	C-org	N	P-org	P-inorg	Al	Ti	Th
635/505	1.00	1.13	1.43	1.21	1.11	1.17	1.62	0.60	1.62
1565/1465	0.72	1.40	1.47	1.49	1.62	1.03	1.20	1.64	1.31
2700/3225	0.63	1.81	1.56	1.49	1.67	1.17	1.72	0.99	2.37
2883/3415	0.57	1.31	1.32	1.32	1.72	1.99	2.77	1.73	3.67
3050/3545	0.56	1.41	1.15	1.13	1.37	1.44	2.19	3.96	2.27

Depth/Depth	Sc	U	Mg	Br	Ba	Sr	Pb	Mn	Fe
635/505	1.28	1.17	1.32	1.38	1.28	0.75	2.49	0.40	1.60
1565/1465	0.85	1.01	1.99	1.62	1.18	0.61	0.37	0.70	1.16
2700/3225	1.68	1.52	1.02	1.24	0.99	0.50	-	1.83	2.98
2883/3415	2.48	1.70	2.00	1.53	1.18	0.54	0.43	3.12	5.01
3050/3545	2.12	1.60	1.40	1.12	1.31	0.55	0.79	1.43	3.75

Depth/Depth	Cu	Co	Ni	Zn	Cr	Cd
635/505	1.19	1.02	1.62	2.25	1.70	0.64
1565/1465	1.38	1.45	0.96	3.02	1.20	1.77
2700/3225	1.18	1.22	0.91	1.26	1.36	0.86
2883/3415	1.36	1.63	1.77	2.43	3.67	-
3050/3545	2.04	1.74	0.75	1.09	2.85	5.86

Table I-12. Site M / Site H - Flux ratios for traps at similar depths at each site.

Depth/Depth	CaCO3	Opal	C-org	N	P-org	P-inorg	Al	Ti	Th
635/505	0.47	0.53	0.67	0.57	0.52	0.55	0.76	0.28	0.76
1565/1465	0.33	0.64	0.67	0.68	0.74	0.47	0.55	0.75	0.60
2700/3225	0.39	1.12	0.96	0.92	1.03	0.72	1.06	0.61	1.46
2883/3415	0.49	1.12	1.13	1.13	1.47	1.70	2.37	1.48	3.14
3050/3545	0.49	1.24	1.01	0.99	1.20	1.26	1.92	3.47	1.99

Depth/Depth	Sc	U	Mg	Br	Ba	Sr	Pb	Mn	Fe
635/505	0.60	0.55	0.62	0.65	0.60	0.35	1.17	0.19	0.75
1565/1465	0.39	0.46	0.91	0.74	0.54	0.28	0.17	0.32	0.53
2700/3225	1.04	0.94	0.63	0.77	0.61	0.31	-	1.13	1.84
2883/3415	2.12	1.45	1.71	1.31	1.01	0.46	0.37	2.67	4.28
3050/3545	1.86	1.40	1.23	0.98	1.15	0.48	0.69	1.25	3.29

Depth/Depth	Cu	Co	Ni	Zn	Cr	Cd	Total
635/505	0.56	0.48	0.76	1.04	0.80	0.30	0.47
1565/1465	0.63	0.61	0.44	1.38	0.55	0.81	0.46
2700/3225	0.73	0.75	0.55	0.78	0.84	0.53	0.62
2883/3415	1.16	1.39	1.51	2.08	3.14	-	0.85
3050/3545	1.79	1.57	0.66	0.96	2.50	5.14	0.87

Biogenic Ratios

Table 13 lists the ratios of selected biogenic components. The C/N ratios of the Soutar traps (1465 m, 3415 m, 1565 m, and 2883 m) are generally higher than the OSU ratios. At Site M, the values fall within a narrow range. At Site H, the C/N ratio varies more, though not with a consistent trend with depth. Karl and Knauer (1983) found a maximum C/N value at ~1100 m. within the region 100-2000 m. The ratio increased from 6 to 12 from 100 to 1100 m, and then dropped to 7 at 2000 m. They associated the change with a region of intense bacterial and animal activity in the 900 m to 1100 m region. Considering the C/N at both sites, the average ratio is 7.7 which is slightly higher than the Redfield ratio of 7. Preferential loss of N compared to C, as would occur if proteins decayed more rapidly than carbohydrates or lipids, is not evident. If levels of chemotrophic bacterial activity exist in the region ~1100 m, C/N would decrease at that level.

C/P ratios are much higher than the Redfield ratio of 106, and indicate the rapid release of organic phosphorus during the initial decay of organic matter (Collier and Edmond, 1983). The values found here are similar to those found in the deep ocean by Knauer et al., 1979. C/P for the Soutar trap are lower than for the OSU trap and may reflect bactericide effects on P as noted above. For most traps, C/P ratios fall within the range 300-400.

Table I-13. Biogenic ratios for traps at each site. Ratios are molar (mol. wt. opal taken to be 73.3 g/mol; van Bennekom and van der Gaast, 1976). C refers to organic carbon, N to total nitrogen, and P to organic phosphorus.

Site H:

Depth, m	C/N	C/P	CaCO3/C	Opal/C	CaCO3/Opal
505	6.9	330	0.72	0.42	1.7
1465	8.1	340	0.99	0.48	2.0
3075	6.7	400	1.4	0.60	2.3
3225	7.3	420	1.4	0.61	2.2
3415	8.3	360	1.3	0.61	2.1
3545	7.7	390	1.3	0.61	2.1

Site M:

Depth, m	C/N	C/P	CaCO3/C	Opal/C	CaCO3/Opal
635	8.1	430	0.50	0.33	1.5
1565	8.1	310	0.48	0.46	1.0
2700	7.7	390	0.55	0.75	0.7
2883	8.3	280	0.56	0.60	0.9
3050	7.9	330	0.64	0.75	0.8

The $CaCO_3$/C ratio increases with depth at both sites, although to a greater degree at Site H, and is the result of greater $CaCO_3$ flux with depth compared to organic carbon. Opal/C also increases with depth at both sites, and the ratios are almost equal at the same depth at each site. Although flux increases with depth occur for all three components, proportionately less carbon is present. This suggests that organic carbon decomposes more rapidly than either shell material dissolves. $CaCO_3$/opal is constant with depth at Site H, whereas this ratio decreases by a factor of two with depth at Site M. The $CaCO_3$/opal ratios are almost the same at the ~600 m level at each site, but by ~1500 m differences in the two sites are apparent. Site H is dominated by $CaCO_3$ deposition relative to opal, whereas at Site M the fluxes of these two components are equivalent.

Since the sediments at Site H contain less carbonate than opal (Table I-14), local resuspension should decrease the $CaCO_3$/opal ratio in the lower traps. This assumes that resuspension occurs without fractionation. Similarly, since the $CaCO_3$/opal value in the sediments at Site M is 1.2, resuspension would result in greater carbonate input relative to opal in the lower traps at M. Neither site exhibits the expected resuspension effects in the near-bottom traps. Consequently, the most probable explanation for these changes is a lateral source of biogenic material.

Table I-14. Estimated trap fluxes to the sediment and sediment accumulation rates at Sites H and M. The trap flux at 3075 m was used at Site H for most components. The top 5 cm of sediment was used for the accumulation rate estimates for all components except manganese, for which the accumulation rate at 37-39 cm was taken. For Site M, the 2700 m trap was used for the fluxes to the sediments. Accumulation rates are calculated from the top 5 cm of sediment, with the exception of Mn, for which the 20-22 cm interval was used. Units are ug/sq-cm/y.

	SITE H		SITE M	
Component	Flux	Accumulation Rate	Flux	Accumulation Rate
CaCO3	1340.	0.61	618.	27.
Opal	419.	17.4	607.	16.5
C-org	112.	0.87	135.	2.7
N	19.7	0.16	20.5	0.35
P-org	0.72	0.032	0.89	0.11
P-inorg	0.57	0.20	0.51	0.37
Al	6.62	6.00	11.9	10.4
detr.-SiO2	42.5	39.0	76.5	67.0
Mg	20.5	1.6	14.2	3.1
Br	1.8	0.016	1.7	0.046
Ba	3.3	1.0	3.0	1.1

Table I-14, continued. Extimated flux to the bottom sediments and accumulation rates at Sites H and M.

	SITE H		SITE M	
Component	Flux	Accumulation Rate	Flux	Accumulation Rate
Sr	1.6	0.053	0.57	0.12
Sc	0.0023	0.0023	0.0035	0.0034
Ti	0.70	0.40	0.74	0.71
Cr	0.017	0.0055	0.021	0.012
Mn	0.47	1.7	1.7	0.35
Fe	3.9	5.0	12.	15.
Co	0.0071	0.0085	0.013	0.0090
Ni	0.048	0.11	0.11	0.060
Cu	0.11	0.063	0.14	0.053
Zn	0.29	0.066	0.32	0.071
Pb	0.11	0.0035	0.05(est.)	0.012
Th	0.0007	0.0004	0.00092	0.00083
U	0.0022	0.00021	0.0022	0.00028
Cd	0.0026	0.00011	0.0016	0.00008
Si-total	181.	24.0	268.	37.6

Comparison of Trap Fluxes to Accumulation Rates

Table I-14 gives the estimated particle fluxes to the bottom at Site H (taken from the 3075 m trap) and the accumulation rates of these elements in the surface 0-5 cm of the sediments. The manganese accumulation rate was taken from the 37-39 cm interval in the sediments, since this should be outside the zone of Mn remobilization and thus provide an estimate of the burial rate of Mn. The 2700 m trap data is used for the estimates of the fluxes to the bottom at Site M. The compositional data for the top 5 cm of sediment was used to estimate the accumulation rates of the elements, again with the exception of Mn, for which the 20-22 cm level was used. Figures I-17 and I-18 compare the flux of each component to the accumulation rate of that component in the sediments at each site. All points lying to the left of the solid line are input in excess of what is preserved in the sediments. Regeneration rate can be calculated for each of these by subtracting the accumulation rate from the particulate flux, which represents the loss to the overlying seawater. Decomposition of organic matter, dissolution of shell material, and the loss of metals associated with these phases result in an accumulation rate which is less than the flux. Points falling on the solid line are elements quantitatively preserved in the sediments. Generally, elements which are enriched in aluminosilicates, such as Al, Th, Ti, Fe, and Si, are

Figure I-17. Comparison of trap flux at Site M to sediment accumulation rate at M. In this figure and Figures I-18 though I-20, the solid line represents a one-to-one correspondence between the designated elements. The upper dashed line represents a factor of two-to-one between the y and x values of the elements. The lower dashed line represents a one-half-to-one correspondence between the y and x values. See Table I-14 and text for further discussion.

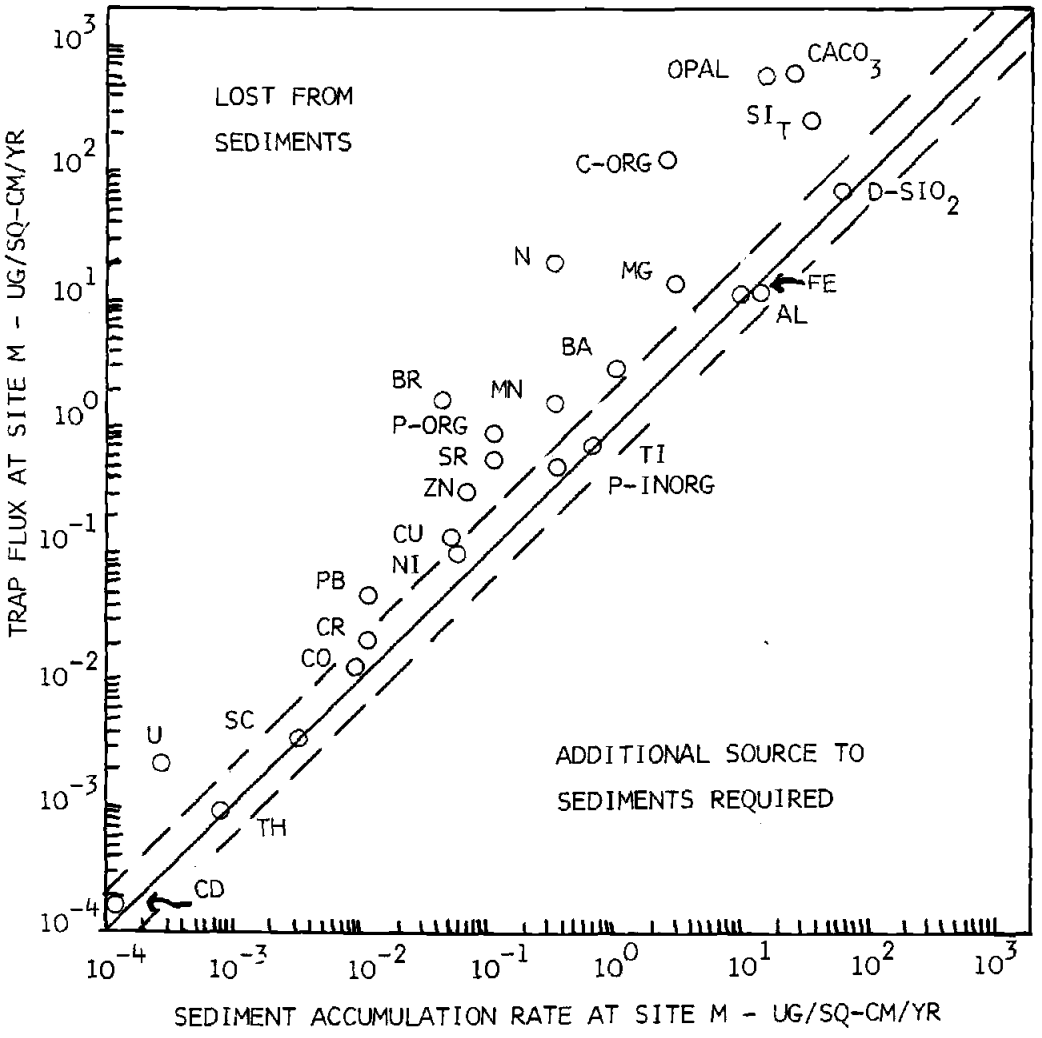
LOST FROM
SEDIMENTS
ADDITIONAL SOURCE TO
SEDIMENTS REQUIRED
OPAL
CACO3
SIT
C-ORG
D-SIO2
N
MG
FE
AL
BA
BR
MN
P-ORG
SR
TI
P-INORG
ZN
CU
NI
PB
CR
CO
SC
U
TH
CD
TRAP FLUX AT SITE M - UG/SQ-CM/YR
SEDIMENT ACCUMULATION RATE AT SITE M - UG/SQ-CM/YR

Figure 17

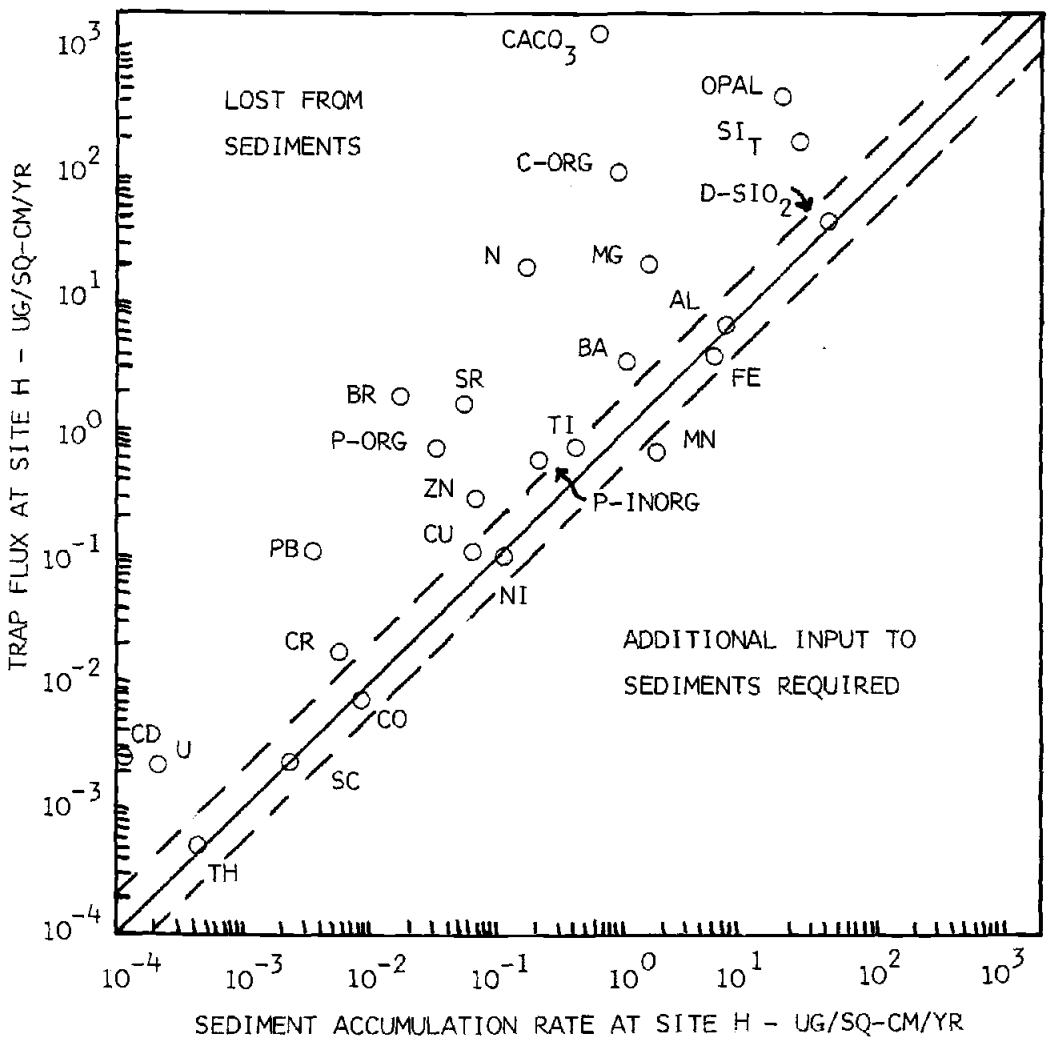

Figure I-18. Comparison of trap flux at Site H to sediment accumulation rate at H.

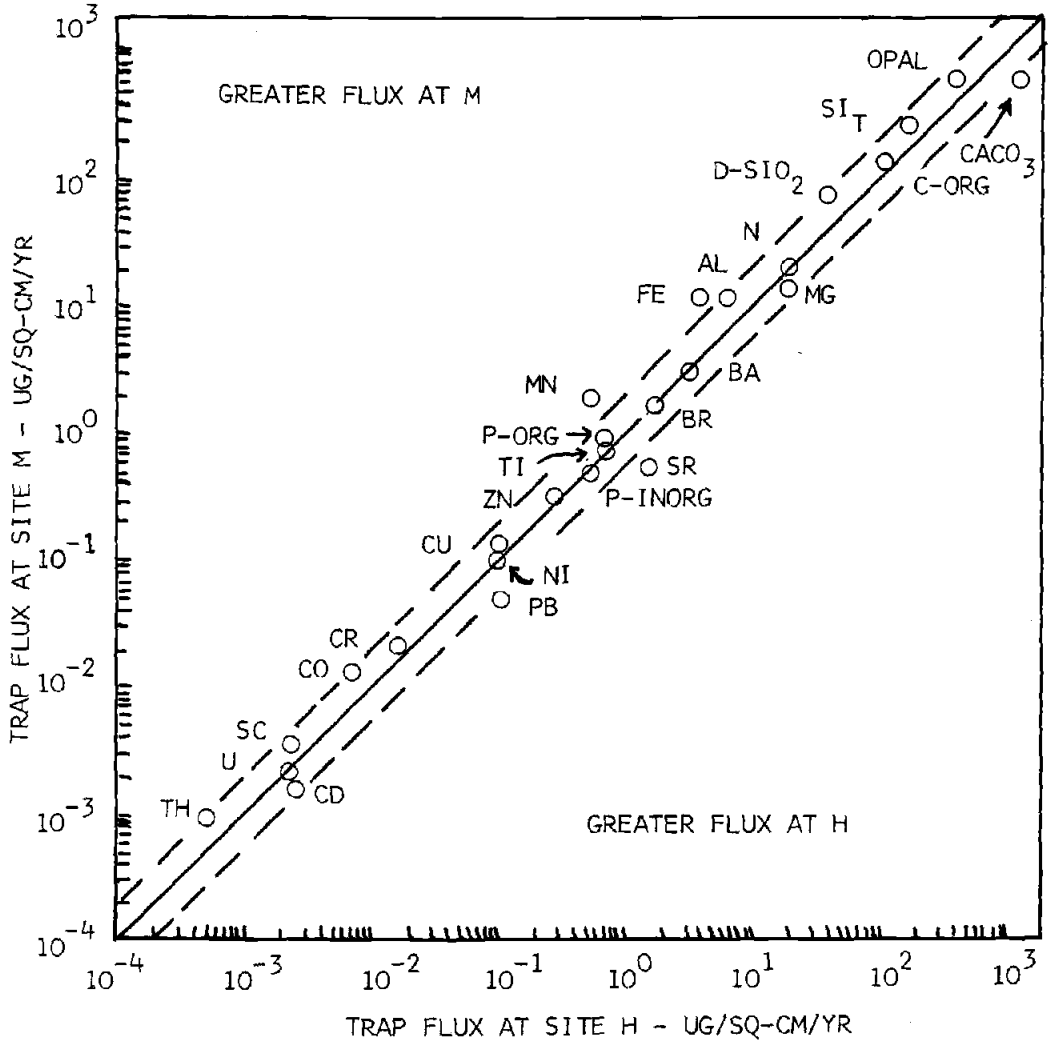

Figure I-19. Comparison of trap flux at Site M to trap flux at Site H.

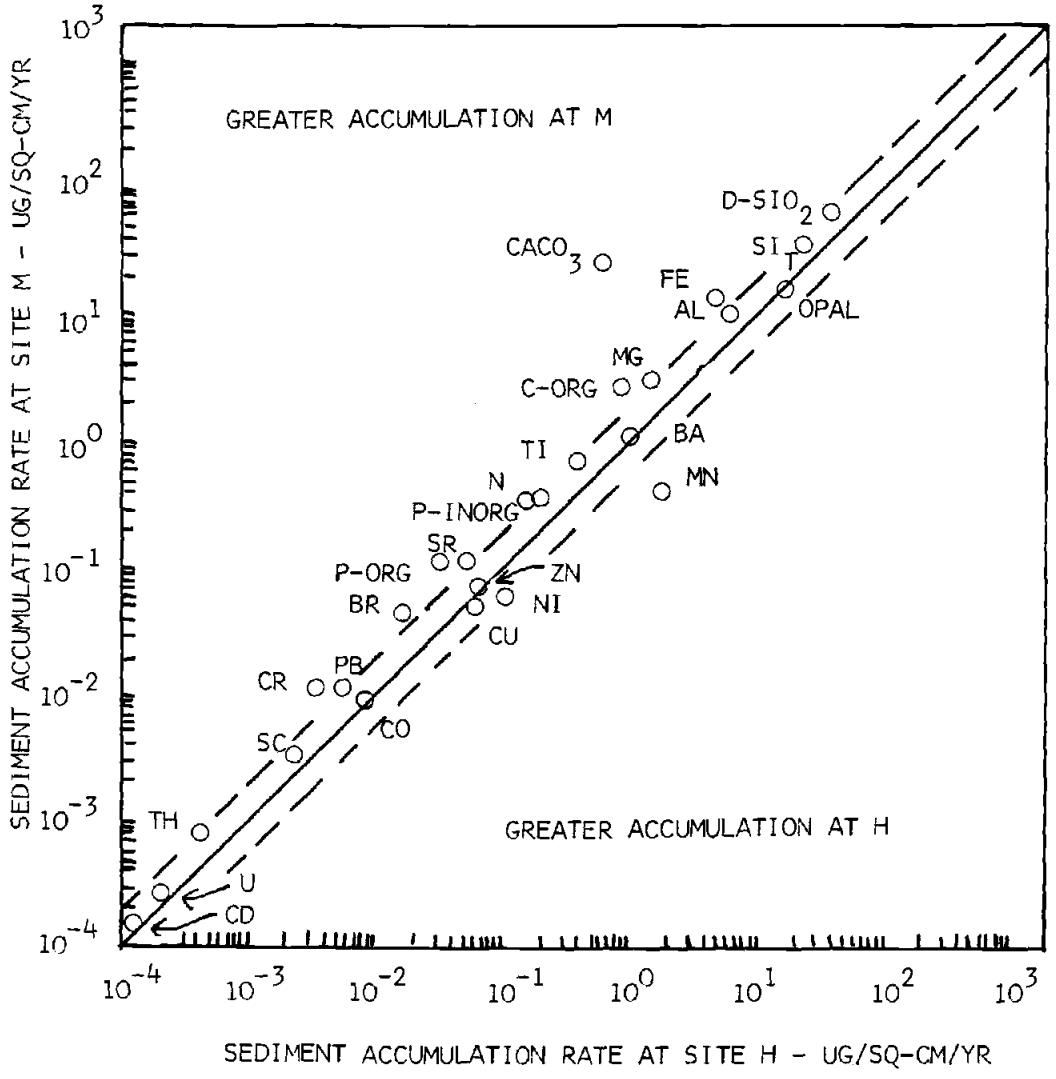

Figure I-20. Comparison of sediment accumulation rate at Site M to sediment accumulation rate at Site H.

expected to be preserved. Elements with accumulation rates greater than the estimated flux require a source in addition to the the flux of particles out of the midwater region. One possibility is that a near-bottom source of particles exists below the level at which the flux was measured. The selection of the level from which the flux to the bottom is taken is critical to this kind of comparison. For this reason, flux measurements at several depths in the near-bottom region are required. Other possibilities are sorption onto particles, hydrogenous precipitation onto sediments, and that the year of measurement is atypical.

At Site H, all elements are input in excess of the accumulation rates except for Mn, Ni, Fe, and Co. The "missing" flux for each of these elements may be added below the level of the 3075 m trap. The sources of these elements may be hydrothermal flux or the precipitation or scavenging of Mn in the lower water column, as discussed above. Al (as well as detrital SiO2 calculated from the Al data), Th, and Sc accumulate without apparent loss from the sediments. This would tend to support that the year of measurement was typical. Most of the biogenic material is regenerated with associated metals.

For Site M, only Fe requires a source other than the particle flux given by the 2700 m trap. Fe is the dominant metal in hydrothermal precipitates, and an

additional flux of Fe may arise through input of hydrothermal material below the 2700 m trap level. Downslope wafting of hydrothermal precipitates from the EPR has been documented elsewhere (Dymond and Veeh, 1975) and is a reasonable explanation for the excess Fe deposition at Site M. Al, Ti, Th, and Sc have fluxes which almost equal the accumulation rates of these elements. The other components and elements plotted show loss from the sediments. These are predominantly biogenic components and associated elements, as at Site H, which decompose or dissolve, and their associated elements.

Comparison of Figures 17 and 18 shows that the regeneration rate of $CaCO_3$, as well as Sr and Mg which is most likely in the form of carbonates, is much greater at Site H.

At M, manganese apppears to be lost from the sediments (Figure 17) and contrasts to Site H where it appears that insufficient Mn is being input to the sediments based on the data from the 3075 m trap. The concentration profile for this element in the bottom sediments at M has a maximum in Mn at the surface (M. Lyle, pers. comm.). Reduced Mn has been found in the surface sediments at Site H (Kalhorn and Emerson, 1983), and dissolved Mn shows a substantial increase in the lower water column at both sites (Edmond, written comm.).

Comparison of Sites M and H

In Figure 19 the estimated flux to Site M is plotted versus the estimated flux to Site H to reveal differences in the particle fluxes to the two sites. Mn and Fe have higher fluxes at M, most probably reflecting the greater hydrothermal input at M. CaCO3 and Sr, most likely in the form of carbonate, have greater inputs at Site H. All other component fluxes are within a factor of two between the two sites.

In Figure 20, the accumulation rate for the elements at Site M are plotted versus the accumulation rate at Site H. The sedimentation rate at Site M is twice that of Site H, and most elements fall along the upper dashed line, which represents a factor of two increase at M. More Mn is accumulating at Site H, despite the greater Mn flux to Site M sediments. This emphasizes the apparent regeneration of Mn at Site M. As discussed above, the very large Mn flux increases in the lower water column cannot be attributed to resuspension, and even hydrothermal material will not supply sufficient Mn without raising the Fe fluxes beyond the measured values. Recycling of Mn from local or nearby sediments may be occuring, and is consistent with the results of the comparison of fluxes and accumulation rates for Mn at both sites.

Conclusions

At both MANOP Sites M and H, particle flux increases with depth. Since our data indicate that this flux increase occurs for the biogenic components as well as the detrital constituents, some process must occur which can move biogenic material into a region at depth. Two explanations seem tenable. One requires some mechanism for large particle generation, i.e. the accumulation of suspended or slowly settling material into more rapidly settling particles which can be sampled by traps. Physical aggregation of particles by currents and bacterial agglutination have been suggested. Packaging into fecal pellets by zooplankton feeding on particles at depth may also increase flux. A second explanation is the movement of water masses containing a greater concentration of rapidly settling particles. Such waters would be transporting surface-produced particles from adjacent areas of higher productivity. Flux increases in the near-bottom region most likely involve resuspension and hydrothermal input.

A second conclusion from this first chapter is that processes exist which greatly increase Mn flux throughout the water column, and that these processes affect Mn to a greater degree than any of the other transition elements. Processes which have been suggested include the input of Mn-rich particles at mid-water depths and the recycling of Mn from the sediments in the lower 200 m of the water column.

CHAPTER 2

SEASONAL FLUXES AT SITES M AND H

Abstract

Multiple sampling sediment traps were deployed at two sites in the eastern tropical Pacific Ocean (MANOP Sites H at 6 30'N, 93 W, and M at 9 N, 104 W). These traps sampled three consecutive intervals for a total deployment period of 13 months and were located between 500 m from the surface and 30 m above bottom. The three sampling periods were: mid-September to the end of January, February to mid-July, and mid-July through mid-October.

At both sites, seasonal differences in flux were apparent. At Site H, the total particle flux for the first period was 3-4 times that of the rest of the year at all depths, and double the yearly average flux. At Site M, the total flux collected during the first period in the upper trap was approximately double the flux for the remainder of the year. At Site H, organic carbon flux during the first period was 2-4 times greater than the rest of the year and 64% greater than the computed average flux for the year. Similar results were found at Site M.

Release of metals associated with decay of organic carbon, dissolution of calcite and opal, or a temporary change in redox conditions in the surface of the sediments may occur in pulses linked to seasonal input of material.

Introduction

Over parts of the ocean, primary production varies with the season. Increased insolation and high nutrient levels combine to produce spring blooms of phytoplankton in certain areas (Russell-Hunter, 1970). Seasonal upwelling of nutrient-rich deep waters occurs along some coasts, resulting in periodic bursts of productivity.

Corresponding increases in particle flux in the waters underlying these regions have been reported. In a study of seasonal variations in particle flux arriving at the 3200 m level in the Sargasso Sea (Deuser et al., 1981), increases in the flux of all major components were concurrent with spring increases in productivity. Upwelling-related increases in the flux of biogenic components, with simultaneous increases in the flux of lithogenic materials, have been measured in the Panama Basin (Honjo, 1982). The pulses of increased flux were recorded simultaneously in traps spanning over 2600 m of water. A bloom of a single species of coccolithophorid accounted for another period of high flux occuring later in the year. At a site 300 km from the typical seaward extent of coastal upwelling, periods of high flux coincided with times when plumes of cold water extended over the mooring location (Fischer et al., 1983). Although principal river runoff occurred December through March, maximum detrital flux was measured during times of peak biogenic flux.

Four important conclusions from these studies are:

1. productivity variations result in variations in flux;

2. increases in flux may transit a 2000-3000 m water column within two months (sampling interval in both the Deuser et al. and the Honjo studies).

3. increases in lithogenic flux, as well as the fluxes of other components, may accompany increases in biogenic fluxes;

4. a bloom of a single species may send a large pulse of shell material to the bottom.

The pathways by which productivity-generated pulses in particle flux travel to the bottom have not been completely defined. Evidence exists for the repeated repackaging of particles into fecal pellets by zooplankton throughout the water column. Pellets of differing size and shape were found at different depths (Karl and Knauer, 1983). Pellets predominantly composed of detrital material have been found in the near-bottom region along with pellets produced higher in the water column (Honjo, 1980), indicating that animals are creating pellets near the bottom. Besides fecal pellets, amorphous particle aggregates ("marine snow", fecal matter, mucous aggregates, etc.) have been collected in traps (Honjo, 1982) and by large-volume filtering (Bishop et al., 1980). These aggregates have been observed and sampled in shallow water by divers (Trent et al., 1978) and as a layer on the surface of bottom sediments in the deep ocean by

camera and coring (Billett et al., 1983).

Seasonal productivity changes have been measured in the eastern tropical Pacific Ocean (Owen and Zeitzschel, 1970). Average seasonal values of primary production for the region vary by a factor of 2.5. These seasonal variations may be linked to upwelling in the Costa Rica Dome (Wyrtki, 1964; Hofmann et al., 1981) and in the Gulf of Tehuantepec (Blackburn, 1962), and possibly to the shoaling of the density gradient at certain times of the year in this region (Owen and Zeitzschel, 1970).

Seasonal sampling sediment traps, as well as traps collecting a bulk sample, were deployed in the eastern tropical Pacific Ocean as part of the Manganese Nodule Project (MANOP). Traps were positioned throughout the water column from 500 m depth to 30 m above bottom at two sites (Site H at 6° 32'N, 93° W; and Site M at 8° 50'N, 104° W). The seasonal traps partitioned the 13-month deployment into three time periods. Variations in the annual flux with depth and the partitioning of the collected material into source-related components are discussed in Chapters 1 and 3, respectively.

Experimental Descriptions

Site H is located in the Guatemala Basin at 6° 32'N, 92° 50'W in 3575 m of water. Site M lies 25 km from the East Pacific Rise spreading center at 8° 50'N, 104° W in 3080 m of water. Table II-1 lists the water depths of the seasonal and average sampling traps at each site, as well as the trap type. Two different traps were used: the single-cone OSU trap, which in most cases is multiple sampling and which uses sodium azide as a preservative; and the Soutar double-cone trap, which collects a bulk sample and which uses buffered formalin as a bactericide. Further descriptions of the sites, traps, sample processing, and analytical procedures can be found in Chapter 1. The performance of the electronic timers on the multiple-sampling traps were checked in a cold room after recovery.

The period of highest particle flux at Site H does not match the period of highest productivity measured in the surface waters. Table II-3 lists primary productivity data collected from April, 1967 through April, 1968 (Owen and Zeitzschel, 1970). The period of highest primary productivity for the area nearest Site H, which was on the eastern edge of the sampling grid, is February - May. Our maximum trap flux was measured in the period September 20 - January 29 (Table II-2). For the regions just to the north or south of Site H, highest productivity was occasionally measured during December through March

Table II-1. Locations and descriptions of traps at Sites H and M.

SITE H (3575 m water depth)

Depth, m	Trap
505	OSU - multiple sample
1465	Soutar - bulk sample
3075	OSU - multiple sample
3225	OSU - bulk sample
3415	Soutar - bulk sample
3545	OSU - multiple sample

SITE M (3080 m water depth)

Depth, m	Trap
635	OSU - multiple sample
1565	Soutar - bulk sample
2700	OSU - multiple sample
2883	Soutar - bulk sample
3050	OSU - bulk sample

Table II-2. Sampling periods at Sites H and M.

	Open	Closed	Days
Site H:			
Cup 1	9-20-80	1-29-81	131
Cup 2	1-29-81	7-12-81	164
Cup 3	7-12-81	10-14/16-81*	95-97
Site M:			
Cup 1	9-10/12-80*	1-30-81	139-141
Cup 2	1-30-81	7-13-81	164
Cup 3	7-13-81	10-23-81	103

*exact date varied with trap

Table II-3. Integrated Surface Production in mgC/sq-cm/y (Owen and Zeitzschel, 1970). Productivities are estimated for the three sampling periods from the measured data.

	7°25'N - 4°25'N 100°30'W - 93°30'W (Site H: 6°32'N, 92°50'W)		10°25'N - 7°25'N 107°30'W - 100°30'W (Site M: 8°50'N, 104°W)	
Oct-Nov	3.2		5.7	
		period 1: 6.3		period 1: 12.0
Dec-Jan	9.3		19.2	
Feb-Mar	21.4		9.6	
		period 2: 15.7		period 2: 9.5
Apr-May	17.1		12.8	
June-July	6.1		4.6	
		period 3: 6.1		period 3: 7.1
Aug-Sept	6.8		8.0	

(Owen and Zeitzschel, 1970). Because the generalized productivity maps of Owen and Zeitzschel are based on a single year of observations, the expected time of maximum productivity at Site H is relatively uncertain and may exhibit variations from year to year.

For Site M, the data of Owen and Zeitzschel suggest that the time of maximum primary productivity is during the December - January period, which coincides with the time of maximum trap flux (September 12 through January 30). In the region to the north or south of Site M, highest productivity was measured during February through May. In general, the Owen and Zeitzschel data indicate that the time of maximum productivity for the region 3 20'S - 16 N, 93 30'W - 121 30'W occurs during December - May, with occasional productivity peaks, generally of lesser magnitude, during June - July or August - September.

Variations in productivity in the vicinity of the two mooring sites may be related to upwelling associated with the Costa Rica Dome (Wyrtki, 1964; 1965). The Costa Rica Dome is centered at 9° N, 89° W, and covers the area from 7 N - 12 N and 89 W - 100 W (Hofmann et al., 1981). Recent examination of wind stress data indicates that upwelling occurs during early spring and summer, and that this feature dissipates in November (Hofmann et al., 1981). Nutrients may be transported to regions to the west of the dome by the North Equatorial current. This would most likely happen at Sites H and M during January - April, since flow past the

sites is predominantly to the east via the Equatorial Countercurrent during the remainder of the year (Wyrtki, 1965). Based on these considerations, highest productivity would be expected during the period January to April. This is confirmed in general by the primary productivity measurements by Owen and Zeitzschel; however, productivity peaks were measured in many cases outside of this four-month time frame.

Seasonal Flux Data - Site H

The seasonal and average flux data for Site H are presented in Table II-4. Period 1 (cup 1) is the time of greatest flux for all elements and components listed. Zn is the only exception, and may reflect in part a contamination signal. The total flux for period 1 is 3 times the flux of period 2 at all three levels. The total flux for period 1 is ~3.5 times the flux of period 3. For most elements, the flux ratio between periods 1 and 2 ranges between 2 and 3, and the flux ratio between periods 1 and 3 ranges between 3 and 5. The simultaneous measurement of maximum flux during period 1 at all three depths demonstrates that surface productivity must transit the 3600 m water column within 4 months. Transit over 3000 m has been found to occur within 2 months (Deuser et al., 1981; Honjo, 1982). Figures II-1 through II-6 show the seasonal changes in the total flux and the flux of the major biogenic components, Al, and Mn.

Seasonal total flux varied by a factor of 3 in the Sargasso Sea, with the fluxes of some components varying by more than an order of magnitude (Deuser et al., 1981). Elements which varied most dramatically in the Sargasso Sea study were Ca, Sr, Al, Ti, and Mn, which reflect the changes in carbonate flux and the increase in aluminosilicate flux with increasing biogenic flux. In our data set, the greatest changes occur between periods 1 and 3 for opal and Ba in the top trap. This most likely reflects

Table II-4. Fluxes for the three sampling periods at Sites H and M. Total fluxes are in units of mg/sq-cm/y. All other fluxes have units of ug/sq-cm/y.

SITE H SEASONAL TRAPS

Trap	Depth,m	Total	C-CO3	CaCO3	Si-total	Opal	C-org	N	P-org	P-inorg
OSU-cup 1	505	2.91	197.	1640.	287.	723.	223.	35.7	1.91	3.02
OSU-cup 2	505	0.93	49.9	416.	87.6	217.	111.	20.0	0.78	1.78
OSU-cup 3	505	0.68	43.3	361.	36.3	87.3	60.7	11.0	0.48	0.93
Average		1.53	97.3	811.	142.	354.	136.	23.1	1.06	1.97
OSU-cup 1	3075	3.85	326.	2710.	302.	690.	180.	30.0	1.26	0.94
OSU-cup 2	3075	1.29	84.2	702.	143.	337.	87.8	15.6	0.48	0.46
OSU-cup 3	3075	1.05	65.9	549.	79.8	192.	62.7	12.3	0.39	0.26
Average		2.09	160.	1340.	181.	419.	112.	19.7	0.72	0.57
OSU-cup 1	3545	4.86	382.	3180.	472.	891.	226.	30.3	1.36	2.10
OSU-cup 2	3545	1.61	97.8	815.	207.	379.	101.	16.7	0.70	0.74
OSU-cup 3	3545	1.58	82.2	685.	208.	372.	104.	19.0	0.86	1.13
Average		2.70	190.	1580.	296.	550.	144.	21.8	0.96	1.29

SITE M SEASONAL TRAPS

Trap	Depth,m	Total	C-CO3	CaCO3	Si-total	Opal	C-org	N	P-org	P-inorg
OSU-cup 1	635	1.05	51.1	426.	140.	348.	149.	22.9	0.84	0.98
OSU-cup 2	635	0.59	40.5	337.	54.2	133.	70.1	9.25	0.38	1.38
OSU-cup 3	635	0.50	47.5	396.	27.2	63.4	48.8	6.74	0.33	0.78
Average		0.72	45.7	381.	76.6	188.	91.3	13.2	0.55	1.09
OSU-cup 1	2700	1.50	65.6	547.	259.	557.	136.	20.8	0.90	0.55
OSU-cup 2	2700	1.12	42.3	352.	230.	561.	104.	15.3	0.78	0.21
OSU-cup 3	2700	2.37	136.	1140.	342.	747.	183.	28.5	1.03	0.94
Average		1.57	74.1	618.	268.	607.	135.	20.5	0.89	0.51

Table II-4, continued. Fluxes for the three sampling periods at Sites H and M. Units are ug/sq-cm/y.

SITE H SEASONAL TRAPS

Trap	Depth,m	d-SiO2	Al	Ti	Th	Sc	U	Ca	Mg	Br
OSU-cup 1	505	21.5	3.36	0.96	0.00032	0.00128	0.00410	667.	24.7	3.00
OSU-cup 2	505	9.2	1.43	0.14	0.00011	0.00048	0.00134	177.	9.6	1.30
OSU-cup 3	505	6.0	0.93	0.05	0.00006	0.00030	0.00120	143.	15.6	1.40
Average		12.5	1.95	0.39	0.00017	0.00070	0.00223	330.	16.1	1.89
OSU-cup 1	3075	80.4	12.5	1.39	0.00142	0.00422	0.00357	1000.	24.6	2.37
OSU-cup 2	3075	29.1	4.54	0.35	0.00038	0.00149	0.00169	264.	12.9	1.31
OSU-cup 3	3075	13.7	2.14	0.36	0.00024	0.00103	0.00099	208.	27.7	2.01
Average		42.5	6.62	0.70	0.00070	0.00229	0.00215	497.	20.5	1.84
OSU-cup 1	3545	279.	43.5	1.59	0.00541	0.0161	0.00408	1160.	32.4	2.60
OSU-cup 2	3545	133.	20.7	0.82	0.00123	0.00690	0.00161	314.	15.6	1.32
OSU-cup 3	3545	139.	21.6	0.93	0.00156	0.00778	0.00126	279.	24.4	2.05
Average		184.	28.6	1.11	0.00272	0.0102	0.00236	592.	23.4	1.93

SITE M SEASONAL TRAPS

Trap	Depth,m	d-SiO2	Al	Ti	Th	Sc	U	Ca	Mg	Br
OSU-cup 1	635	15.2	2.36	0.10	0.00023	0.00065	0.00185	172.	10.0	1.61
OSU-cup 2	635	7.1	1.10	0.10	0.00006	0.00029	0.00101	134.	6.3	0.75
OSU-cup 3	635	6.2	0.96	0.14	0.00008	0.00031	0.00071	145.	15.7	1.44
Average		9.6	1.49	0.11	0.00013	0.00042	0.00122	149.	9.9	1.22
OSU-cup 1	2700	96.7	15.1	0.88	0.00126	0.00422	0.00195	234.	14.1	1.61
OSU-cup 2	2700	32.5	5.07	0.31	0.00033	0.00164	0.00211	144.	9.5	1.22
OSU-cup 3	2700	119.	18.5	1.25	0.00140	0.00560	0.00275	449.	21.6	2.58
Average		76.5	11.9	0.74	0.00092	0.00353	0.00222	252.	14.2	1.70

Table II-4, continued. Fluxes for the three sampling periods at Sites H and M. Units are ug/sq-cm/y.

SITE H SEASONAL TRAPS

Trap	Depth,m	Ba	Sr	Pb	Mn	Fe	Cu	Co	Ni	Zn
OSU-cup 1	505	2.78	2.08	0.067	0.083	1.32	0.0616	0.00371	0.035	0.301
OSU-cup 2	505	0.88	0.46	0.023	0.070	0.69	0.0191	0.00138	0.017	0.245
OSU-cup 3	505	0.44	0.34	0.042	0.023	0.41	0.0119	0.00085	0.010	0.421
Average		1.41	0.97	0.042	0.062	0.83	0.0315	0.00203	0.021	0.307
OSU-cup 1	3075	6.09	3.31	0.153	0.943	6.91	0.194	0.0121	0.083	0.319
OSU-cup 2	3075	2.25	0.77	0.075	0.274	2.80	0.0721	0.00523	0.034	0.210
OSU-cup 3	3075	1.32	0.53	0.096	0.146	1.75	0.0444	0.00359	0.023	0.367
Average		3.31	1.56	0.106	0.466	3.92	0.106	0.00714	0.048	0.286
OSU-cup 1	3545	12.0	3.78	0.214	22.5	36.1	0.583	0.0606	0.759	0.667
OSU-cup 2	3545	4.66	0.94	0.116	10.8	15.6	0.249	0.0343	0.330	0.389
OSU-cup 3	3545	5.04	0.82	0.299	10.3	16.8	0.257	0.0501	0.302	0.635
Average		7.23	1.87	0.193	14.6	22.8	0.363	0.0470	0.468	0.542

SITE M SEASONAL TRAPS

Trap	Depth,m	Ba	Sr	Pb	Mn	Fe	Cu	Co	Ni	Zn
OSU-cup 1	635	1.53	0.45	0.050	0.017	0.93	0.0271	0.00150	0.028	0.484
OSU-cup 2	635	0.45	0.27	0.047	0.006	0.44	0.0115	0.00041	0.006	0.243
OSU-cup 3	635	0.56	0.29	0.050	0.013	0.49	0.0147	0.00121	0.017	0.222
Average		0.85	0.34	0.049	0.012	0.62	0.0176	0.00098	0.016	0.319
OSU-cup 1	2700	3.68	0.54	0.252	3.28	14.5	0.152	0.0124	0.094	0.415
OSU-cup 2	2700	1.42	0.35	0.072	0.444	4.42	0.0718	0.00436	0.047	0.148
OSU-cup 3	2700	4.66	0.98	-	1.36	20.5	0.224	0.0289	0.211	0.451
Average		3.02	0.57	-	1.65	12.0	0.138	0.0134	0.105	0.316

Table II-4, continued. Fluxes for the three sampling periods at Sites H and M. Units are ug/sq-cm/y.

SITE H SEASONAL TRAPS

Trap	Depth,m	Cr	Cd
OSU-cup 1	505	0.0100	0.0106
OSU-cup 2	505	0.0059	0.0035
OSU-cup 3	505	0.0029	0.0011
Average		0.0065	0.0053
OSU-cup 1	3075	0.0283	0.0041
OSU-cup 2	3075	0.0105	0.0021
OSU-cup 3	3075	0.0117	0.0012
Average		0.0168	0.0026
OSU-cup 1	3545	0.0596	0.0037
OSU-cup 2	3545	0.0212	0.0014
OSU-cup 3	3545	0.0284	0.0009
Average		0.0359	0.0021

SITE M SEASONAL TRAPS

Trap	Depth,m	Cr	Cd
OSU-cup 1	635	0.0065	0.0026
OSU-cup 2	635	0.0037	0.0016
OSU-cup 3	635	0.0058	0.0001
Average		0.0052	0.0016
OSU-cup 1	2700	0.0235	0.0026
OSU-cup 2	2700	0.0100	0.0007
OSU-cup 3	2700	0.0367	0.0017
Average		0.0214	0.0016

Figures II-1a and II-1b. Total fluxes for the three sampling periods at Sites H and M. Calculated yearly average fluxes, as well as fluxes from traps which collected a bulk sample for the deployment period, are shown. Bottom at Site H is 3575 m. Bottom at Site M is 3080 m.

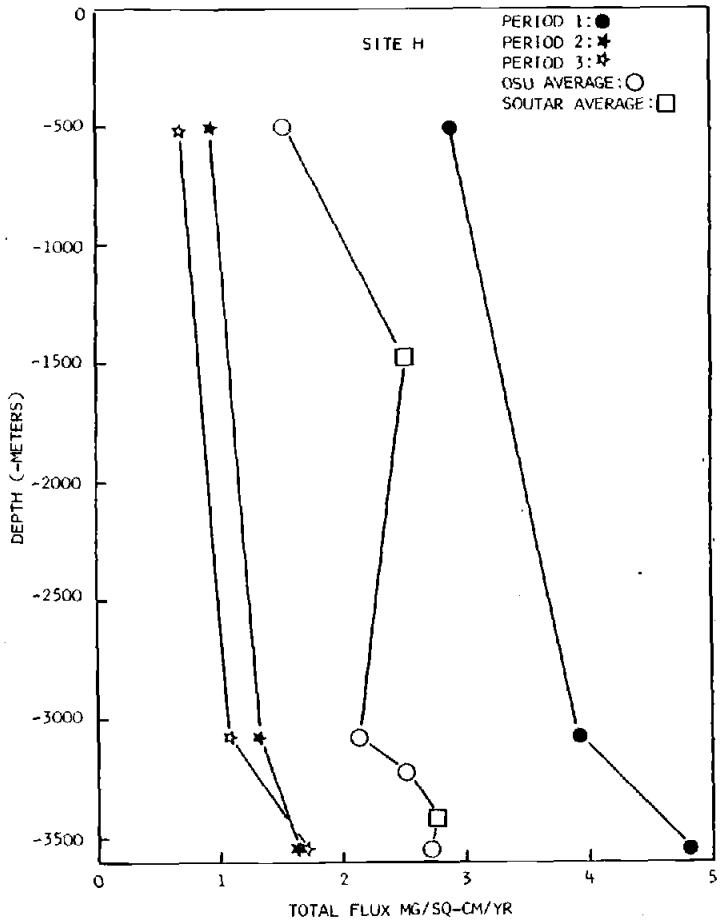

Figure II-1a

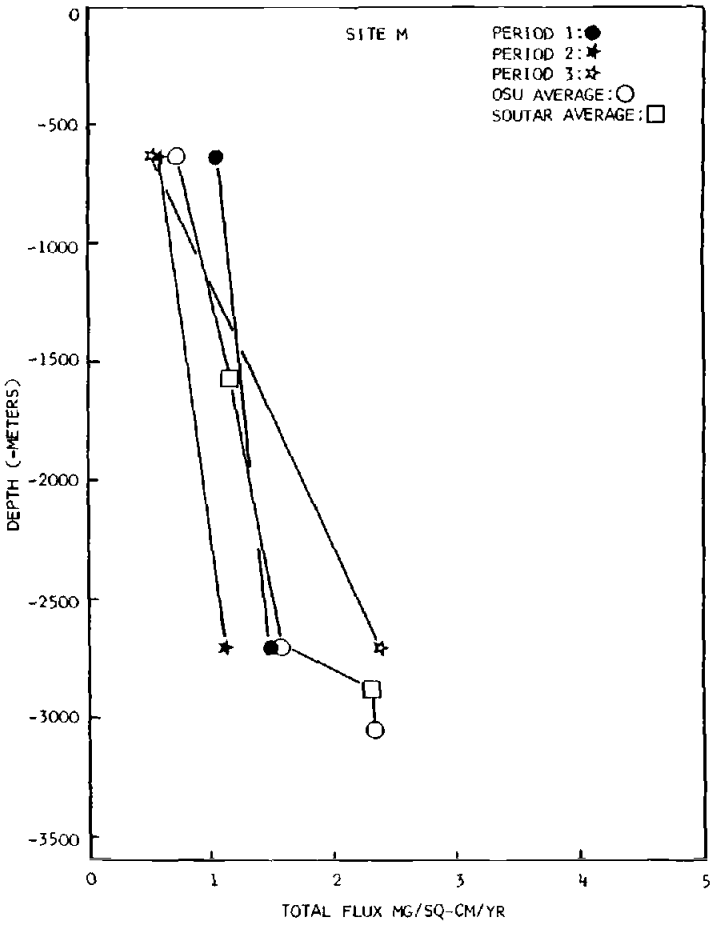

Figure II-1b

Figures II-2a and II-2b. $CaCO_3$ fluxes for the three sampling periods at Sites H and M. Calculated yearly average fluxes, as well as fluxes from traps which collected a bulk sample for the deployment period, are shown. Bottom at Site H is 3575 m. Bottom at Site M is 3080 m.

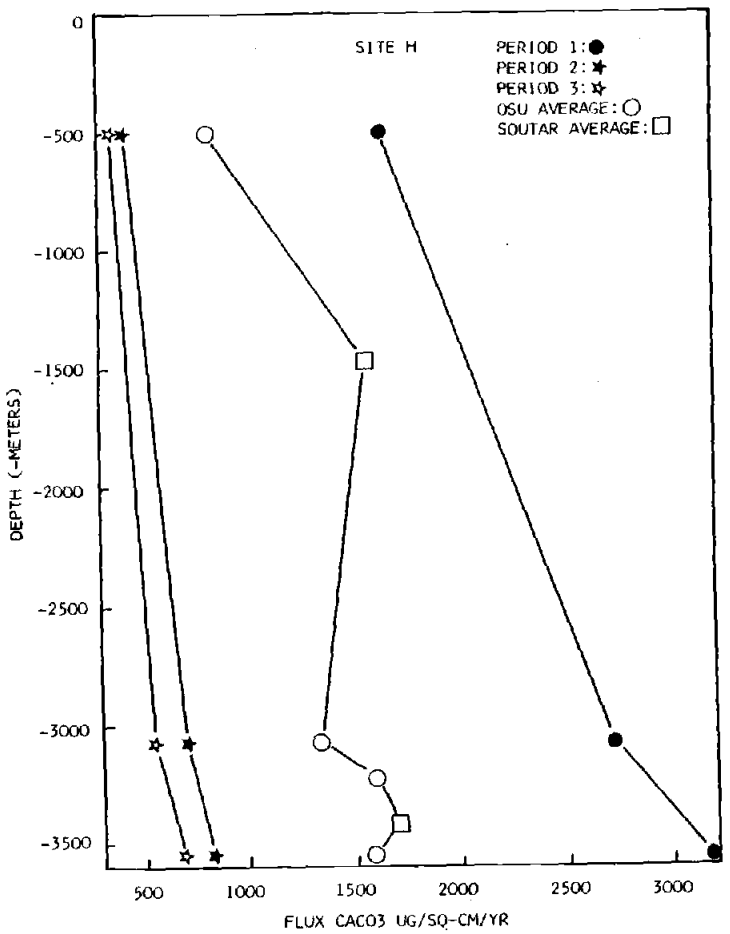

Figure II-2a

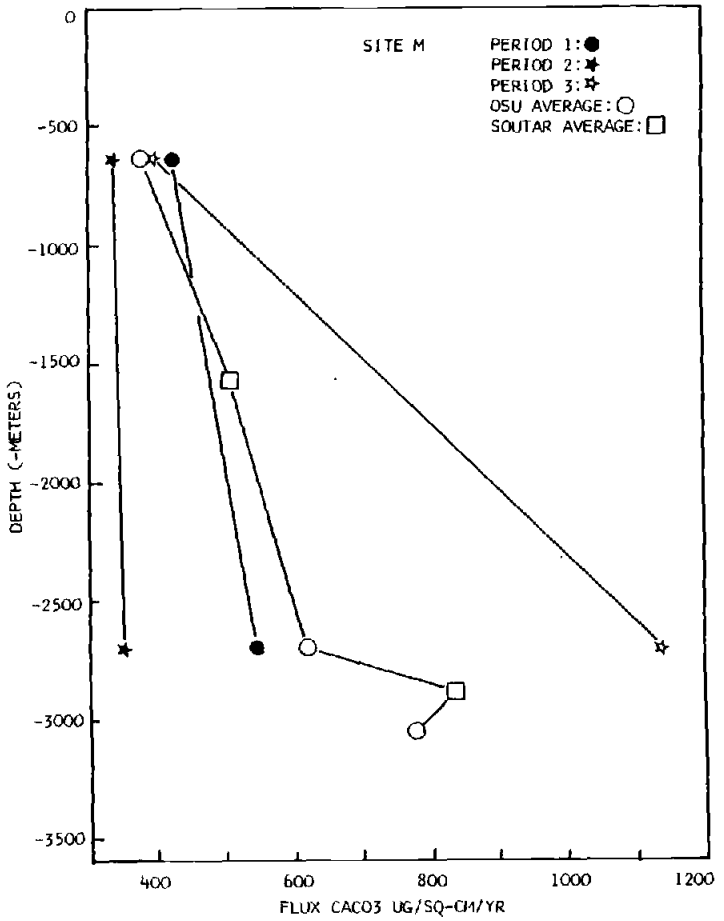

Figure II-2b

Figures II-3a and II-3b. Opal fluxes for the three sampling periods at Sites H and M. Calculated yearly average fluxes, as well as fluxes from traps which collected a bulk sample for the deployment period, are shown. Bottom at Site H is 3575 m. Bottom at Site M is 3080 m.

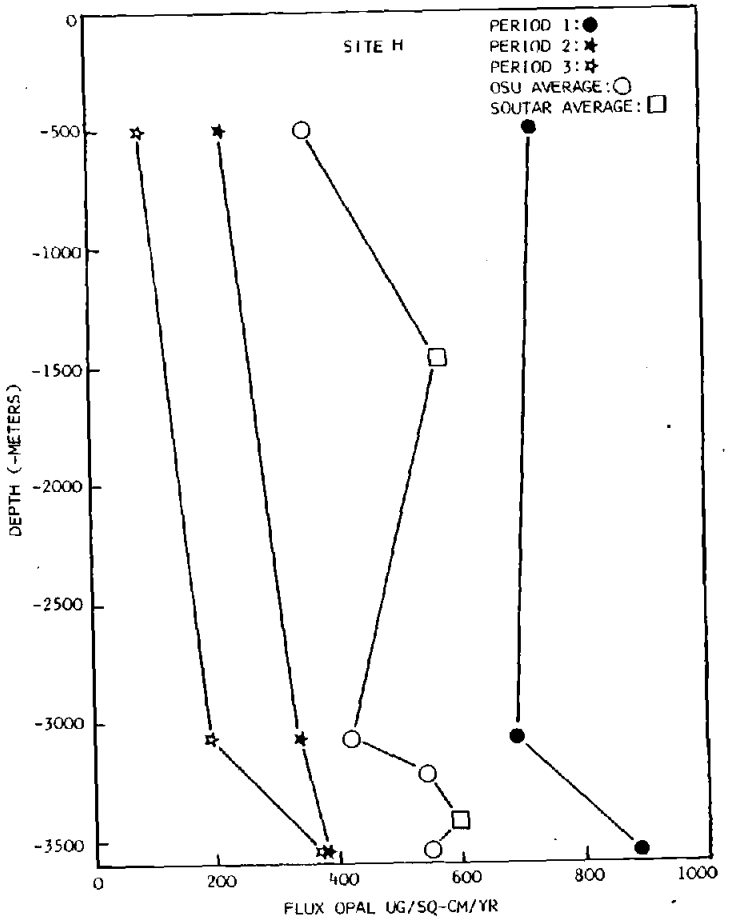

Figure II-3a

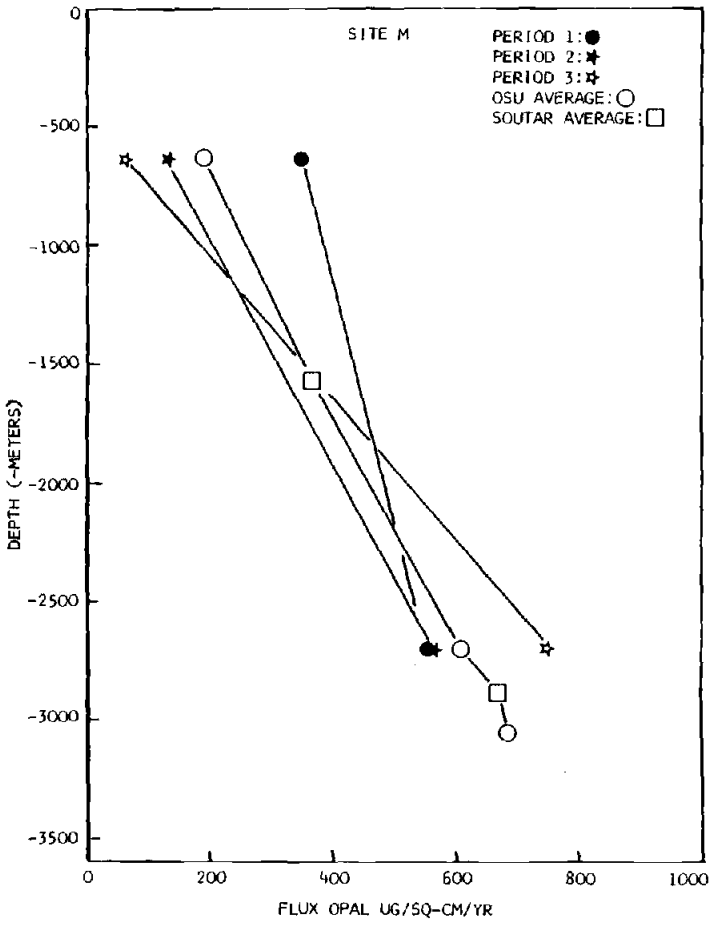

Figure II-3b

Figures II-4a and II-4b. Organic carbon fluxes for the three sampling periods at H and M. Calculated yearly average fluxes, as well as fluxes from traps which collected a bulk sample for the deployment period, are shown. Bottom at Site H is 3575 m. Bottom at Site M is 3080 m.

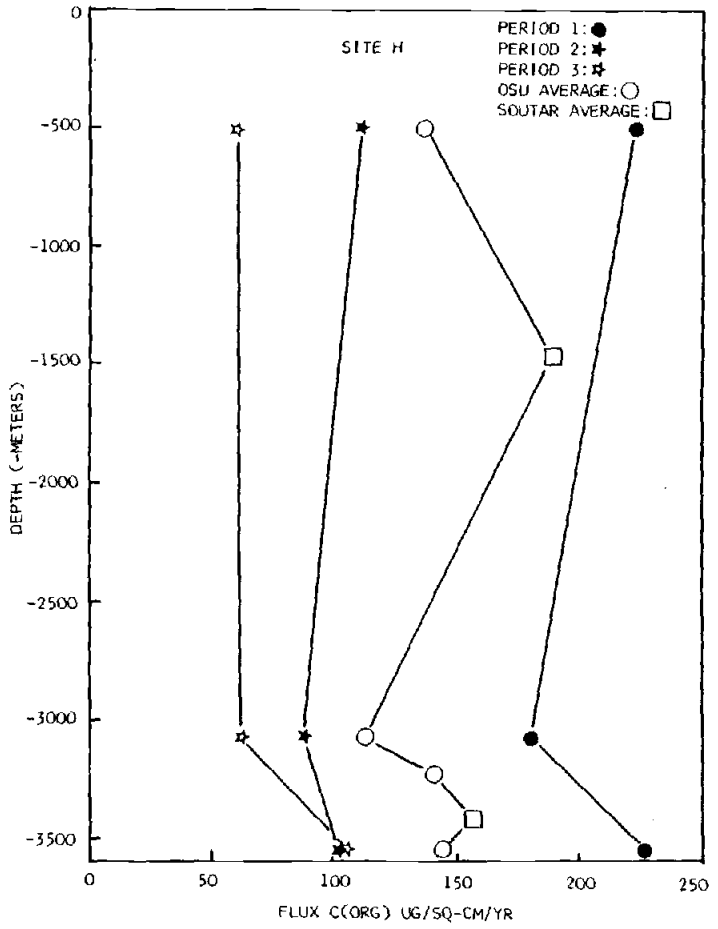

Figure II-4a

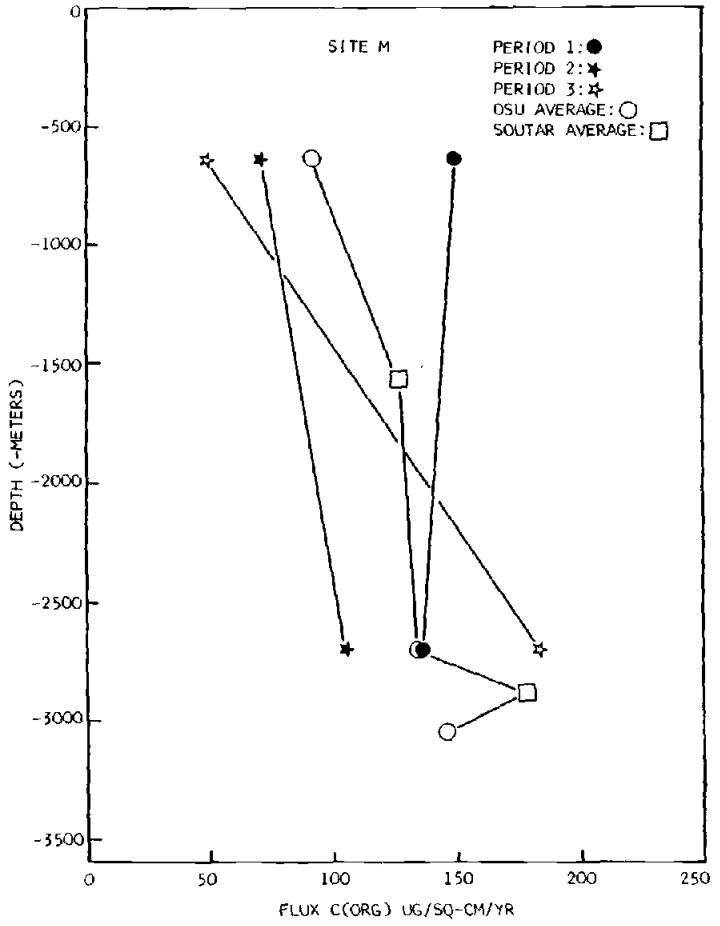

Figure II-4b

Figures II-5a and II-5b. Aluminum fluxes for the three sampling periods at Sites H and M. Calculated yearly average fluxes, as well as fluxes from traps which collected a bulk sample for the deployment period, are shown. Bottom at Site H is 3575 m. Bottom at Site M is 3080 m.

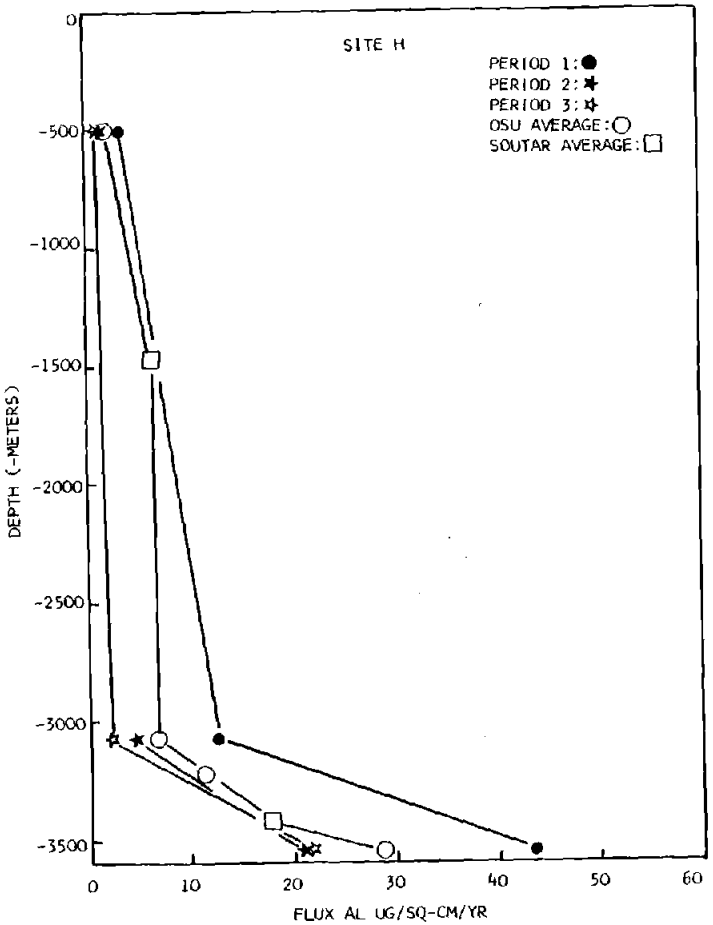

Figure II-5a

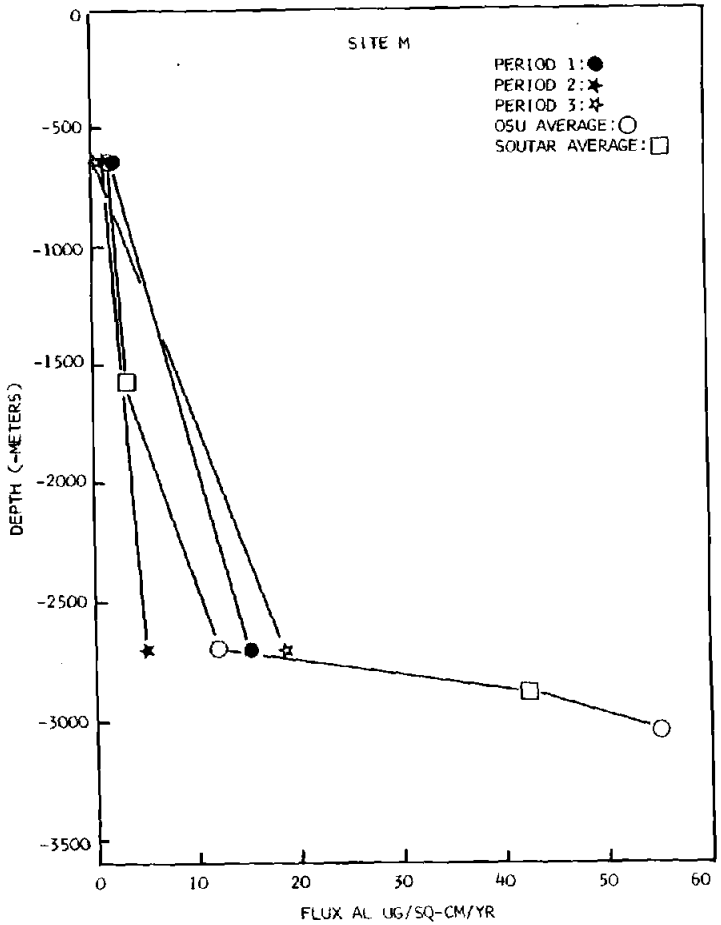

Figure II-5b

Figures II-6a and II-6b. Manganese fluxes for the three sampling periods at Sites H and M. Calculated yearly average fluxes, as well as fluxes from traps which collected a bulk sample for the deployment period, are shown. Bottom at Site H is 3575 m. Bottom at Site M is 3080 m.

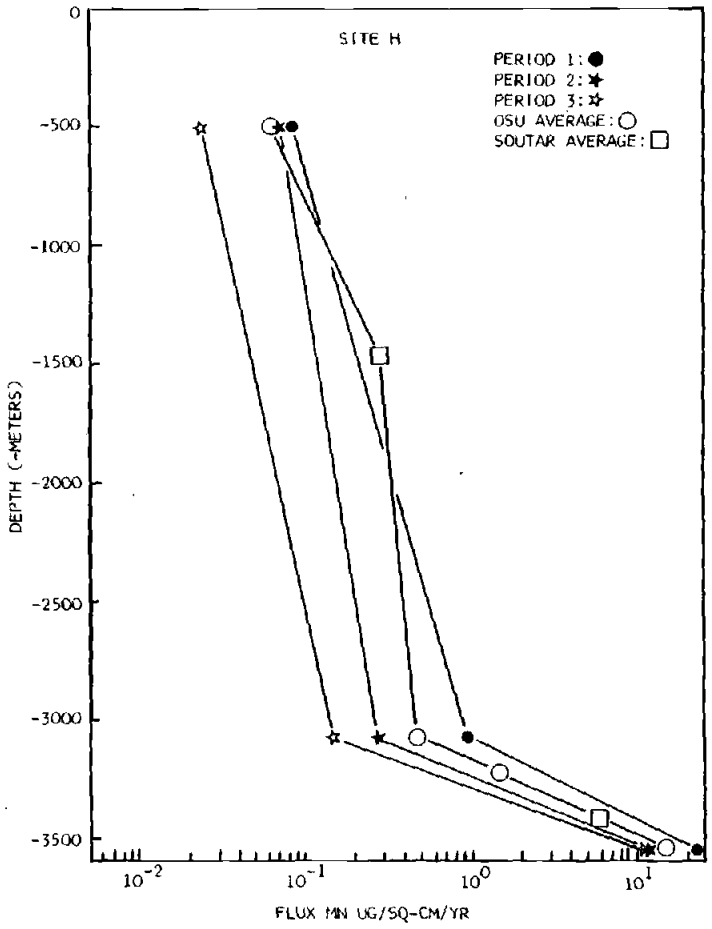

Figure II-6a

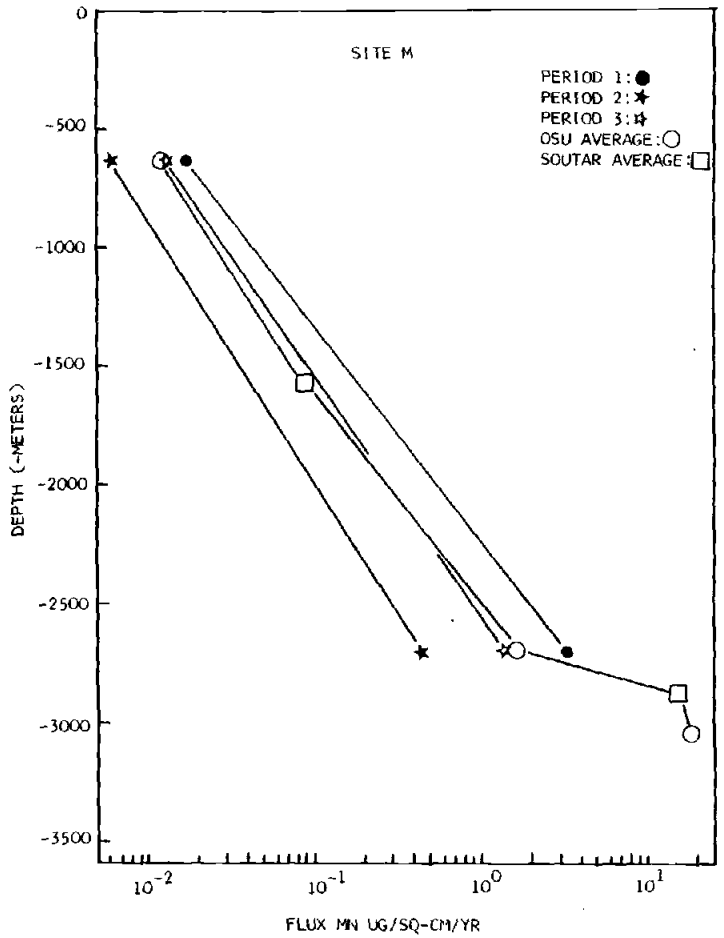

Figure II-6b

changes in phytoplankton communities over the year, with less opal-producing species occuring during period 3 (Matherne and Fischer, 1982).

The flux ratios between periods decrease in the lowest traps (Table II-5), particularly for elements enriched in the sediments (Al, Ti, Th, Sc, Ba, Mn, Fe, Cu, Co). The damping of the seasonal signal is most likely the result of resuspended input to the lowest trap which varies less over the year than the seasonal fluxes. If Al is used as a measure of resuspended flux, comparison of the 3075 m trap flux (assume no resuspended flux) and the 3545 m trap flux (3075 m flux plus resuspended flux) shows that resuspension during period 1 is twice the resuspension during periods 2 and 3. This difference does not appear to be related to current activity. Bottom currents at Site H range from 0.8 to 10 cm/sec, with a mean of 3.05 cm/sec (See Appendix 1). Currents during period 3 are slightly greater in velocity and are more persistent in direction than during the other two periods. The apparent increase in resuspension during period 1 must be linked to the greater flux during period 1. This may happen either through an actual increase in resuspension or through increased scavenging of resuspended material due to the increased biogenic flux. In the case of increased resuspension, fresh material, before it has been worked into the sediment, would be easier to resuspend than more consolidated sediment. Increased flux may also

Table II-5. Flux ratios between sampling periods at Sites H and M. Cup number is the same as sampling period.

Site H

Depth, m	Cup/Cup	Total	CaCO3	Si-total	Opal	C-org	N	P-org	P-inorg
505	1/2	3.1	3.9	3.3	3.3	2.0	1.8	2.4	1.7
3075	1/2	3.0	3.9	2.1	2.0	2.1	1.9	2.6	2.0
3545	1/2	3.0	3.9	2.3	2.4	2.2	1.8	1.9	2.8
505	1/3	4.3	4.5	7.9	8.3	3.7	3.2	4.0	3.2
3075	1/3	3.7	4.9	3.8	3.6	2.9	2.4	3.2	3.6
3545	1/3	3.1	4.6	2.3	2.4	2.2	1.6	1.6	1.9

Site M

Depth, m	Cup/Cup	Total	CaCO3	Si-total	Opal	C-org	N	P-org	P-inorg
635	1/2	1.8	1.3	2.6	2.6	2.1	2.5	2.2	0.7
2700	1/2	1.3	1.6	1.1	1.0	1.3	1.4	1.2	2.6
635	1/3	2.1	1.1	5.1	5.4	3.1	3.4	2.5	1.3
2700	1/3	0.6	0.5	0.8	0.7	0.7	0.7	0.9	0.6

Table II-5, continued. Flux ratios between sampling periods at Sites H and M. Cup number is the same as sampling period.

Site H

Depth, m	Cup/Cup	d-SiO2	Al	Ti	Th	Sc	U	Ca	Mg	Br
505	1/2	2.3	2.3	6.9	2.9	2.7	3.1	3.8	2.6	2.3
3075	1/2	2.8	2.8	4.0	3.7	2.8	2.1	3.8	1.9	1.8
3545	1/2	2.1	2.1	1.9	4.4	2.3	2.5	3.7	2.1	2.0
505	1/3	3.6	3.6	19.2	5.3	4.3	3.4	4.7	1.6	2.1
3075	1/3	5.8	5.8	4.0	5.9	4.1	3.6	4.8	0.9	1.2
3545	1/3	2.0	2.0	1.7	3.5	2.1	3.2	4.2	1.3	1.3

Site M

Depth, m	Cup/Cup	d-SiO2	Al	Ti	Th	Sc	U	Ca	Mg	Br
635	1/2	2.1	2.1	1.0	3.8	2.2	1.8	1.3	1.6	2.1
2700	1/2	3.0	3.0	2.8	3.8	2.6	0.9	1.6	1.5	1.3
635	1/3	2.5	2.5	0.7	2.9	2.1	2.6	1.2	0.6	1.1
2700	1/3	0.8	0.8	0.7	0.9	0.8	0.7	0.5	0.7	0.6

Table II-5, continued. Flux ratios between sampling periods at Sites H and M. Cup number is the same as sampling period.

Site H

Depth, m	Cup/Cup	Ba	Sr	Pb	Mn	Fe	Cu	Co	Ni	Zn
505	1/2	3.2	4.5	2.9	1.2	1.9	3.2	2.7	2.1	1.2
3075	1/2	2.7	4.3	2.0	3.4	2.5	2.7	2.3	2.4	1.5
3545	1/2	2.6	4.0	1.8	2.1	2.3	2.3	1.8	2.3	1.7
505	1/3	6.3	6.1	1.6	3.6	3.2	5.2	4.4	3.5	0.7
3075	1/3	4.6	6.2	1.6	6.5	3.9	4.4	3.4	3.6	0.9
3545	1/3	2.4	4.6	0.7	2.2	2.1	2.3	1.2	2.5	1.1

Site M

Depth, m	Cup/Cup	Ba	Sr	Pb	Mn	Fe	Cu	Co	Ni	Zn
635	1/2	3.4	1.7	1.1	2.8	2.1	2.4	3.7	4.7	2.0
2700	1/2	2.6	1.5	3.5	7.4	3.3	2.1	2.8	2.0	2.8
635	1/3	2.7	1.6	1.0	1.3	1.9	1.8	1.2	1.6	2.2
2700	1/3	0.8	0.6	-	2.4	0.7	0.7	0.4	0.4	0.9

Table II-5, continued. Flux ratios between sampling periods at Sites H and M. Cup number is the same as sampling period.

Site H

Depth, m	Cup/Cup	Cr	Cd
505	1/2	1.7	3.0
3075	1/2	2.7	2.0
3545	1/2	2.8	2.6
505	1/3	3.4	9.6
3075	1/3	2.4	3.4
3545	1/3	2.1	4.1

Site M

Depth, M	Cup/Cup	Cr	Cd
635	1/2	1.8	1.6
2700	1/2	2.4	3.7
635	1/3	1.1	26.0
2700	1/3	0.6	1.5

result in increased biological activity and bioturbation, which might increase the resuspension of sediments. Camera observations of the sediment surface have recorded the appearance and resuspension of pulses of material originating from surface waters (Billett et al., 1983).

Alternatively, or possibly in addition to increased resuspension, the greater Al flux during period 1 may arise via increased scavenging during times of high flux. Organic carbon to aluminum ratios are reasonably constant over the course of the year, although the ratios vary with depth, as can be seen in Table 4. Increase in aluminosilicate flux with increase in carbon flux has been reported (Deuser et al., 1981; Honjo, 1982), and has been best explained by the incorporation of aluminosilicate particles into fecal pellets or marine snow (Deuser et al., 1981; Honjo, 1982). The Al/C-org over a more than two year period ranged from 0.1 - 0.2 for a single trap 1000 m above bottom in the Sargasso Sea (taken from figures, Deuser et al., 1981). For our traps, Al/C-org also did not vary with season, but did change with depth. This ratio is 0.015 at 505 m, 0.03 - 0.07 at 1465 m, and 0.2 at 3545 m. The lithogenic/C-org ratio in the Panama Basin also varied with depth (Honjo, 1982), ranging from 0.6 - 2.6 at 890 m, 2.9 - 6.0 at 2590 m, and 5.2 - 10.0 at 3560 m (300 m above bottom). The changes with depth of this ratio in the Panama Basin was attributed to a greater standing stock of aluminosilicates at depth due to resuspension from the slope.

Increased scavenging would occur during times of high biological production. Karl and Knauer (1983) measured increasing particulate Al in traps as suspended Al concentrations increased. These increases occurred steadily from ~100 m to 1000 m, and then decreased slowly below 1000 m to the deepest data point at 2000 m. The mooring location for their study was 100 km northeast of Point Sur, considerably closer to land than our site. Although we do not have data for the concentration of suspended particulates for Site H, near-bottom increases in the Al/C-org ratio may be due to increased Al concentration from resuspension. The Al/C-org ratio at any depth would be a function of particulate Al concentration and biogenic flux. Unless a substantial animal population is present to provide packaging into fecal pellets, marine snow would seem a more likely particle type to provide increased scavenging of Al particles via agglutination.

Table II-6 lists the seasonal ratios for the biogenic components. C/N ratios vary between 6.0 - 8.7 at Site H, with some indication of an increase with depth. Karl and Knauer (1983) found constant to increasing C/N trap ratios between 100 m and 1100 m, with a range of 6 - 12. Below 1100 m, the ratio decreased to ~7. Their fecal pellet counts indicate that the region 600 m to 1100 m is a region of increased animal activity, with different animals present at slightly different depths. In addition, particulate carbon and nitrogen fluxes increase at the

Table II-6. Biogenic ratios for seasonal traps at each site. Ratios are molar. The molecular weight for opal is assumed to be 73.3 (van Bennekom and van der Gaast, 1976). C refers to organic carbon, N to total nitrogen, and P to organic phosphorus.

Site H:

Depth,m	Period	C/N	C/P	CaCO3/C	Opal/C	CaCO3/Opal
505	1	7.3	300.	0.88	0.52	1.7
	2	6.5	370.	0.45	0.31	1.4
	3	6.4	330.	0.71	0.23	3.0
3075	1	7.0	370.	1.8	0.61	2.9
	2	6.6	470.	0.96	0.61	1.5
	3	6.0	420.	1.1	0.49	2.1
3545	1	8.7	430.	1.7	0.63	2.6
	2	7.1	370.	0.97	0.60	1.6
	3	6.4	310.	0.79	0.57	1.3

Site M:

Depth,m	Period	C/N	C/P	CaCO3/C	Opal/C	CaCO3/Opal
635	1	7.6	460.	0.34	0.37	0.89
	2	8.8	480.	0.58	0.30	1.9
	3	8.5	380.	0.97	0.21	4.56
2700	1	7.6	390.	0.48	0.65	0.72
	2	7.9	340.	0.41	0.86	0.46
	3	7.5	460.	0.75	0.65	1.1

900 m level, associated with increased microbial growth. They have proposed that this region within or just below the oxygen minimum zone at their site is the location of intense metabolic activity.

At Site H, the C/N ratios are greatest during period 1, the time of high flux, and lowest during period 3, the time of lowest flux, at all three depths. The reason for this may be that, during times of high production, N becomes depleted in the surface waters, resulting in a higher higher C/N ratio. Sufficient N is available, however, to maintain production. C/P ratio shows no consistent trends with season or depth. Generally, the values fall within the range 300-400, which is consistent with values reported by Knauer et al., 1979 for open ocean and nonupwelling coastal locations.

Period 1 is the time of high CaCO3/C at all three levels. This ratio is much reduced during the remainder of the year, particularly at the two lower depths. The CaCO3/C is 0.71 during period 3 in the top trap, which almost equals the ratio found during period 1. Peaks in primary productivity were measured during off-seasons (Owen and Zeitzschel, 1970) and bloom were recored in a trapping experiment in the Panama Basin (Honjo, 1982).

Opal/C is highest during period 1 in the top trap, and the differences between sampling periods decrease with depth. Opal flux increases with depth during

periods 2 and 3 in the lower traps, but the reason for this is uncertain.

CaCO3/opal is greatest during period 1 as well for the two lower traps, but period 3 shows the greatest value of this ratio in the top trap, possibly due to a bloom of carbonate-producing species. These ratios demonstrate the dominance of carbonate production at Site H compared to opal throughout the year.

Seasonal Flux Data - Site M

The time of maximum flux at Site M occurs during the first sampling period at 635 m, and during period 3 at 2700 m. The reasons for this are not apparent. This maximum in flux at the 2700 m level occurs for all the biogenic components, which implies a surface source. Yet periods 2 and 3 are substantially lower than period 1. Either the peak in flux during period 3 in the 2700 m trap was produced during period 1, and consequently took almost a year to transit 2000 m of water, which is contradictory to the results at Site H, or lateral transport of material is occuring from adjacent waters. Only Mn and Cd do not show peak fluxes during period 3 at 2700 m.

Flux ratios between seasons (Table 5) show that period 1 is a factor of 1-3 greater than period 2 for most components at the two trap levels. The ratios of period 1 to period 3 fluxes are greater than 1 at 635 m and less than 1 at 2700 m as a consequence of the high fluxes during period 3 at 2700 m. Mn and Cd are the exceptions to this statement.

The biogenic ratios (Table II-6) at Site M show rather constant C/N and C/P with depth and season. Period 3 at both trap depths is the time of high CaCO3/C. High CaCO3/opal is also seen during period 3 at both depths.

Effects of Seasonal Variations on the Sediments

If 2-4 times the organic carbon is passed to the bottom during one season relative to another, it may be speculated that decomposition of this material will result in significant reduction of the surface sediments. This would be the case if bioturbation is unable to process the pulse of material rapidly enough to dilute the input organic carbon. Benthos may respond to the pulse with higher activity, and animal reproductive cyles may be keyed to seasons of high food input (see Billett et al., 1983 for brief review). Bioturbation rates at Sites H and M have been estimated (J. Kirk Cochran, pers. comm.), and are a factor of 10 higher at Site H than at M. Whether such a difference can result in substantial surface chemistry changes is not known through direct measurement; however, modelling may help assess the effects of these differences. A recent analysis of sediment and porewater data (Emerson et al., 1983) using a model involving bioturbation rates and decomposition rates of organic carbon indicates that all of the organic carbon input to Sites M and H is decomposed at depth in the sediments. If this modelling accurately reflects the conditions in the bottom sediments, then the high flux of material may be worked into the sediments before substantial organic decomposition occurs. Whether the same is true for the dissolution of carbonate and opal at these two sites is

unknown. Reduced forms of Mn have been found in the surface sediments at both sites (Kalhorn and Emerson, 1983), but whether this is linked to periods of high productivity is still speculation.

Conclusions

The major conclusion from the second chapter is that a strong seasonal signal exists at both sites, and this seasonality is reflected in all elements. Comparisons of average flux values to the flux values obtained during the season of highest flux indicate that consideration of average values alone may not present an adequate picture of the possible diagenetic processes which may be occuring at the sediment surface.

CHAPTER 3

SOURCES AND PROCESSES CONTROLLING FLUXES AT SITES M AND H

Abstract

Using linear programming, four models are constructed which partition sediment trap flux data from the eastern tropical Pacific Ocean into contributions from sources with distinct compositions. These source materials, called end members, suggest the origin of the collected material and the oceanic processes involved in transporting them. The trap data span the water column from ~500 m depth to 30 m above bottom at two sites: MANOP Site H at 6°30'N, 93° N, and Site M at 9°N, 104° W. Compositions of end members were taken from the literature or from within the data set. The elements used to define the trap and end member compositions are: organic-C, organic-P, inorganic-P, N, Al, Si, Ca, Ti, Mn, Fe, Co, Ni, Cu, Zn, and Ba.

In the first model, the trap fluxes were partitioned into the following six end members: calcareous material, opal, organic matter, aluminosilicate detritus, hydrothermal precipitates, and authigenic/adsorbed matter. At Site H, >98% of the flux at each level in the water column could be accounted for by a combination of these six end members. According to this partitioning, at Site H the detrital and authigenic/adsorbed fluxes increased in the lower 350 m both by more than a factor of three. Since these two factors are enriched in the surface sediments relative to the traps, the model suggests local resuspension or lateral

reworking are important sources to the near-bottom traps. Hydrothermal input was not necessary to account for the measured fluxes, and less than 1% hydrothermal material is found in surface sediments at Site H.

At Site M, >96% of the flux can be explained by this model. At this site, the detrital and authigenic fluxes in the lower 300 m increased by a factor of 5. Hydrothermal precipitate contributed to the fluxes of the lower traps, increasing by a factor of 6 in the bottom 300 m. These three components are enriched in the surface sediments at M.

A second model in which the lower trap fluxes were partitioned into two end members, vertical flux (input from the upper water column) and resuspended surface sediments, was developed to quantify the resuspension effects. Combination of these two components can account for >99% of the fluxes in the near-bottom region at Site H and >94% of these fluxes at Site M. Resuspended surface sediments contribute ~10% of the flux 30 m above bottom at H and ~40% at M. The resuspended flux 160 m above bottom at Site H accounts for 3% of the total flux. At Site M, the resuspended flux 197 m above bottom is ~30% of the total flux. Resuspension of surface sediments in these amounts can supply the near-bottom increases in detrital, authigenic/adsorbed, and hydrothermal fluxes found by the first model.

The results of this and other modelling using linear programming suggest that the near-bottom flux data are significantly influenced by resuspension of surface sediments at these two sites, with greater resuspension occuring at Site M. Bottom currents at both sites were similar, ~3 cm/sec. The greater degree of resuspension seen at M may be due to greater relief at that site.

Introduction

Recent sediment trap data have shown flux increases with depth for various elements (Honjo et al., 1982c; Spencer, 1981b; Karl and Knauer, 1983; Martin and Knauer, 1982; Gardner et al., 1982b, 1982c). These increases have been attributed to resuspension of slope and bottom sediments and to the action of bacteria. Although it has not previously been demonstrated with sediment trap data, analyses of bottom sediments indicate hydrothermal precipitates from active spreading centers are transported at least 1000 km from their source (Heath and Dymond, 1977; Dymond, 1981). Thus, sediment trap flux data from a given level in the water column may include not only the input from surface waters, but also additional input from the slope, bottom sediments, and hydrothermal activity.

Partitioning of the measured flux into inputs from from various sources is useful for estimating the true flux to bottom sediments. Local resuspension would not be included as new flux to the bottom sediments, since this process recycles previously input material. Comparison of the true flux to the bottom to the accumulation rate in the sediments indicates whether elements are preserved in the sediments, recycled back into the bottom waters, or require some additional source of flux not collected by the trap from which the flux to bottom was taken. Additionally, a greater understanding of the

processes occuring in the water column and near-bottom region may be gained from examining changes in flux with depth.

Linear programming (normative analysis) has been used successfully to partition deep sea sediments into contributions from various sources (Dymond and Eklund, 1978; Dymond, 1981). In the following study, this technique is used to estimate the inputs from various sources to sediment traps deployed at two sites in the eastern tropical Pacific Ocean.

Description of Linear Programming

In linear programming, the composition of any sample is partitioned into contributions from various sources, called end members. The compositions of these end members must be known or estimated. Linear programming calculates the fraction of each end member which best accounts for the measured sample composition. This calculation involves the simultaneous solution of a system of n equations, where n is the number of variables used to define the composition. These variables may be the percentages of elements or minerals in a sample or any other measurable way of specifying a composition. As for any solution to a system of linear equations, the number of composition variables must equal or exceed the number of end members. In the following discussion, elements are used as the composition variables, since all linear programming runs presented in this paper were based on elemental compositions. An example of an equation for a particular sample using aluminum as one of the compostion variables is given below:

% Al-sample = % Al-1 x a + % Al-2 x b + ... + % Al-m x z

In the above equation, % Al-1 through % Al-m represent the percentages of Al in the m end members, and the letters a through z stand for the fractions of the end members which are the unknowns to be determined. Similar equations (one for each element) are written, and this system of equations is simultaneously solved for that particular sample.

A weighting factor for a each element is calculated and then multiplied by the equation for that element. The system of equations is then solved for the best solution as described below. Weighting factors are used to prevent elements with high concentration from dominating the solution. The weighting factors for runs presented in this paper are calculated from the average composition for the data set by the following equation, written for Al as an example:

weighting factor for Al = avg % M-sample/ avg % Al-sample

where M represents the element with the highest concentration. In this study, a maximum weighting factor was used in some cases to limit the affect on the solution of trace elements with chemistries that are poorly understood.

Since a perfect fit of the sample composition by the mixing of end member compositions is seldom obtained, an infinite number of solutions can be generated with varying degrees of fit to the sample composition. This closeness of fit is found by calculating the percent residual for each element:

%residual = % estimated by linear programming - % measured.

In the linear programming runs covered in this paper, the best solution is taken to be the solution which minimizes the sum of the absolute values of the residuals for all elements considered.

Evaluation of the solution may be done in several ways. The method chosen in this paper is to define the

"% accounted for". This is an estimate of the percent of total flux which can be explained by the model. It is calculated by dividing the sum of the absolute values of the percent residuals (as defined above) by the sum of all concentrations input to the model and multiplying by 100:

$$\%\ \text{accounted for} = \left(\text{sum}|\%\text{res}| \ /\ \text{sum of concentrations}\right) \times 100.$$

In deciding how well a model accounts for a particular element, the percent overestimated (>100%) or underestimated (100%) is used, calculated in the following way:

$$\%\ \text{over/underestimated} = 100 \times (\text{estimated}\ \% \ /\ \text{measured}\ \%)$$

One of the limitations to the applicability of a linear programming run to the real world may be the choice of end members and their compositions. The choice of weighting factors is also an important consideration in setting up a run, and affects the solution obtained.

End Member Compositions

Table III-1 gives the compositions of six end members used in linear programming runs 1 and 2 described below. The 15 elements are the major components of the end member compositions. The end members may be described as source-related. At Sites M and H, calcareous matter, opal, and organic matter originate from biogenic material from the upper water column. Detrital silicates have an upper-water column source associated with biological particles and originating most likely from wind-transported continental debris (Rea, 1982). Detrital silicates may also have a near-bottom source, i.e. resuspension and down-slope movement. Hydrothermal precipitates are transported from the East Pacific Rise, and authigenic/adsorbed material originates from resuspended bottom sediments or by sorption of elements onto particles as they settle through the water column. The hydrothermal, detrital, and authigenic components of the sediments may be resuspended in the near-bottom zone, and this resuspension input may provide some of these fractions in near-bottom traps. Table III-1 also lists the references for and describes these six end members.

In Table III-1, the end member compositions using these same 15 elements are given for runs 3 and 4. The models on which these runs are based will be described below.

Table III-1. Compositions of end members used in linear programming Runs 1, 2, 3, and 4.

Compositions of six source-related end members used in linear programming Runs 1 and 2. Compositions are given as % by weight.

Element	calc	opal	orgm	detr	hdth	auth
C-organic	0	0	40.	0	0	0
P-organic	0	0	0.28	0	0	0
P-inorganic	0.03	0	0	0.1	0	0
N	0	0	6.6	0	0	0
Al	0	0.72	0	8.4	0.21	1.17
Si	0	36.	0	25.2	4.52	4.93
Ca	40.	0	0	5	0	2.5
Ti	0	0	0	0.6	0	0.49
Mn	0.01	0.00083	0	0.134	10.1	21.7
Fe	0.001	0.036	0	5.9	34.8	18.3
Co	0	0	0	0.005	0	0.12
Ni	0.001	0.0014	0	0.013	0.031	0.52
Cu	0.01	0.0018	0	0.01	0.146	0.063
Zn	0.002	0.0029	0	0.012	0.066	0.076
Ba	0.020	0.072	0	0.100	0.174	0.138

Table III-1, continued. Description of end members for linear programming Runs 1 and 2.

calc: Calcareous shell material, either aragonite or calcite, from Dymond, 1981.

opal: Opaline shell material, from Dymond, 1981.

orgm: Organic matter, a C/N molar ratio of 7 and a N/P molar ratio of ~50 were assumed from trap compositional data. This member may contain trace metals which have not been included in the above composition.

detr: Detrital silicates, most probably wind-transported in the upper traps, and a combination of wind-blown input from above and resuspended material from the bottom sediments in the lowest traps. The composition is from Dymond, 1981.

hdth: Hydrothermal precipitate, emanating from the rise crest and transported by currents. May also be the resuspended hydrothermal component of bottom sediments. Composition from Dymond, 1981.

auth: Authigenic/adsorbed component, a precipitate formed as crusts directly from seawater, though elemental ratios indicate that detrital particles may be incorporated into these crusts. The compostion is taken from measurements of crusts dredged from Sites M and H (Dymond et al., 1983; K. Murphy, unpublished). In the case of traps above the zone of resuspension, contribution to the collected material from this source may occur by sorption from the water column.

Table III-1, continued. Compositions as % by weight for end members used in linear programming Runs 3 and 4. Hydrothermal composition is from Table III-1, preceding page.

element	vertical flux H- 3075 trap	vertical flux M- 1565 trap	resuspended flux H- 0-2 cm seds.	resuspended flux M- 0-2 cm seds.
C-org	5.29	10.41	0.86	1.46
P-org	0.034	0.091	0.020	0.046
P-inorg	0.027	0.033	0.127	0.159
N	0.94	1.58	0.135	0.207
Al	0.24	0.22	6.04	5.28
Si	8.65	12.93	24.3	20.2
Ca	23.5	17.8	1.51	7.35
Ti	0.034	0.037	0.41	0.39
Mn	0.023	0.0076	5.4	1.79
Fe	0.18	0.16	5.1	7.6
Co	0.00034	0.0007	0.0085	0.0048
Ni	0.0023	0.0036	0.109	0.0316
Cu	0.0051	0.0039	0.063	0.0259
Zn	0.0137	0.019	0.063	0.0368
Ba	0.159	0.165	1.03	0.59

Sample Compositions and Weighting Factors

Table III-2 lists the weighting factors used in all four runs.

Table III-3 presents the sample compositions which are partitioned in the various runs. For runs 1, 3, and 4, these are yearly average trap compositions at the indicated depths at Sites H and M. Table III-3 gives the excess flux compositions for the lower three traps at each site. These compositions are calculated as the difference between the measured trap flux at the indicated depth and the assigned vertical flux, taken as the 3075 m trap at Site H and the 1565 m trap at Site M. The vertical flux may be thought of as the flux from the upper water column, with no contributions from hydrothermal or resuspended material. The 1565 m trap at M and the 3075 m trap at H were selected, as discussed below.

Table III-2. Weighting factors for samples partitioned in linear programming runs.

Weighting factors for samples partitioned in linear programming Runs 1, 3, and 4.

Element	H traps	M traps	H sediments	M sediments
C-org	3.3	1.9	28.	14.
P-org	460.	260.	1000.	440.
P-inorg	390.	250.	190.	130.
N	20.	13.	180.	97.
Al	52.	24.	4.	3.8
Si	2.3	1.2	1.	1.
Ca	1.	1.	16.	2.7
Ti	660.	330.	59.	52.
Mn	130.	88.	4.5	11.
Fe	65.	20.	4.8	2.7
Co	1000.	1000.	1000.	1000.
Ni	1000.	1000.	220.	640.
Cu	1000.	1000.	390.	780.
Zn	1000.	1000.	390.	550.
Ba	130.	91.	24.	34.

Table III-2, continued. Weighting factors for samples partitioned in linear programming Run 2.

Element	H excess flux (= flux - flux,3075m)	M excess flux (= flux - flux,1565m)
C-org	3.6	8.5
P-org	610.	800.
P-inorg	660.	460.
N	77.	47.
Al	18.	9.
Si	1.6	1.
Ca	1.1	2.4
Ti	280.	220.
Mn	59.	34.
Fe	23.	6.9
Co	1000.	1000.
Ni	640.	890.
Cu	760.	770.
Zn	820.	900.
Ba	54.	68.

Table III-3. Compositions of traps and excess fluxes at Sites H and M.

Sediment trap compositions as % by weight at Site H.

Element	505m	1465m	3075m	3225m	3415m	3545m
C-org	9.77	6.46	5.29	5.89	5.67	5.09
P-org	0.069	0.056	0.034	0.034	0.040	0.036
P-inorg	0.129	0.032	0.027	0.028	0.027	0.048
N	1.51	1.07	0.94	0.88	0.79	0.81
Al	0.107	0.221	0.238	0.353	0.543	0.930
Si	9.26	9.34	8.65	9.44	10.11	11.0
Ca	21.5	24.8	23.5	24.7	22.7	21.8
Ti	0.0255	0.0231	0.0336	0.0474	0.0429	0.0410
Mn	0.00402	0.0112	0.0230	0.0570	0.207	0.545
Fe	0.0562	0.133	0.176	0.263	0.421	0.845
Co	0.000133	0.000512	0.000342	0.000697	0.00252	0.00174
Ni	0.00139	0.00377	0.00229	0.00743	0.00918	0.0173
Cu	0.00206	0.00283	0.00508	0.00723	0.00988	0.0135
Zn	0.0201	0.00619	0.0137	0.0159	0.00865	0.0201
Ba	0.0922	0.140	0.159	0.195	0.219	0.268

For 0-2 cm sediment composition, see Table III-1, resuspended flux, Site H.

Table III-3, continued. Sediment trap compositions as % by weight from Site M.

Element	635m	1565m	2700m	2883m	3050m
C-org	12.4	10.4	8.27	7.40	6.51
P-org	0.0757	0.0909	0.0566	0.0695	0.0488
P-inorg	0.152	0.0330	0.0326	0.0531	0.0684
N	1.84	1.58	1.31	1.05	0.911
Al	0.125	0.221	0.661	1.63	2.23
Si	10.6	12.9	17.1	16.1	18.0
Ca	20.3	17.8	15.9	14.2	13.4
Ti	0.0153	0.0374	0.0473	0.0741	0.163
Mn	0.0014	0.0076	0.106	0.642	0.771
Fe	0.0848	0.157	0.760	2.14	2.90
Co	0.000137	0.000679	0.000851	0.00411	0.00312
Ni	0.00227	0.00357	0.00666	0.0162	0.0130
Cu	0.00244	0.00387	0.00880	0.0134	0.0275
Zn	0.0443	0.0186	0.0202	0.0212	0.0221
Ba	0.118	0.165	0.192	0.260	0.352

For 0-2 cm sediment composition, see Table III-1, resuspended flux, Site M.

Table III-3, continued. Composition as % by weight of excess flux partitioned in Run 2. Excess flux is equal to the measured flux less the assigned vertical flux which is taken from the 3075 m trap at Site H and the 1565 m trap at Site M.

Element	H: 3225m	3415m	3545m	M: 2700m	2883m	3050m
C-org	8.70	6.96	4.43	2.20	4.55	2.75
P-org	0.030	0.058	0.039	0.	0.049	0.008
P-inorg	0.030	0.025	0.120	0.032	0.073	0.103
N	0.435	0.290	0.328	0.732	0.579	0.330
Al	0.88	1.47	3.28	1.91	2.99	4.18
Si	13.3	14.6	19.0	28.5	19.1	22.9
Ca	30.0	20.0	15.6	9.8	10.9	9.17
Ti	0.11	0.07	0.07	0.07	0.11	0.28
Mn	0.21	0.77	2.33	0.39	1.25	1.51
Fe	0.66	1.17	3.13	2.46	4.04	5.56
Co	0.0024	0.0091	0.0066	0.0012	0.0074	0.0055
Ni	0.0309	0.0300	0.0688	0.0154	0.0283	0.022
Cu	0.0170	0.0245	0.042	0.0227	0.0226	0.0503
Zn	0.026	0.	0.042	0.0241	0.0236	0.0255
Ba	0.361	0.403	0.643	0.268	0.351	0.534

Experimental Description

Trap deployments were part of the Manganese Nodule Project (MANOP) and were located at Site H at 6°32'N, 92°50'W and at Site M at 8°50'N, 104°W. Traps were deployed at Site H at depths of 505 m, 1465 m, 3075 m, 3225 m, 3415 m, and 3545 m (30 m above bottom). At Site M, traps were deployed at 635 m, 1565 m, 2700 m, 2883 m, and 3050 m (30 m above bottom). Two types of traps were used: the OSU single-cone trap and the double-cone Soutar trap (located at 1465 m and 3415 m at H, and 1565m and 2883 m at M). Both traps were constructed of fiberglass with minimal usage of metal parts. The Soutar trap contained buffered formalin as a bactericide. Sodium azide was used in the OSU trap to reduce bacterial activity. Further descriptions of traps and moorings, as well as Sites H and M, can be found in Chapter 1.

Partitioning into Major Source Components - Run 1

The purpose of this model is to separate the trap and surface sediment compositions into fundamental components. The average trap compositions at all depths and the top layer of sediments are partitioned into the six end members: calcareous material, opal, organic matter, aluminosilicate detritus, hydrothermal precipitate, and authigenic/adsorbed matter.

Table III-4 gives the results of Run 1. These results are displayed in Figures III-1a and III-1b. At Site H, the fluxes of the calcareous, opal, and detrital fractions approximately double from the 505 m trap to the 1465 m trap. These increases, as discussed in Chapter 1, are most likely due to the lateral movement of waters which contain a greater abundance of settling particles, as might be produced in regions with greater overlying productivity. Alternatively, biological effects, such as particle repackaging or vertical movement of nekton, could cause increased particle flux with depth (Honjo, 1980; Karl and Knauer, 1983). Because of the presence of a oxygen minimum between 350-450 m at Site H and 100-600 m at Site M, reduced animal activity is expected in the top trap at each site. Increased animal activity, with possible flux enhancement due to repackaging of slowly settling particles might be expected at the trap below the oxygen minimum, i.e. ~1500 m. However, this repackaging must be matched by an input of particles. If this is not the case, the repackaging organisms will

Table III-4. Compositional and flux results from the partitioning of traps and sediments into six end members - Run 1.
Results for Site H.

trap	%calc	%opal	%orgm	%detr	%hdth	%auth	%accounted for
505m	51.5	24.0	23.5	1.0	0.	0.	99.2
1465m	59.0	23.2	15.5	2.3	0.	0.	99.0
3075m	60.5	23.0	13.7	2.7	0.	0.1	99.4
3225m	59.9	22.9	13.1	3.9	0.	0.2	98.1
3415m	55.5	23.5	14.1	6.1	0.	0.9	98.9
3545m	53.0	25.4	12.6	6.5	0.	2.4	98.4
0-2cm sed.	0.	54.1	2.3	21.4	0.6	21.7	91.3

Results of Partitioning as flux, in mg/sq-cm/yr: (assumes all flux accounted for)

	calc	opal	orgm	detr	hdth	auth
505m	0.79	0.37	0.36	0.02	0.	0.
1465m	1.50	0.59	0.39	0.06	0.	0.
3075m	1.26	0.48	0.29	0.06	0.	0.01
3225m	1.53	0.58	0.33	0.10	0.	0.01
3415m	1.54	0.65	0.39	0.17	0.	0.02
3545m	1.43	0.69	0.34	0.18	0.	0.07
0-2cm sed.	0.	0.057	0.003	0.023	0.006	0.023

Table III-4, continued. Results of linear programming Run 1 for Site H. Fraction overestimated (>1) or underestimated (<1) by model is listed.

element	trap: 505m	1465m	3075m	3225m	3415m	3545m	surface sed.
C-org	1.00	1.00	1.00	0.90	1.00	1.00	1.00
P-org	0.99	0.81	1.08	1.11	0.99	1.00	0.30
P-inorg	0.13	0.66	0.74	0.80	0.86	0.47	0.16
N	1.07	1.00	0.93	1.00	1.19	1.04	1.05
Al	1.00	1.00	1.00	1.00	1.00	0.64	0.32
Si	1.00	1.00	1.00	1.00	1.00	1.00	1.00
Ca	1.00	1.00	1.00	1.00	1.00	1.00	1.00
Ti	0.25	0.63	0.48	0.53	0.96	1.25	0.54
Mn	1.75	1.00	1.00	1.00	1.00	1.00	0.83
Fe	1.28	1.15	1.00	1.07	1.27	1.00	1.00
Co	1.00	0.20	0.67	0.57	0.56	1.94	2.99
Ni	0.71	0.34	0.70	0.34	0.68	0.84	1.00
Cu	0.52	0.46	0.25	0.22	0.22	0.24	0.26
Zn	0.09	0.35	0.16	0.16	0.37	0.22	0.31
Ba	0.32	0.23	0.19	0.17	0.16	0.15	0.08

Table III-4, continued. Results of linear programming Run 1 for Site M.

trap	%calc	%opal	%orgm	%detr	%hdth	%auth	% accounted for
635m	46.7	26.4	25.7	1.2	0.	0.	96.6
1565m	41.4	32.0	24.3	2.3	0.	0.	99.2
2700m	35.3	38.3	18.4	7.2	0.7	0.1	99.0
2883m	31.4	29.5	17.6	17.9	1.8	1.8	98.9
3050m	27.9	29.1	15.0	23.5	2.7	1.9	98.8
0-2cm sed.	10.4	10.9	3.6	61.9	9.2	3.9	83.0

Results of Partitioning as flux, in mg/sq-cm/yr: (assumes all flux accounted for)

trap	calc	opal	orgm	detr	hdth	auth
635m	0.34	0.20	0.19	0.01	0.	0.
1565m	0.48	0.37	0.28	0.03	0.	0.
2700m	0.55	0.60	0.29	0.11	0.01	0.01
2883m	0.73	0.68	0.41	0.42	0.04	0.04
3050m	0.66	0.69	0.35	0.55	0.06	0.04
0-2 cm sed.	0.021	0.022	0.007	0.126	0.025	0.004

Table III-4, continued. Results of linear programming Run 1 for Site M. Fraction overestimated (>1) or underestimated (<1) by model is listed.

element	trap: 635m	1565m	2700m	2883m	3050m	surface sed.
C-org	0.90	1.00	0.98	1.00	1.00	1.00
P-org	1.03	0.80	1.00	0.75	0.93	0.22
P-inorg	0.11	0.48	0.60	0.54	0.51	0.41
N	1.00	1.09	1.02	1.16	1.18	1.16
Al	1.01	1.04	1.05	1.00	0.98	1.00
Si	1.00	1.00	1.00	1.00	1.00	1.00
Ca	1.00	1.00	1.00	1.00	1.00	1.00
Ti	0.49	0.39	1.00	1.65	1.00	1.00
Mn	5.00	1.05	1.00	1.00	1.00	1.05
Fe	1.00	1.00	1.00	1.00	1.00	1.00
Co	1.00	0.14	0.56	0.80	1.19	1.63
Ni	0.49	0.33	0.37	0.86	1.19	1.00
Cu	0.46	0.33	0.35	0.51	0.32	0.87
Zn	0.05	0.12	0.17	0.31	0.36	0.46
Ba	0.27	0.22	0.25	0.21	0.18	0.16

Figures III-1a and III-1b. Results of Run 1 - Partitioning of trap fluxes into six end members. The flux of each end member is plotted versus depth at each site. Bottom at H is 3575 m. Bottom at M is 3080 m.

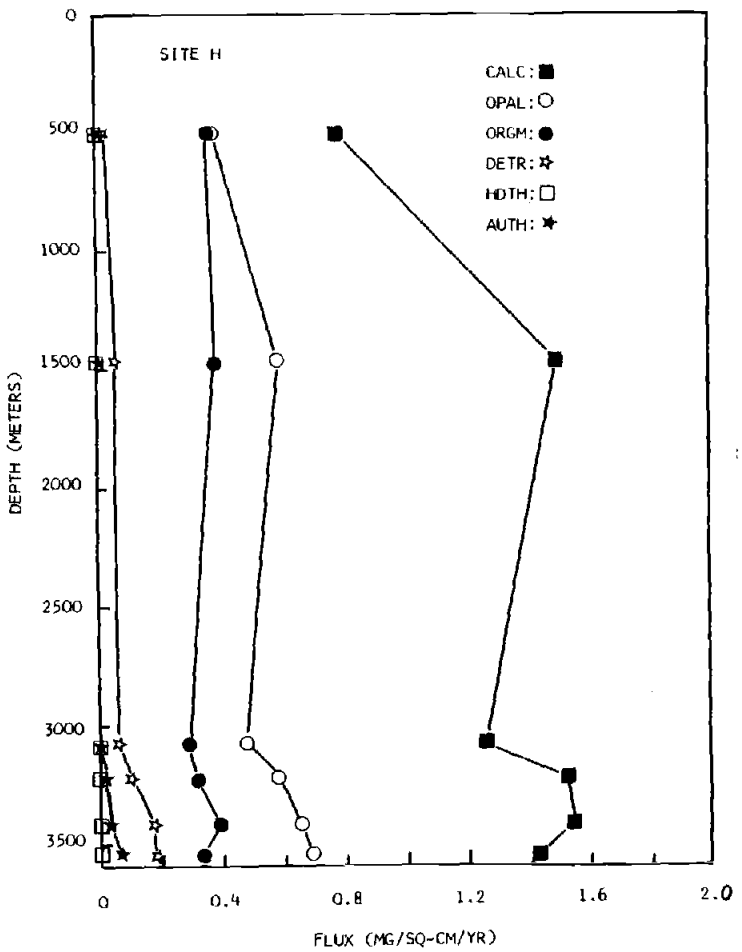

Figure III-1a

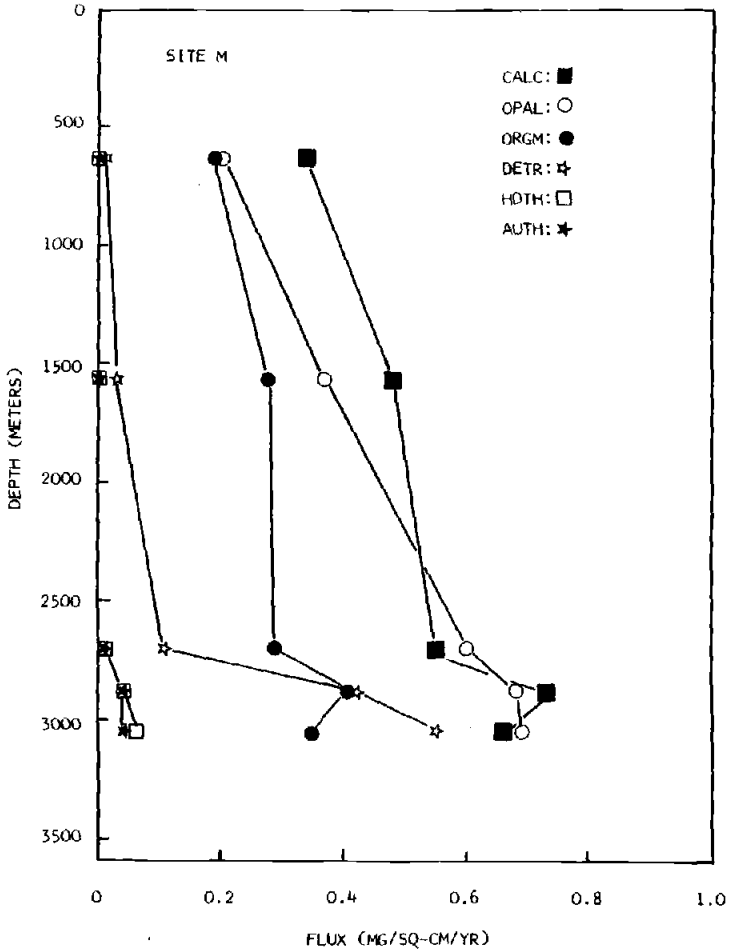

Figure III-1b

deplete the particle standing stock, shutting off this mode of input. Since current speeds are not markedly different from the ~500 m level to the ~1500 m at each site (see Appendix I), marked differences in collection efficiency are not likely from the 500 m level to the 1500 m level. Near-bottom comparisons of the Soutar and OSU traps (see Chapter 1) also rule out these differences as due to the collection efficiency of each trap.

The biogenic fluxes decrease by approximately 20% from the 1465 m trap to the trap at 3075 m at Site H. The 3075 m trap is 500 m above bottom and should be outside the zone of resuspension. Whether a decrease in biogenics similar to that at Site H would be observed at M in a trap located 500 m above bottom is not known. The 2700 m trap at Site M is 380 m above bottom, and may collect some resuspended material.

The detrital flux at H remains constant from the 1465 m level to the 3075 m level, while authigenic/adsorbed and hydrothermal fluxes are low or nonexistent in the three shallowest traps. Consequently, the 3075 m trap was selected as representing the vertical flux. The increases in biogenic fluxes in the lower three traps at Site H, however, are puzzling. Since there is no reason to suspect that the 3075 m trap has undertrapped biogenic components, the increased biogenic flux in the lower 350 m at H is believed to be due to resuspension of relatively fresh material (Walsh et al., 1983). This may occur at Site M as well.

A striking result of this model is that the opal, detrital silicates, and authigenic material, which are components enriched in the sediments, are found in increasing quantities in the traps as the bottom is approached. Hydrothermal material is not necessary to account for the compositions of the Site H traps. This component is found in small quantities (<1%) in the sediments. The fit of the trap data to these end members is good, with >98% of the flux accounted for in each trap. The sediment data does not fit as well. At Site M, sediments are very rich in detrital silicates (62%) with high authigenic and hydrothermal compositions relative to the traps. The lower three traps at Site M are enriched in these components. Greater than 96% of the flux for all traps can be accounted for by a combination of these end members.

Table III-5 compares analytically determined fractions, such as carbonate, to the percentages of these components found through linear programming. Descriptions of analytical techniques and precisions, and the equation by which opal is calculated, can be found in Chapter 1. In most cases, the linear programming results compare well with the measured carbonate and organic carbon. The two methods for estimating opal rest upon a common assumption: that the Si/Al of detritus is known for the material being studied. The linear programming method uses additional elementary ratios in constraining the amount of opal estimated.

Table III-5. Comparison of analytically determined biogenic components versus linear programming results.

Carbonate results.

Site	Depth	%CaCO3 measured	%CaCO3 from LP	LP/measured
H	505m	53.0	51.5	.97
	1465m	61.4	59.0	.96
	3075m	64.1	60.5	.94
	3225m	62.4	59.9	.96
	3415m	61.2	55.5	.91
	3545m	58.5	53.0	.91
M	635m	52.9	46.7	.88
	1565m	43.7	41.4	.95
	2700m	39.4	35.3	.90
	2883m	35.2	31.4	.89
	3050m	32.9	27.9	.85

Table III-5, continued. Comparison of % opal calculated from equation * versus % opal determined by linear programming.

Site	Depth	%Opal *	%Opal from LP	LP/*
H	505m	23.1	24.0	1.04
	1465m	22.4	23.2	1.04
	3075m	20.1	23.0	1.14
	3225m	21.2	22.9	1.08
	3415m	21.4	23.5	1.10
	3545m	20.4	25.4	1.25
M	635m	26.1	26.4	1.01
	1565m	31.6	32.0	1.01
	2700m	38.7	38.3	.99
	2883m	28.2	29.5	1.05
	3050m	28.9	29.1	1.01

*calculated from measured Al concentration by the following equation: Opal = 2.61 x (Si - 3 x Al). This assumes that the ratio of Si/Al bound in detrital aluminosilicates is 3. The factor of 2.61 is the ratio of the molecular weights of opal to Si (van Bennekom and van der Gaast, 1976).

Table III-5, continued. Comparison of analytically determined % CH_2O versus % CH_2O determined by linear programming.

Site	Depth	%CH2O (measured C-org)	%orgm from LP	LP/measured
H	505m	22.2	23.5	1.06
	1465m	18.6	15.5	.83
	3075m	13.4	13.7	1.02
	3225m	13.8	13.1	.95
	3415m	14.1	14.1	1.00
	3545m	13.3	12.6	.95
M	635m	31.7	25.7	.81
	1565m	27.4	24.3	.89
	2700m	21.5	18.4	.86
	2883m	18.8	17.6	.94
	3050m	15.4	15.0	.97

Partitioning of Excess Flux - Run 2

In this model, the primary flux from the upper water column is assigned using a trap sufficiently above the bottom so that there is little hydrothermal or resuspended input. The results of run 1 indicate that resuspension/ hydrothermal input are contributing to the lower 350 m at each site. Consequently, for Site H the 3075 m trap was chosen to estimate the primary flux. The Al flux of this trap almost equals the Al accumulation rate in the sediments, which suggests that this trap collects the true flux to the bottom. At Site M, the 2700 m trap, which is 350 m above bottom, had an Al flux approximately the same as that in the sediments, suggesting that it may provide a good estimate of the primary flux. However, according to run 1, the 2700 m trap has both hydrothermal and authigenic (most likely from resuspension) components. Site M also has more topographic relief (+/- 100 m locally, and the rise crest 25 km to the west), higher current speeds, and increased detrital flux between 1500 m and the 2700 m trap. For these reasons the 1565 m trap data was selected as the primary flux. At both sites, the primary flux of each of the 15 elements was subtracted from the elemental fluxes measured deeper in the water column. The net flux, refered to as the excess flux at each depth, is the flux unexplained by input from above. Changes in the primary flux with depth due to carbonate and opal dissolution or organic carbon decomposition in the

bottom waters have not been made. Changes in opal, carbonate, and organic carbon fluxes due to decomposition and dissolution losses in the bottom 500 m at H are probably small. Although carbonate dissolution in the bottom waters at Site M may be minimal since this site is relatively shallow, losses due to opal dissolution and organic carbon decomposition may be significant below 1565 m.

At Site H, most of the excess flux is calcareous and opaline material, with some organic, detrital, and authigenic contributions (Table III-6, Figures III-2 and III-3). The excess flux is similar to the primary flux at 350 m above bottom, except it is relatively enriched in detrital silicates and authigenic components and depleted in organic matter. Deeper traps show even greater detrital and authigenic contributions and somewhat more opal input. The enhanced detrital-authigenic contributions are compatible with resuspension of surface sediments; however, the enhanced carbonate fluxes cannot be accounted for by this mechanism since H sediments are essentially carbonate-free. The model accounts for >86% of the flux, with organic carbon, Al, and Ba the chief components of the unaccounted fraction.

At Site M, opal and detritus are the main components of the of the excess flux, with contributions from calcareous, hydrothermal, organic, and authigenic matter (Table 6, Figure III-2 and III-3). Compositionally, the excess flux differs from the primary flux by being relatively depleted in CaCO3 and organic matter and enriched in detrital sili-

Table III-6. Compositional and flux results from the partitioning of near-bottom excess fluxes into six end members - Run 2.

Results for Site H.

trap	mab*	%calc	%opal	%orgm	%detr	%hdth	%auth	% accounted for
3225m	350	61.0	24.6	5.5	8.3	0.	0.7	88.0
3415m	160	49.0	34.1	4.4	9.1	0.	3.5	86.3
3545m	30	32.9	34.4	4.6	18.4	0.	9.7	90.3

*mab: meters above bottom

Results of partitioning above on a flux basis, in mg/sq-cm/yr:
(assumes all flux accounted for)

trap	mab	calc	opal	orgm	detr	hdth	auth
3225m	350	0.28	0.11	0.03	0.04	0.	0.01
3415m	160	0.34	0.24	0.03	0.06	0.	0.02
3545m	30	0.20	0.21	0.03	0.11	0.	0.06

Table III-6, continued. Results from Run 2 - Site H. Fraction overestimated (>1) or underestimated (<1) by model is listed.

element excess flux at:	3225m	3415m	3545m
C-org	0.30	0.25	0.45
P-org	0.62	0.21	0.36
P-inorg	1.07	0.94	0.26
N	1.00	1.00	1.00
Al	1.00	0.56	0.56
Si	1.00	1.00	1.00
Ca	1.00	1.00	1.00
Ti	0.59	1.00	2.56
Mn	1.00	1.00	1.00
Fe	1.16	1.01	1.00
Co	0.63	0.51	2.08
Ni	0.23	0.67	0.85
Cu	0.16	0.17	0.23
Zn	0.16	-	0.29
Ba	0.13	0.12	0.11

Table III-6, continued. Results of partitioning by Run 2 - Site M.

trap	mab*	%calc	%opal	%orgm	%detr	%hdth	%auth	% accounted for
2700m	380	18.7	54.7	4.7	19.1	2.7	0.2	98.5
2883m	197	21.8	26.7	10.9	33.4	3.5	3.7	98.5
3050m	30	15.7	28.3	4.6	40.9	8.3	2.2	95.1

*mab: meters above bottom

Results of partitioning on a flux basis, in mg/sq-cm/yr:
(assumes all flux accounted for)

trap	mab	calc	opal	orgm	detr	hdth	auth
2700m	380	0.08	0.22	0.02	0.08	0.01	0.01
2883m	197	0.26	0.32	0.13	0.40	0.04	0.04
3050m	30	0.19	0.32	0.06	0.49	0.10	0.03

Table III-6, continued. Results of Run 2 - Site M. Fraction overestimated (>1) or underestimated (<1) by model is listed.

element excess flux at:	2700m	2883m	3050m
C-org	1.00	1.00	0.73
P-org	-	0.65	1.87
P-inorg	0.89	0.57	0.48
N	0.50	1.30	1.00
Al	1.00	1.00	0.91
Si	1.00	1.00	1.00
Ca	1.00	1.00	1.00
Ti	1.88	2.06	1.00
Mn	1.00	1.00	1.00
Fe	1.00	1.00	1.12
Co	1.08	0.85	0.96
Ni	0.38	0.92	1.00
Cu	0.37	0.53	0.40
Zn	0.29	0.46	0.56
Ba	0.29	0.20	0.17

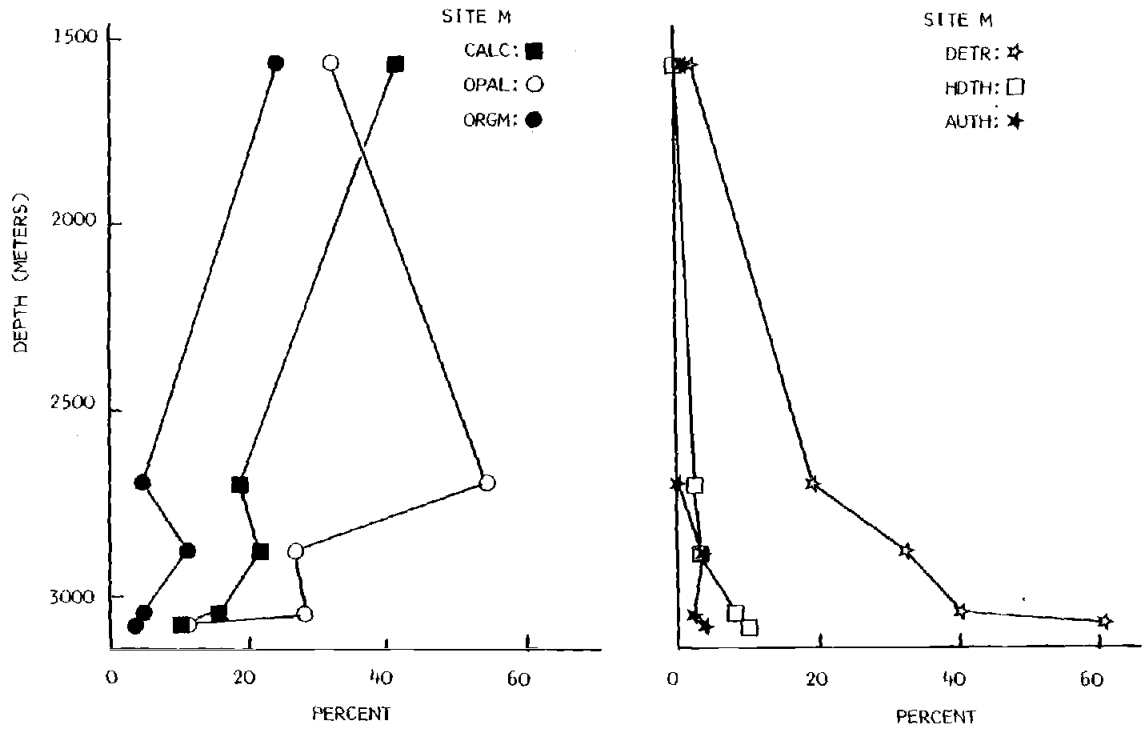

Figure III-2. Results of Run 2 - Partitioning of Site M excess near-bottom flux into six source-related end members. "Excess flux" refers to the flux in excess of an assigned vertical flux. For clarity, only three of these end members are plotted on each side of this figure. The depth axis is common to both sides of the figure. The plot is percent of end member versus depth. Bottom points are the results for the top 2 cm of sediment from Run 1.

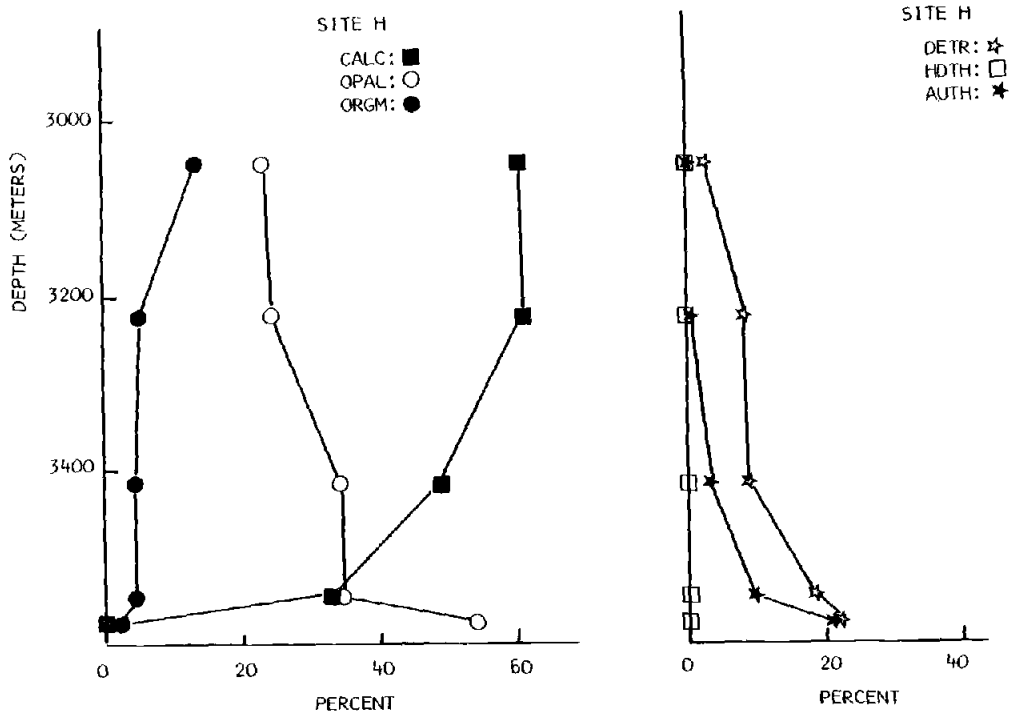

Figure III-3. Results of Run 2 - Partitioning of Site H excess near-bottom flux into six source-related end members. "Excess flux" refers to the flux in excess of an assigned vertical flux. For clarity, only three of these end members are plotted on each side of this figure. The depth axis is common to both sidesof the figure. The plot is percent of end member versus depth. Bottom points are the results for the top 2 cm of sediment from Run 1.

cates, hydrothermal precipitates, and authigenic components. This result also suggests a bottom source for the excess material; however, I will demonstrate in linear programming run 3 that resuspension alone cannot fully account for the near-bottom flux increases.

Partitioning into Primary Flux and Resuspended Flux - Run 3

In this model the sediment trap samples are partitioned into two components: vertical flux as described in run 2, and resuspended sediments defined by the composition of the top 2 cm of sediment. This model accounts for >92% of the flux at H (Table III-7, Figure III-4a) and 86% of the flux at M (Table III-7, Figure III-4b). The individual elemental fluxes are not well explained by this model.

Moreover, the model requires more primary flux in the deeper traps than is measured in either the 3075 m trap at H or the 1565 m trap at M. The flux for the 3075 m trap at H was 2.09 mg/sq-cm/yr and contrasts to the results of run 2 which call for a primary flux of ~2.5 mg/sq-cm/yr. Similarly, the flux for the 1565 m trap at M was 1.16 mg/sq-cm/yr, compared to the ~1.5 mg/sq-cm/yr primary flux needed according to run 2. These results suggest that either the flux measurements from which the vertical fluxes at each site were taken were too low, or that relatively unaltered primary flux is added to the deepest traps. These results are compatible with those of Walsh et al. (1983).

The sediment partitioning from run 1 can be combined with the results of run 3 to check if sufficient hydrothermal, authigenic, and detrital material are provided by

Table III-7. Results of partitioning lower water column traps into vertical flux and resuspended material - Run 3.

Results for Site H.

trap	mab*	% vertical flux (3075m trap)	% resuspended+	% accounted for
3225m	350	98.6	1.4	98.6
3415m	160	96.9	3.1	92.9
3545m	30	89.1	10.9	97.7

*mab: meters above bottom
+Resuspended material is 0-2 cm sediment.

Results of partitioning above on a flux basis, in mg/sq-cm/yr:
(assumes all flux is accounted for)

trap	mab*	vertical flux	resuspended flux
3225m	350	2.51	0.04
3415m	160	2.69	0.09
3545m	30	2.41	0.29

Table III-7, continued. Results of Run 3 - Site H. Fraction overestimated (>1) or underestimated (<1) by model is given.

element	trap: 3225m	3415m	3545m
C-org	0.95	1.00	1.00
P-org	1.07	0.92	0.97
P-inorg	1.08	1.24	0.84
N	1.13	1.28	1.11
Al	0.96	0.85	0.99
Si	1.00	0.99	1.00
Ca	1.00	1.11	1.03
Ti	0.88	1.17	1.93
Mn	1.79	1.00	1.18
Fe	1.00	0.87	0.89
Co	0.71	0.28	0.76
Ni	0.54	0.66	0.85
Cu	0.88	0.77	0.90
Zn	0.96	1.93	1.00
Ba	0.93	0.93	1.00

Table III-7, continued. Results of partitioning of lower water column traps at Site M into vertical flux and resuspended material - Run 3.

trap	mab*	% vertical flux (1565m trap)	% resuspended+	% accounted for
2700m	380	90.8	9.2	86.3
2883m	197	70.1	29.9	90.3
3050m	30	56.7	43.3	88.6

*mab: meters above bottom
+Resuspended material is 0-2 cm sediment.

Results of partitioning above on a flux basis, in mg/sq-cm/yr:
(assumes all flux accounted for)

trap	mab*	vertical flux	resuspended flux
2700m	380	1.43	0.14
2883m	197	1.66	0.71
3050m	30	1.34	1.02

Table III-7, continued. Results of Run 3 - Site M. Fraction overestimated (>1) or underestimated (<1) by model is given.

element	trap: 2700m	2883m	3050m
C-org	1.04	0.94	0.93
P-org	1.38	1.00	1.35
P-inorg	1.23	1.19	1.18
N	1.00	1.00	1.00
Al	0.93	0.95	1.00
Si	0.72	0.84	0.82
Ca	0.96	0.93	0.91
Ti	1.32	1.73	1.08
Mn	1.45	0.76	0.74
Fe	1.00	1.00	1.12
Co	1.11	0.41	0.45
Ni	0.84	0.66	1.12
Cu	0.60	0.70	0.45
Zn	0.92	1.03	1.12
Ba	0.96	1.01	0.92

Figures III-4a and III-4b. Results of Run 3 - Partitioning of lower trap fluxes into primary flux and resuspended flux. Flux of each end member versus depth is plotted.

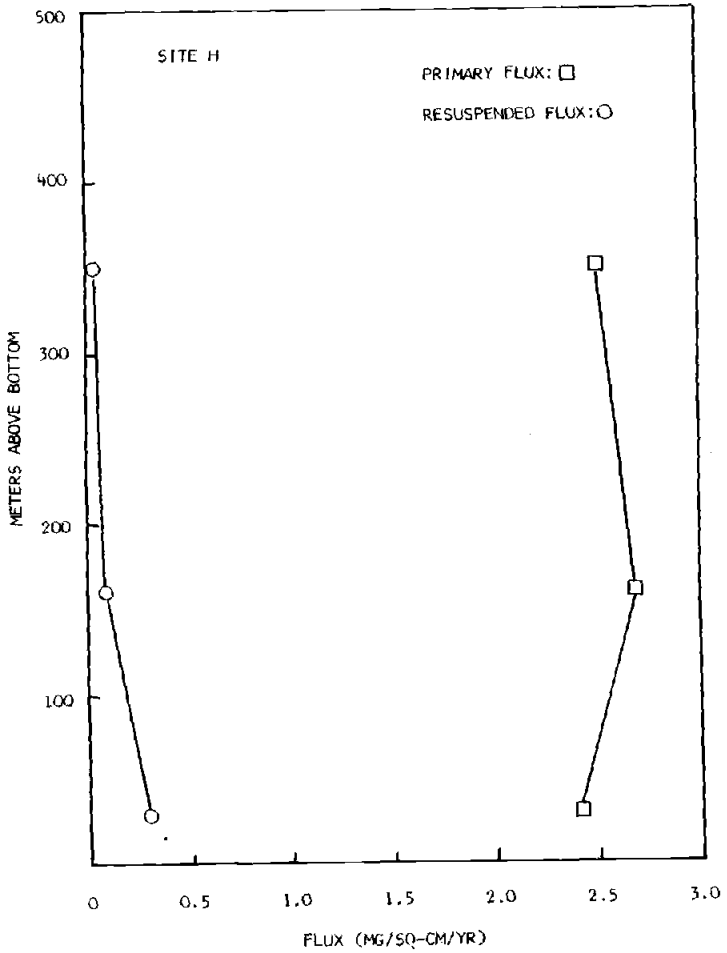

Figure III-4a

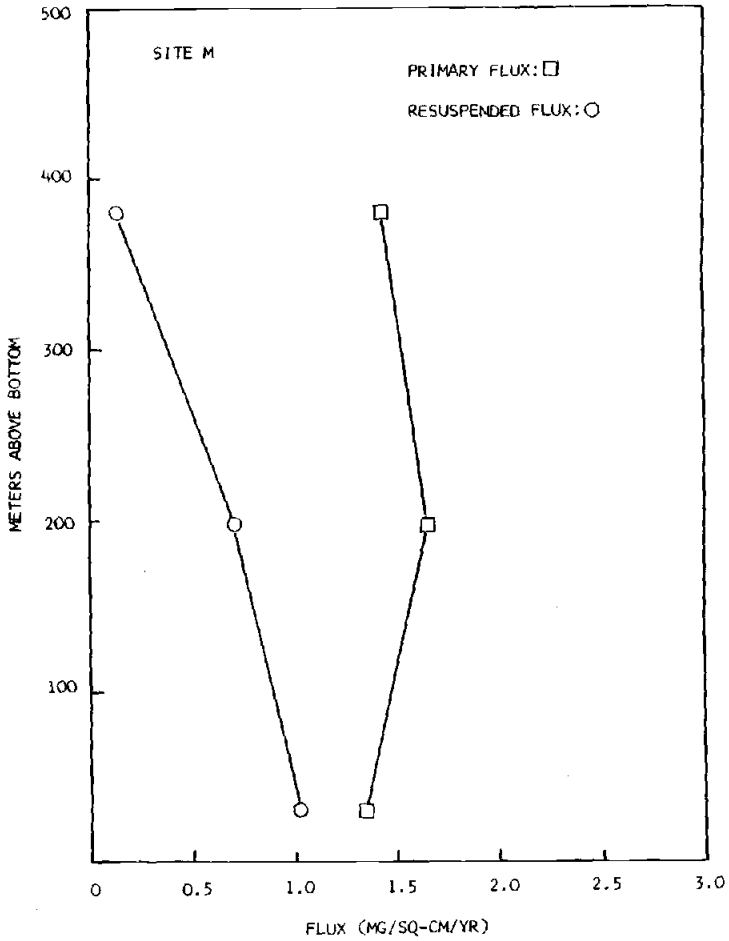

Figure III-4b

resuspension of surface sediments to match the near-bottom increases in these components seen in the traps in run 1. For example, if 1.02 mg/sq-cm/yr of unfractionated resuspended sediment is added to the 3050 m trap at Site M, and this input is 9% hydrothermal (see Table III-4), then 0.09 mg/sq-cm/yr of hydrothermal flux to the 3050 m trap can be accounted for on the basis of resuspension alone. Only 0.06 mg/sq-cm/yr is added to this trap according to run 1. This would require no input from the rise crest (at least during the time of our trap deployments). These results may suggest that the sediment is fractionated somewhat, with less hydrothermal material resuspended than detrital, for example. A similar treatment of the detrital component at Site H shows that 0.06 mg/sq-cm/yr may be due to resuspension, with an added 0.07 mg/sq-cm/yr due to primary flux input. This total, 0.13 mg/sq-cm/yr, is less than the 0.18 mg/sq-cm/yr partitioned in run 1.

Site M results show more than three time the resuspended flux of Site H. This may be due to differences in sediment type (Site M has more carbonate preservation) or the greater relief found at M, which is an area of numerous fault blocks located 25 km east of the East Pacific Rise. The bottom currents are similar at each site, ~3 cm/sec average speed (see Appendix I). The greater interaction of currents with the bottom because of the topography at M may result in more resuspension.

Partitioning into Primary Flux and Hydrothermal Flux - Run 4

In this model, the only two contributors to trap flux in the lower water column are vertical flux from above and hydrothermal input from the rise crest. Table III-8 lists the results shown in Figures III-5a and III-5b. At Site H, >76% of the flux can be accounted for by this model, and Co, Ni, and Cu are not supplied in sufficient abundance by these two sources alone. The increasing Al flux with depth in the near-bottom region also cannot be accounted for. Although this model does not completely rule out hydrothermal input at Site H, the fluxes measured appear to be predominantly the result of the combination of vertical flux and resuspended material, whether as pure bottom sediment, or a mixture of bottom sediments and freshly deposited material. The results for Site M show that >70% of the measured near-bottom fluxes can be produced by a simple combination of these two end members. Again, Al, Co, Ni, and Cu are not well explained by the model.

Table III-8. Results of partitioning lower water column traps into vertical flux and hydrothermal precipitate - Run 4.
Results for Site H.

trap	mab*	% vertical flux (3075m trap)	% hydrothermal+	% accounted for
3225m	350	99.8	0.2	95.1
3415m	160	99.5	0.5	85.4
3545m	30	98.5	1.5	76.4

*mab: meters above bottom
+Hydrothermal material composition is from Dymond, 1981.

Results of partitioning above on a flux basis, in mg/sq-cm/yr:
(assumes all flux accounted for)

trap	mab*	vertical flux	hydrothermal flux
3225m	350	2.54	0.01
3415m	160	2.77	0.01
3545m	30	2.66	0.04

Table III-8, continued. Results of Run 4 - Site H. Fraction overestimated (>1) or underestimated (<1) by model is given.

element trap:	3225m	3415m	3545m
C-org	1.00	1.09	1.25
P-org	1.12	0.99	1.15
P-inorg	1.08	1.18	0.68
N	1.19	1.39	1.40
Al	0.76	0.52	0.32
Si	1.02	1.00	0.96
Ca	1.06	1.21	1.30
Ti	0.80	0.92	1.00
Mn	0.76	0.43	0.39
Fe	1.00	1.00	1.00
Co	0.57	0.16	0.24
Ni	0.35	0.29	0.19
Cu	0.82	0.69	0.65
Zn	0.97	1.89	0.88
Ba	0.91	0.85	0.73

Table III-8, continued. Results of partitioning of lower water column traps at Site M into vertical flux and hydrothermal precipitate - Run 4.

trap	mab*	% vertical flux (1565m trap)	% hydrothermal+	% accounted for
2700m	380	98.3	1.7	80.0
2883m	197	92.7	7.3	80.6
3050m	30	91.8	8.2	68.6

*mab: meters above bottom
+Hydrothermal material composition is from Dymond, 1981.

Results of partitioning above on a flux basis, in mg/sq-cm/yr:
(assumes all flux accounted for)

trap	mab*	vertical flux	hydrothermal flux
2700m	380	2.51	0.04
2883m	197	2.58	0.20
3050m	30	2.48	0.22

Table III-8, continued. Results of Run 4 - Site M. Fraction overestimated (>1) or underestimated (<1) by model is given.

element trap:	2700m	2883m	3050m
C-org	1.25	1.12	1.44
P-org	1.59	1.04	1.66
P-inorg	1.00	0.50	0.43
N	1.19	1.20	1.54
Al	0.33	0.12	0.10
Si	0.75	0.66	0.66
Ca	1.11	1.00	1.18
Ti	0.77	0.40	0.20
Mn	1.71	1.00	1.05
Fe	1.00	1.08	1.00
Co	0.78	0.15	0.19
Ni	0.61	0.30	0.44
Cu	0.73	0.92	0.55
Zn	0.99	0.91	1.00
Ba	0.86	0.55	0.46

Figures III-5a and III-5b. Results of Run 4 - Partitioning of lower trap fluxes into primary flux and hydrothermal precipitate. Flux of each end member versus depth is plotted.

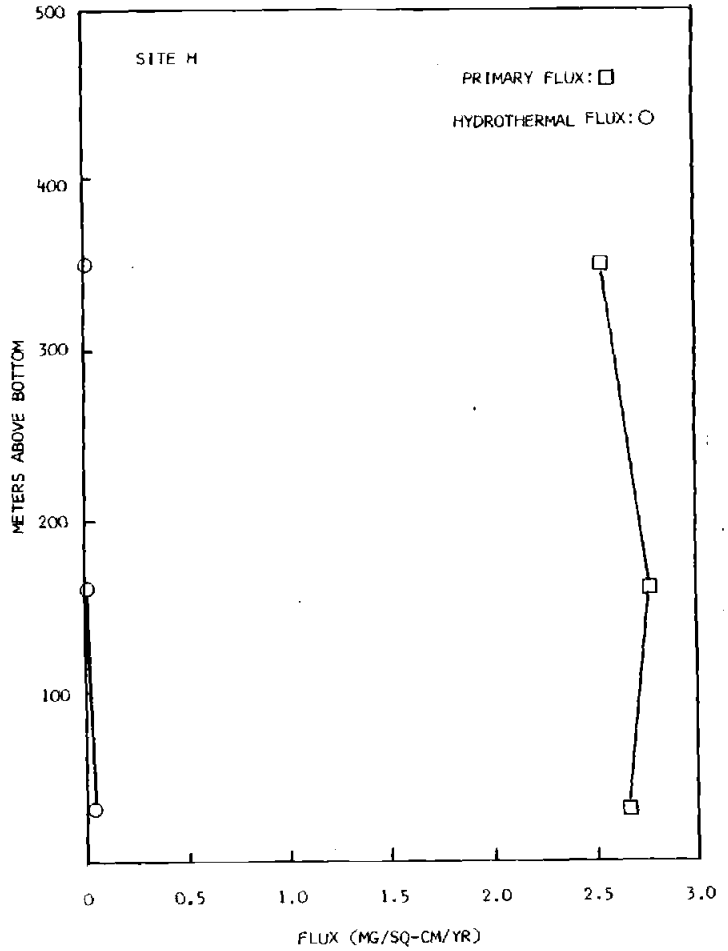

Figure III-5a

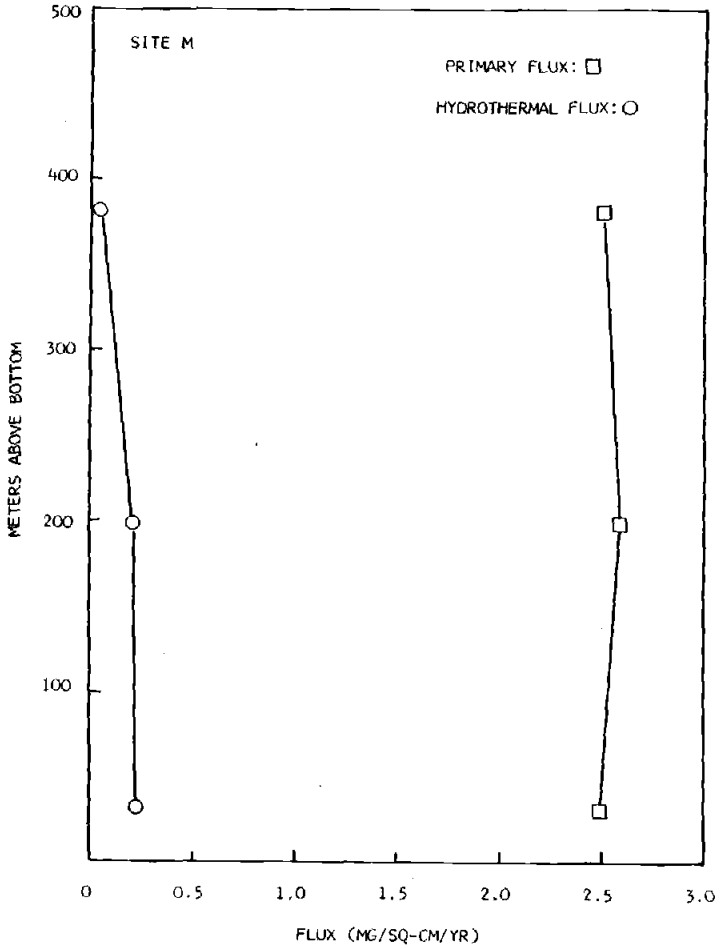

Figure III-5b

Conclusions

The results of the linear programming runs presented herein suggest that the near-bottom flux increases for several components can be explained by a combination of primary flux and resuspension. Near-bottom increases in Fe may be due to a hydrothermal flux in addition to the primary flux and resuspended flux. Mn fluxes increase throughout the water column, but the greatest increases are seen near the bottom. Recycling of Mn from the sediments into the the bottom waters with subsequent reprecipitation onto particles may explain the large increases in Mn flux in this zone.

Flux increases at mid-water depths involve carbonate and opal, as well as organic carbon and detrital silicates. These increases may be the results of lateral transport or biological repackaging.

BIBLIOGRAPHY

Aspila, K.I., H. Agemian, and A.S.Y. Chau, 1976. A Semi-automated Method for the Determination of Inorganic, Organic, and Total Phosphate in Sediments. Analyst, 101, 187-197.

Billett, D.S.M., R.S. Lampitt, A.L. Rice, and R.F.C. Mantoura, 1983. Seasonal sedimentation of phytoplankton to the deep-sea benthos. Nature, 302, 520-522.

Bishop, J.K.B., R.W. Collier, D.R. Kettens, and J.M. Edmond, 1980. The chemistry, biology, and vertical flux of particulate matter from the upper 1500 m of the Panama Basin. Deep-Sea Res., 27, 615-640.

Blackburn, Maurice, 1962. An oceanographic study of the Gulf of Tehuantepec. U.S. Dept. of the Interior, Fish and Wildlife Service, Special Scientific Report - Fisheries No. 404, 28 pp.

Bremner, J.M., 1960. Determination of nitrogen in soil by the Kjeldahl method. J. Agric. Sci., 55, 11-33.

Brewer, P.G., Y. Nozaki, D.W. Spencer, and A.P. Fleer, 1980. Sediment trap experiments in the deep North Atlantic: isotopic and elemental fluxes. J. Mar. Res., 38, 703-728.

Brun-Cottan, J.-C., 1976. Stokes Settling and Dissolution Rate Model for Marine Particles as a Function of Size Distribution. J. Geophys. Res., 81, 1601-1606.

Cobler, R., and J. Dymond, 1980. Sediment Trap Experiment on the Galapagos Spreading Center, Equatorial Pacific. Science, 209, 801-803.

Collier, R.W., and J.M. Edmond, 1983. Plankton compositions and trace element fluxes from the surface ocean. In Wong, C.S., and others (eds.), Trace Metals in Sea Water. Plenum Press, New York, 789-810.

Conard, R., 1976. A Study of the Chemical Composition of Ca-Al-rich Inclusions from the Allende Meteorite. Unpubl. M.S. thesis, Oregon State University, Corvallis, 129 pp.

Deuser, W.G., E.H. Ross, and R.F. Anderson, 1981. Seasonality in the supply of sediment to the deep Sargasso Sea and implications for the rapid transfer of matter to the deep ocean. Deep-Sea Res., 28, 495-505.

Dunbar, R.B., and W.H. Berger, 1981. Fecal pellet flux to modern bottom sediment of Santa Barbara Basin (California) based on sediment trapping. Geol. Soc. Am. Bull. 92, 212-218.

Dymond, J., 1981. Geochemistry of Nazca plate surface sediments: An evaluation of hydrothermal, biogenic, detrital, and hydrogenous sources. In Kulm, L.D., and others (eds.), Nazca Plate: Crustal Formation and Andean Convergence, Geol. Soc. Am. Memoir 154, Boulder, CO., 133-174.

Dymond, J., and W. Eklund, 1978. A microprobe study of metalliferous sediment components. Earth Planet. Sci. Lett., 40, 243-251.

Dymond, J., K. Fischer, M. Clauson, R. Cobler, W. Gardner, M.J. Richardson, W. Berger, A. Soutar, and R. Dunbar, 1981. A sediment trap intercomparison study in the Santa Barbara Basin. Earth Planet. Sci. Lett., 53, 409-418.

Dymond, J., D.Z. Piper, M. Lyle, B. Finney, K. Murphy, R. Conard, and N. Pisias, 1983. Ferromanganese Nodules from MANOP Site H -- Control of mineralogical and chemical composition by multiple accretionary processes. Submitted to Geochim. Cosmochim. Acta.

Dymond, Jack, and H.H. Veeh, 1975. Metal accumulation rates in the southeast Pacific and the origin of metalliferous sediments. Earth Planet. Sci. Lett., 28, 13-22.

Emerson, S., S. Kalhorn, L. Jacobs, B.M. Tebo, K.H. Nealson, and R.A. Rosson, 1982. Environmental oxidation rate of manganese (II): bacterial catalysis. Geochim. Cosmochim. Acta, 46, 1073-1079.

Emerson, S., K. Fischer, C. Reimers, and D. Heggie, 1983. Organic dynamics at the sediment-water interface of the deep sea. In preparation.

Fischer, K., and R. Cobler, 1979. Antibiotic Poisoning of Sediment Trap. EOS: Trans. Am. Geophys. Union, 60, 851.

Fischer, K., J. Dymond, C. Moser, D. Murray, and A. Matherne, 1983. Seasonal variations in particulate flux in an offshore area adjacent to coastal upwelling. In Suess, E., and J. Thiede (eds.), Coastal Upwelling: Its Sediment Record, vol. 1. Plenum Press, New York, 209-224.

Gardner, W.D., 1980a. Sediment trap dynamics and calibration: laboratory evaluation. J. Mar. Res., 38, 17-39.

Gardner, W.D., 1980b. Field assessment of sediment traps. J. Mar. Res., 38, 41-52.

Gardner, W.D., 1982. A re-evaluation of sediment trap dynamics based on experiments with tilted sediment traps. In preparation.

Gardner, W.D., K.R. Hinga, and J. Marra, 1982a. Observations on the degradation of biogenic material in the deep ocean and the effect on sediment trap fluxes. In preparation.

Gardner, W.D., C.D. Hollister, and J.B. Southard, 1982b. Sedimentation and Resuspension in the Northwest Atlantic. Submitted to Mar. Geol.

Gardner, W.D., M. J. Richardson, K.R. Hinga, and P.E. Biscaye, 1982c. Large Particle Vertical Fluxes in High Energy Environments. In preparation.

Gunther, E.B., 1981. Eastern North Pacific Tropical Cyclones of 1980. Mon. Weather Rev., 109., 1701-1712.

Gunther, E.B., 1982. Eastern North Pacific Tropical Cyclones of 1981. Mon. Weather Rev., 110, 839-851.

Hargrave, B.T. and N.M. Burns, 1979. Assessment of sediment trap collection efficiency. Limnol. Oceanogr., 24, 1124-1136.

Heath, G.R., and J. Dymond, 1977. Genesis and transformation of metalliferous sediments from the East Pacific Rise, Bauer Deep, and Central Basin, northwest Nazca plate. Geol. Soc. Am. Bull., 88, 723-733.

Heath, G.R., and M.W. Lyle, 1982. Modification of a Hydrothermal Sediment by Suboxic Diagenesis: Evidence for Manganese Loss at MANOP Site M (8°45'N, 104°W). EOS: Trans. Am. Geophys. Union, 63, 999.

Heggie, D., and M. Bender, 1983. Fate of organic carbon reaching the seafloor: a status report. Geochim. Cosmochim. Acta, in press.

Hofmann, E.E., A.J. Busalacchi, and J.J. O'Brien, 1981. Wind Generation of the Costa Rica Dome. Science, 214, 552-554.

Honjo, S., 1980. Material fluxes and modes of sedimentation in the mesopelagic and bathypelagic zones. J. Mar. Res., 38, 53-97.

Honjo, S., 1982. Seasonality and Interaction of Biogenic and Lithogenic Particulate Flux at the Panama Basin. Science, 218, 883-884.

Honjo, S., S.J. Manganini, and J. Cole, 1982a. Sedimentation of biogenic matter in the deep ocean. Deep-Sea Res., 29, 609-625.

Honjo, S., S.J. Manganini, and L.J. Poppe, 1982b. Sedimentation of Lithogenic Particles in the Deep Ocean. Mar. Geol., 50, 199-220.

Honjo, S., D.W. Spencer, and J.W. Farrington, 1982c. Deep Advective Transport of Lithogenic Particles in Panama Basin. Science, 216, 516-518.

Kalhorn, S., and S. Emerson, 1983. Oxidation state of manganese in surface sediments of the Pacific Ocean. Submitted to Geochim. Cosmochim. Acta.

Karl, D.M., and G.A. Knauer, 1983. Vertical distribution, transport and exchange of organic matter in the Northeast Pacific Ocean: Evidence for multiple zones of biological activity. Submitted to Deep-Sea Res.

Klinkhammer, G.P., and M.L. Bender, 1980. The distribution of manganese in the Pacific Ocean. Earth Planet. Sci. Lett., 46, 361-384.

Knauer, G.A., J.H. Martin, and K.W. Bruland, 1979. Fluxes of particulate carbon, nitrogen, and phosphorus in the upper water column of the northeast Pacific. Deep-Sea Res., 26, 97-108.

Lal, D., and A. Lerman, 1973. Dissolution and Behavior of Particulate Biogenic Matter in the Ocean: Some Theoretical Considerations. J. Geophys. Res., 78, 7100-7111.

Lonsdale, P., and F.N. Spiess, 1980. Deep-tow observations at the East Pacific Rise, 8°45'N, and some interpretations. In Rosendahl, B.R., Hekinian, R., et al., Initial Reports of the Deep Sea Drilling project, 54: Washington (U.S. Government Printing Office, 43-62.

Lyle, M., 1983. The brown-green color transition in marine sediments: A marker of the Fe(III)-Fe(IV) redox boundary. Limnol. Oceanogr., 28.

Martin, J.H., and G.A. Knauer, 1973. The elemental composition of plankton. Geochim. Cosmochim. Acta, 37, 1639-1653.

Martin, J.H., and G.A. Knauer, 1982. Manganese cycling in northeast Pacific equatorial waters. J. Mar. Res., 40, 1213-1225.

Matherne, A.M., and K. Fischer, 1982. Biogenic Fluxes in Sediment Trap Samples from MANOP Sites M and H. EOS: Trans. Am. Geophys. Union, 63, 1016.

McCave, I.N., 1975. Vertical flux of particles in the ocean. Deep-Sea Res., 22, 491-502.

Owen, R.W., and B. Zeitzschel, 1970. Phytoplankton production: seasonal change in the oceanic eastern tropical Pacific. Mar. Biol., 7, 32-36.

Pillsbury, R.D., J.S. Bottero, R.E. Still, and W.E. Gilbert, 1974. A Compilation of Observations from Moored Current Meters, Vol. VI, Oregon Continental Shelf, April-October 1972. Oregon State University, School of Oceanography, Corvallis. Data Report 57. Reference 74-2, 189-230.

Pillsbury, R.D., F. Sciremammano, Jr., J.S. Bottero, and R.E. Still, 1980. A Compilation of Observations from Moored Current Meters, Vol. XII, Currents, Temperature and Pressure in the Drake Passage During F DRAKE 77, 78. Oregon State University, School of Oceanography, Corvallis. Data Report 82. Reference 80-11, 5-12.

Powell, H., and K. Fischer, 1982. Comparison Study of Bactericides for Sediment Traps. EOS: Trans. Am. Geophys. Union, 63, 1016.

Rea, D.K., 1982. Fluctuation in eolian sedimentation during the past five glacial-interglacial cycles: A preliminary examination of data from Deep Sea Drilling Project Hole 503B, eastern equatorial Pacific. In Prell, W.L., J.V. Gardner, and others (eds.), Initial Reports of the Deep Sea Drilling Project, Vol. 54. Washington (U.S. Government Printing Office), 409-415.

Richman, S., D.R. Heinle, and R. Huff, 1977. Grazing by Adult Estuarine Calanoid Copepods of the Chesapeake Bay. Mar. Biol., 42, 69-84.

Robbins, J.G., G.R. Heath, and M.W. Lyle, 1983. A sequential extraction procedure for partitioning elements among coexisting phases in marine sediments. Submitted to Geochim. Cosmochim. Acta.

Russell-Hunter, W.D., 1970. Aquatic Productivity. The Macmillan Company, New York, 306 pp. See Chap. 3.

Schrader, H.-J., 1971. Fecal Pellets: Role in Sedimentation of Pelagic Diatoms. Science, 174, 55-57.

Soutar, A., S.A. Kling, P.A. Crill, E. Duffrin, and K.W. Bruland, 1977. Monitoring the marine environment through sedimentation. Nature, 266, 136-139.

Spencer, D.W., 1981a. The Sediment Trap Intercomparison Experiment. Some preliminary data. In Anderson, R.F., and M.P. Bacon (eds.), Sediment Trap Intercomparison Experiment, Woods Hole Oceanographic Institution Technical Memorandum WHOI-1-81, 57-104.

Spencer, D.W., 1981b. Aluminum concentrations and fluxes in the ocean. In Anderson, R.F., and M.P. Bacon (eds.), Sediment Trap Intercomparison Experiment, Woods Hole Oceanographic Institution Technical Memorandum WHOI-1-81, 105-120.

Suess, E., 1980. Particulate organic carbon flux in the oceans--surface productivity and oxygen utilization. Nature, 288, 260-263.

Trent, J.D., A.L. Shanks, and M.W. Silver, 1978. In situ and laboratory measurements on macroscopic aggregates in Monterey Bay, California. Limnol. Oceanogr. 23, 626-635.

Wedepohl, K.H., 1969a. Composition and abundance of common igneous rocks. In Wedepohl, K.H., exec. ed., Handbook of Geochemistry. Springer-Verlag, New York, 227-249.

Wedepohl, K.H., 1969b. Composition and abundance of common sedimentary rocks. In Wedepohl, K.H., exec. ed., Handbook of Geochemistry. Springer-Verlag, New York, 250-271.

van Bennekom, A.J., and S.J. van der Gaast, 1976. Possible clay structures in frustules of living diatoms, Geochim. Cosmochim. Acta, 40, 1149-1152.

Walsh, I.D., K. Fischer, J. Dymond, 1983. Particle Fluxes and Resuspension in the eastern tropical Pacific Ocean. Submitted to Nature.

Weliky, K., E. Suess, C. Ungerer, P. Muller, and K. Fischer, 1983. Problems with accurate carbon measurements in marine sediments and water column particulates: A new approach. Limnol. Oceanogr. In press.

Wyrtki, K., 1964. Upwelling in the Costa Rica Dome. Fish. Bull., 63, 355-372.

Wyrtki, K., 1965. Surface currents of the eastern tropical Pacific Ocean. Inter-Am. Tropical Tuna Comm., Bull. IX (5), 271-294. Publ. also in: Scripps Institution of Oceanography Contributions, No. 1792, 1965, 35, 63-88.

APPENDICES

APPENDIX I

CURRENT METER DATA

Introductory Comments

Current meter data from Sites H and M. H-1, H-BOM, M-1, and M-2 are the designations for the moorings on which the current meters were located. (BOM refers to a tripod called the Bottom Ocean Monitor, which held a camera in addition to a current meter). The Aanderra current meters used in these deployments have a moving vane, which tracks the direction of the current, and a revolving wheel which records current speed. Current vector data is recorded once every ten minutes. These data may then be averaged over an hour or a day, depending upon the subsequent handling of the data. The meters also record temperature and pressure (depth).

The projection of the current vector on directional axes are given by S and U vectors. Directions are indicated by: $S > 0$ equals north; $S < 0$ equals south; $U > 0$ equals east; and $U < 0$ equals west. V refers to current speed, without directional indications. N refers to the number of hourly averaged current vectors obtained from a meter. S. D. is standard deviation. Skew and kurt (kurtosis) are mathematical techniques for describing the deviation of a distribution from normality. (See any standard Statistics text for a definition and explanation of these terms.)

A progressive vector diagram is constructed by placing the the mean vectors (speed and direction averaged for one day) end-to-end. The net result gives a picture of water mass movement past the current meter. These diagrams are useful for showing water mass movement in the area.

LLP stands for low low pass filtering, which removes any frequency with a period greater than 12 hours. For further information on the current meters, their calibration, and data handling, see Pillsbury et al, 1974 and 1980.

The OSU Current Meter Group under Dale Pillsbury prepared the current meters for deployment and processed the data presented here.

Table AI-1. Current meter data at Site M. See introductory comments to Appendix I for explanations of symbols and parameters.

M-2

620 METERS

	MEAN	S.D.	SKEW	KURT	MIN	MAX	N
S(cm/sec)	7.58	4.37	0.89	3.65	0.70	25.50	6232
U(cm/sec)	-1.62	6.45	-0.13	2.78	-23.50	18.80	6232
V(cm/sec)	0.47	5.66	-0.49	3.86	-22.20	16.80	6232
T(°C)	6.86	0.28	1.24	4.81	6.24	8.07	6232
P(decibars)	628.96	7.82	4.07	22.99	624.20	701.40	6232

1550 METERS

S(cm/sec)	4.86	2.89	0.45	2.74	0.70	16.30	4452
U(cm/sec)	1.66	4.25	0.08	2.80	-13.40	15.50	4452
V(cm/sec)	0.71	3.26	-0.14	3.52	-13.90	12.30	4452
T(°C)	2.95	0.11	-0.05	2.34	2.69	3.63	5149
P(decibars)	1571.39	2.79	-1.47	5.13	1563.70	1581.10	5149

Table AI-1, continued. Current meter data at Site M. See introductory comments to Appendix I for symbol and parameter explanations.

M-1

2900 METERS

	MEAN	S.D.	SKEW	KURT	MIN	MAX	N
S(cm/sec)	4.08	2.17	0.50	3.13	0.80	13.40	9673
U(cm/sec)	-0.28	2.83	-0.05	2.79	-12.30	8.50	9673
V(cm/sec)	-1.79	3.18	-0.13	2.62	-13.40	7.50	9673
T(°C)	1.87	0.01	-0.49	2.28	1.81	1.88	9673
P(decibars)	2956.95	0.94	-6.19	40.01	2945.10	2957.10	9673

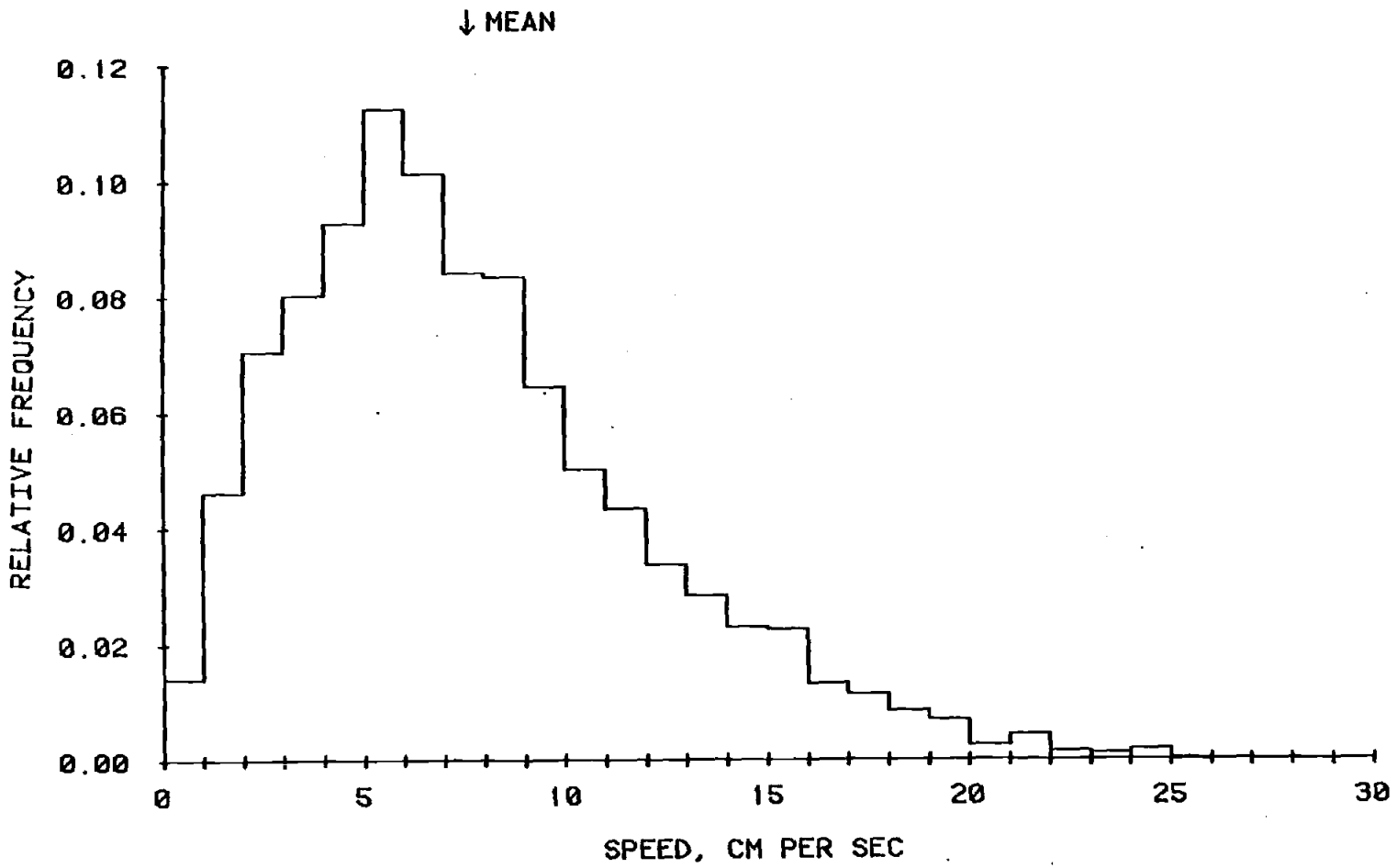

Figure AI-1. Current speed distribution for 620 m current meter at Site M.

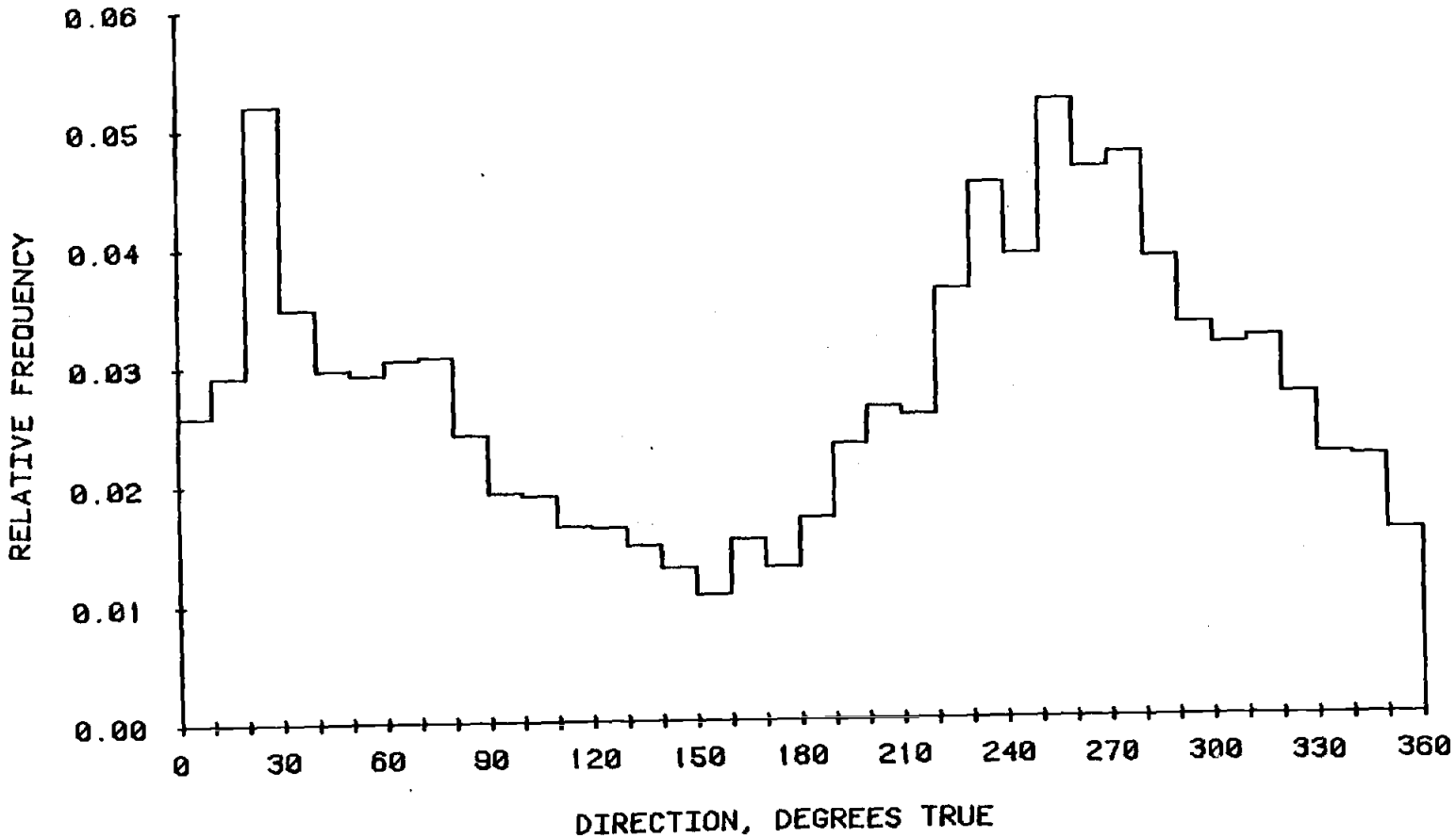

Figure AI-2. Current direction distribution for 620 m current meter at Site M.

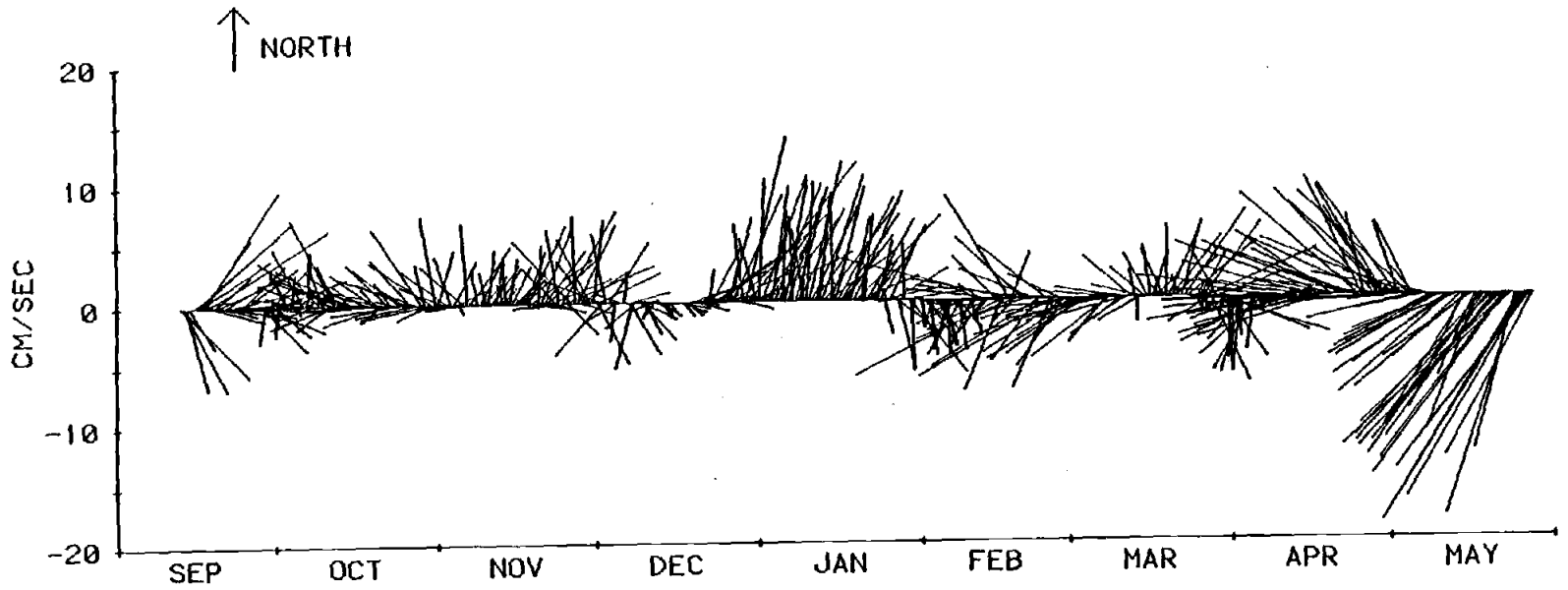

Figure AI-3. Plot of current speed and direction versus time at 620 m at Site M.

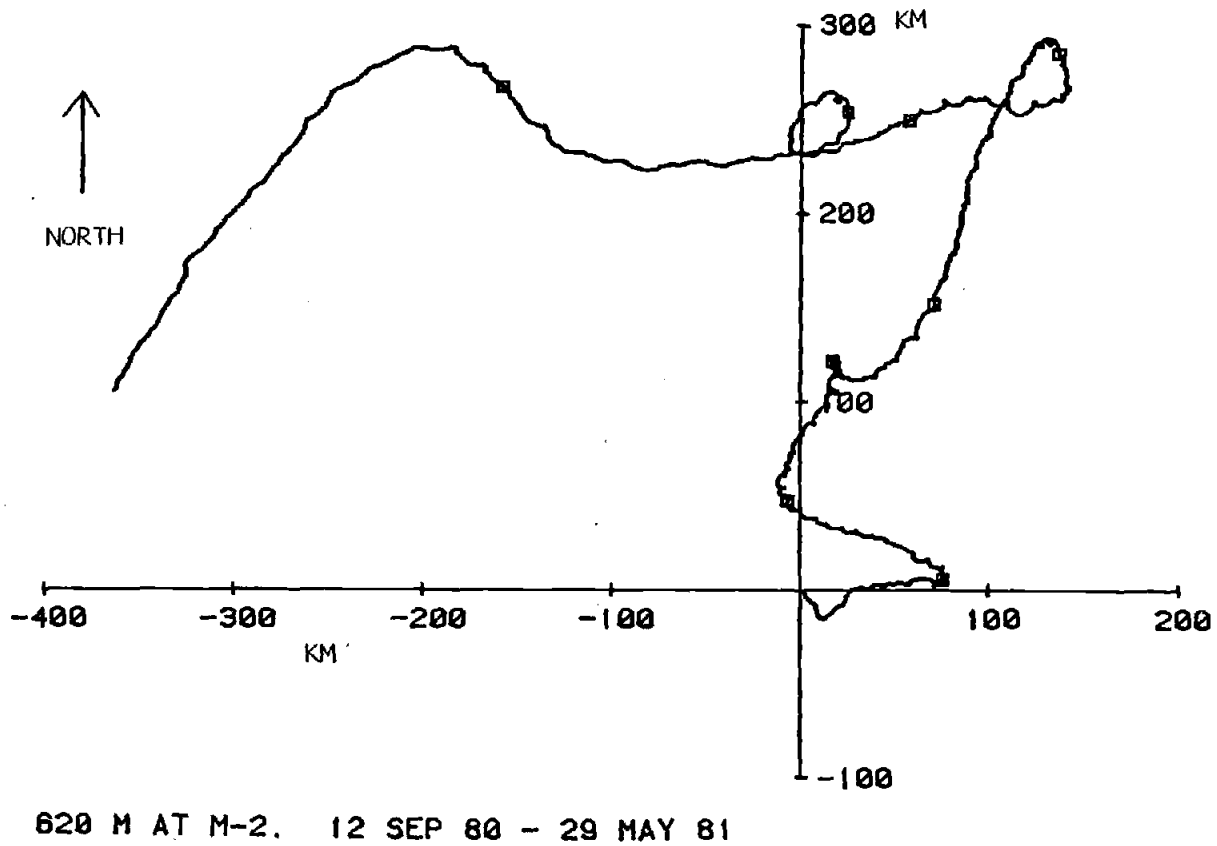

Figure AI-4. Progressive vector diagram for 620 m current meter at Site M. Axes are in kilometers. See introductory comments to Appendix I for explanation of this type of diagram.

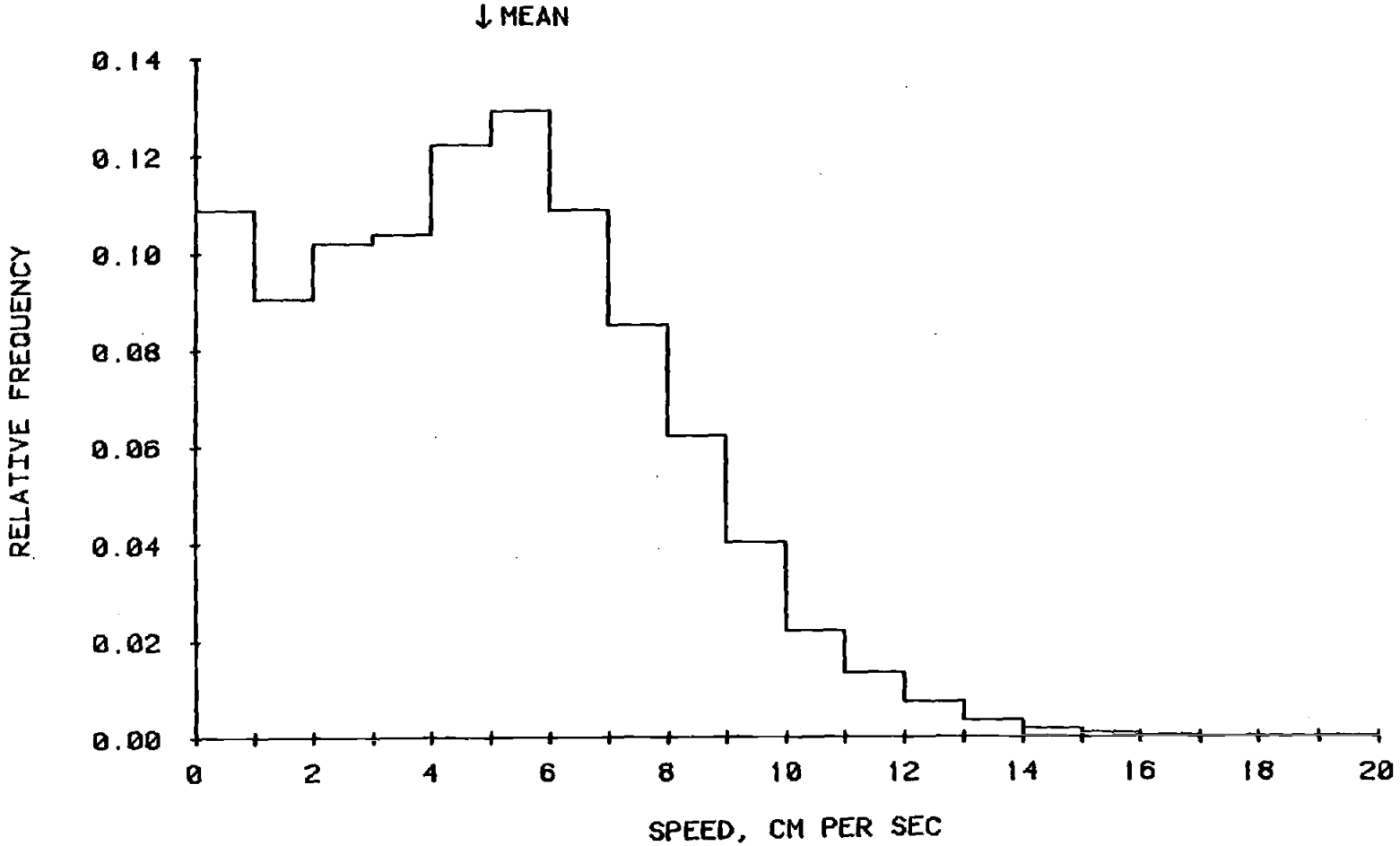

Figure AI-5. Current speed distribution for the 1550 m current meter at Site M.

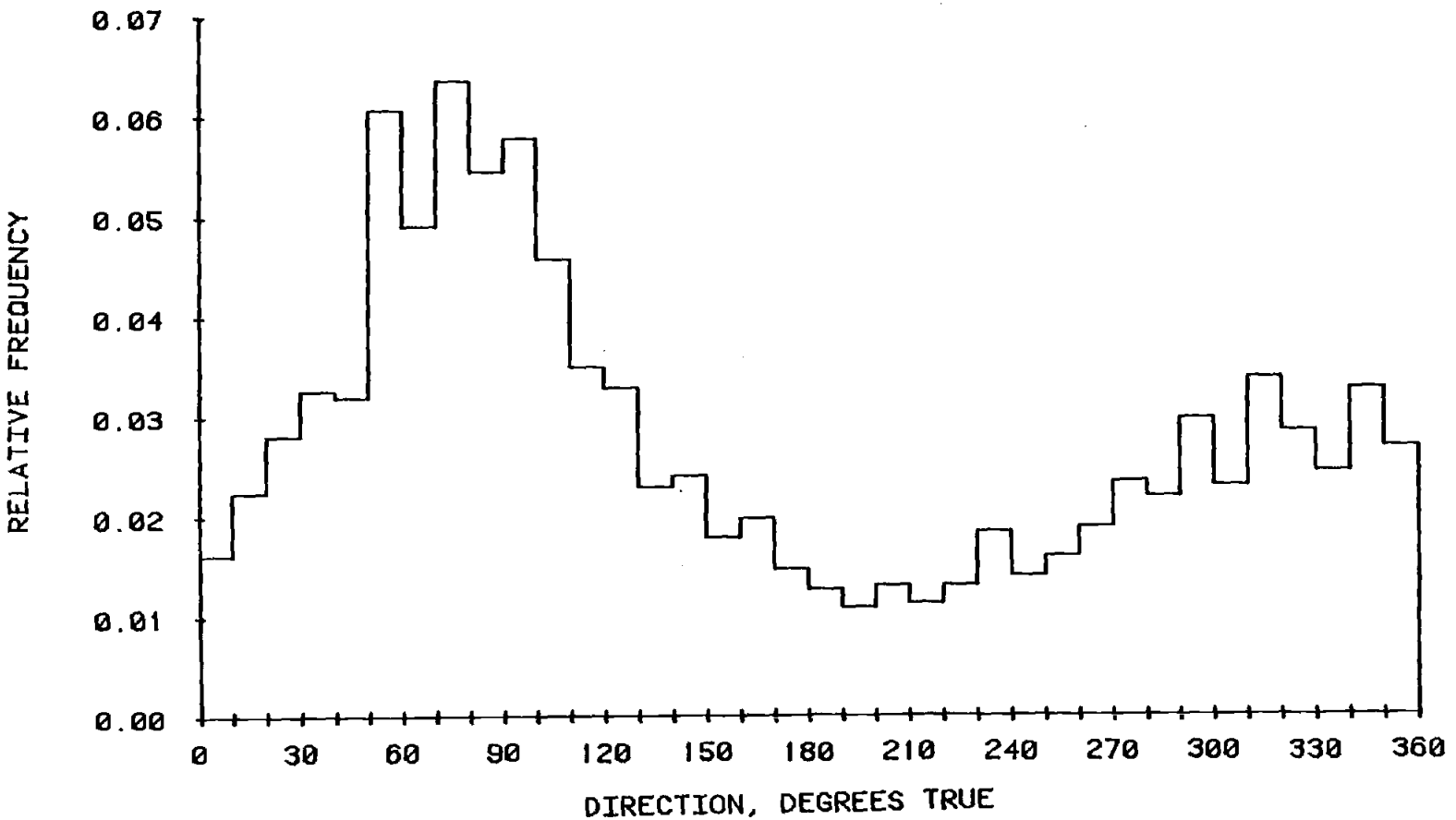

Figure AI-6. Current direction distribution for the 1550 m current meter at Site M.

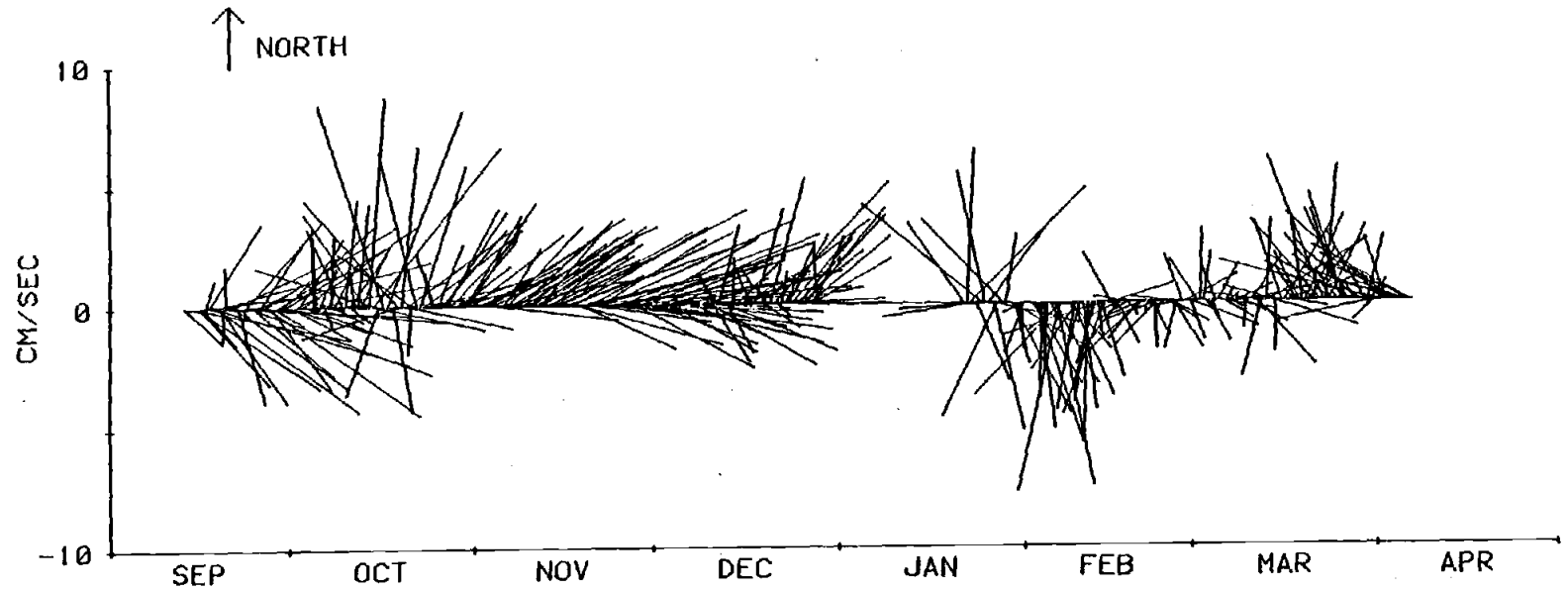

Figure AI-7. Plot of current speed and direction versus time at 1550 m at Site M.

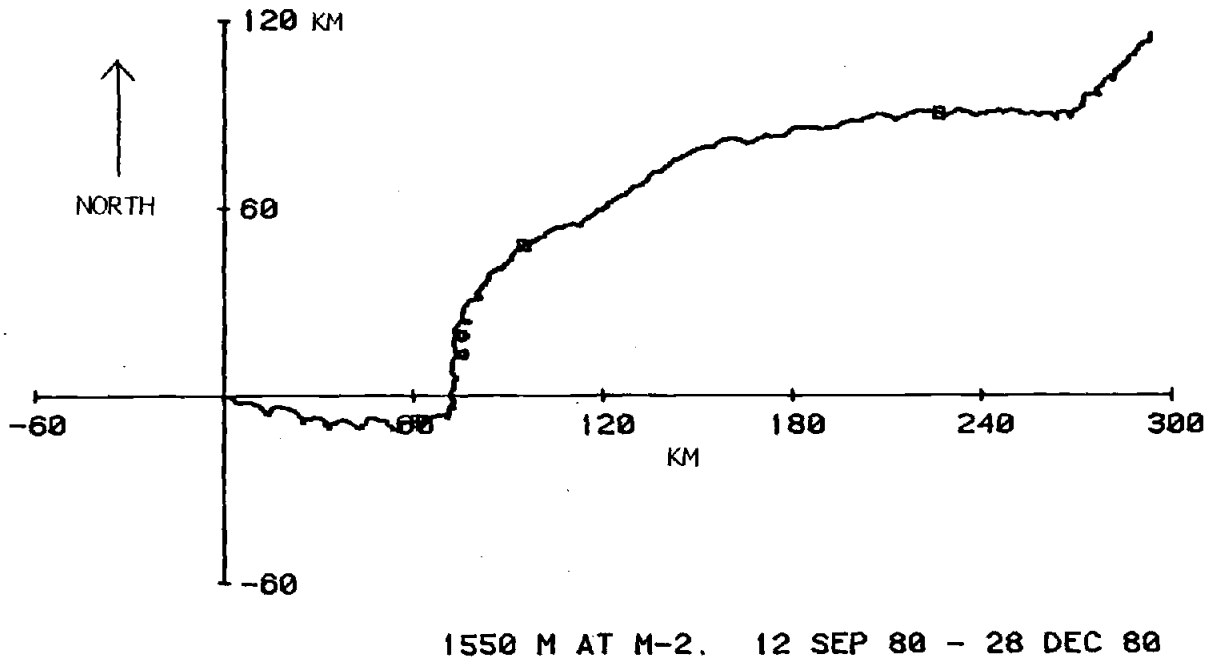

Figure AI-8a. Progressive vector diagram for the 1550 m current meter at Site M. Axes are in kilometers. See Figure AI-8b for the second period of operation during deployment. Introductory comments to Appendix I explain this type of diagram.

Figure AI-8b. Progressive vector diagram for the second period of operation during deployment for the 1550 m current meter at Site M. Axes are in kilometers. See the introductory comments to Appendix 1 for an explanation of this type of diagram.

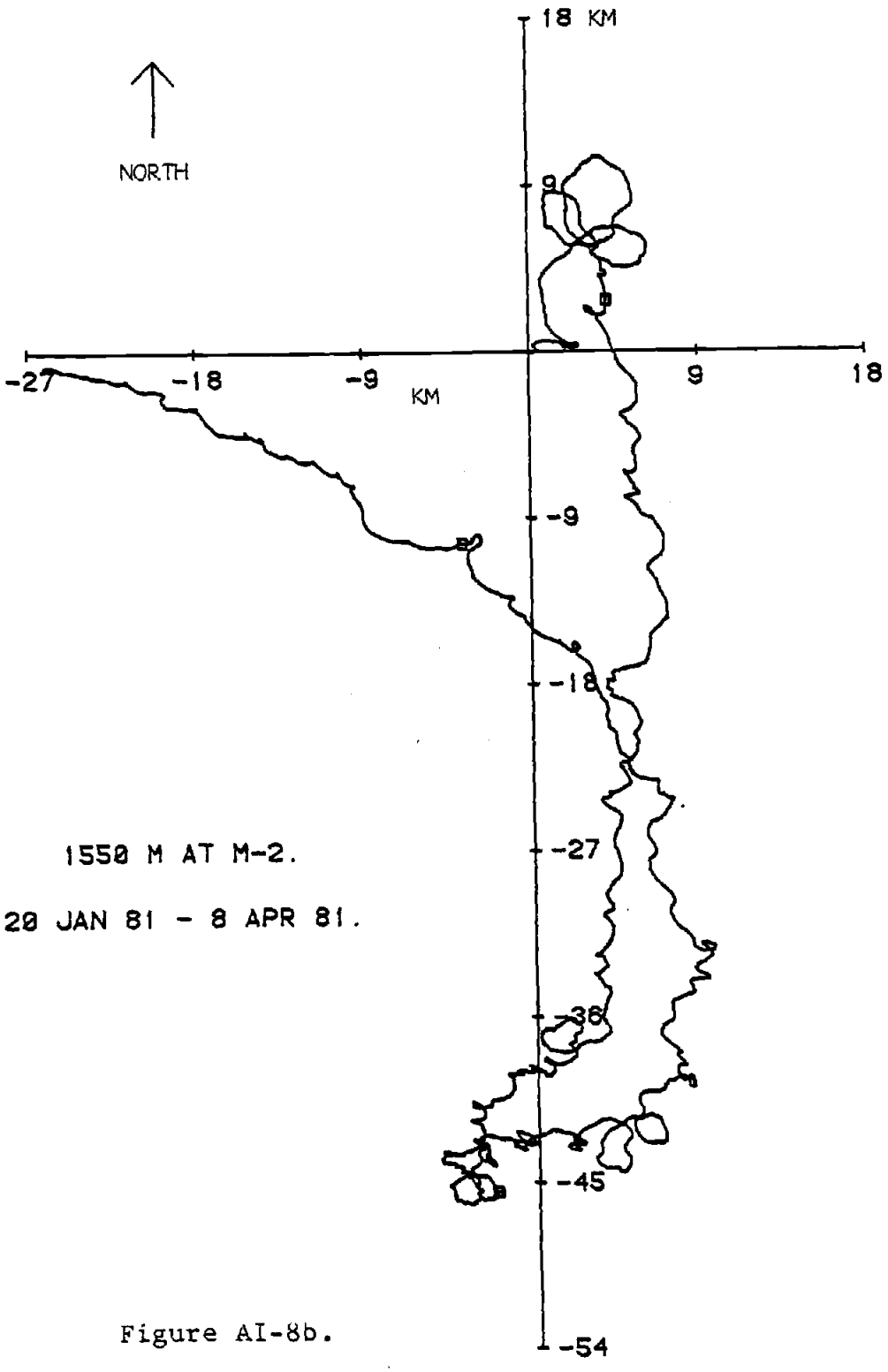
18 KM
NORTH
9
-27
-18
-9
KM
9
18
-9
-18
-27
-36
-45
-54
1550 M AT M-2.
20 JAN 81 - 8 APR 81.

Figure AI-8b.

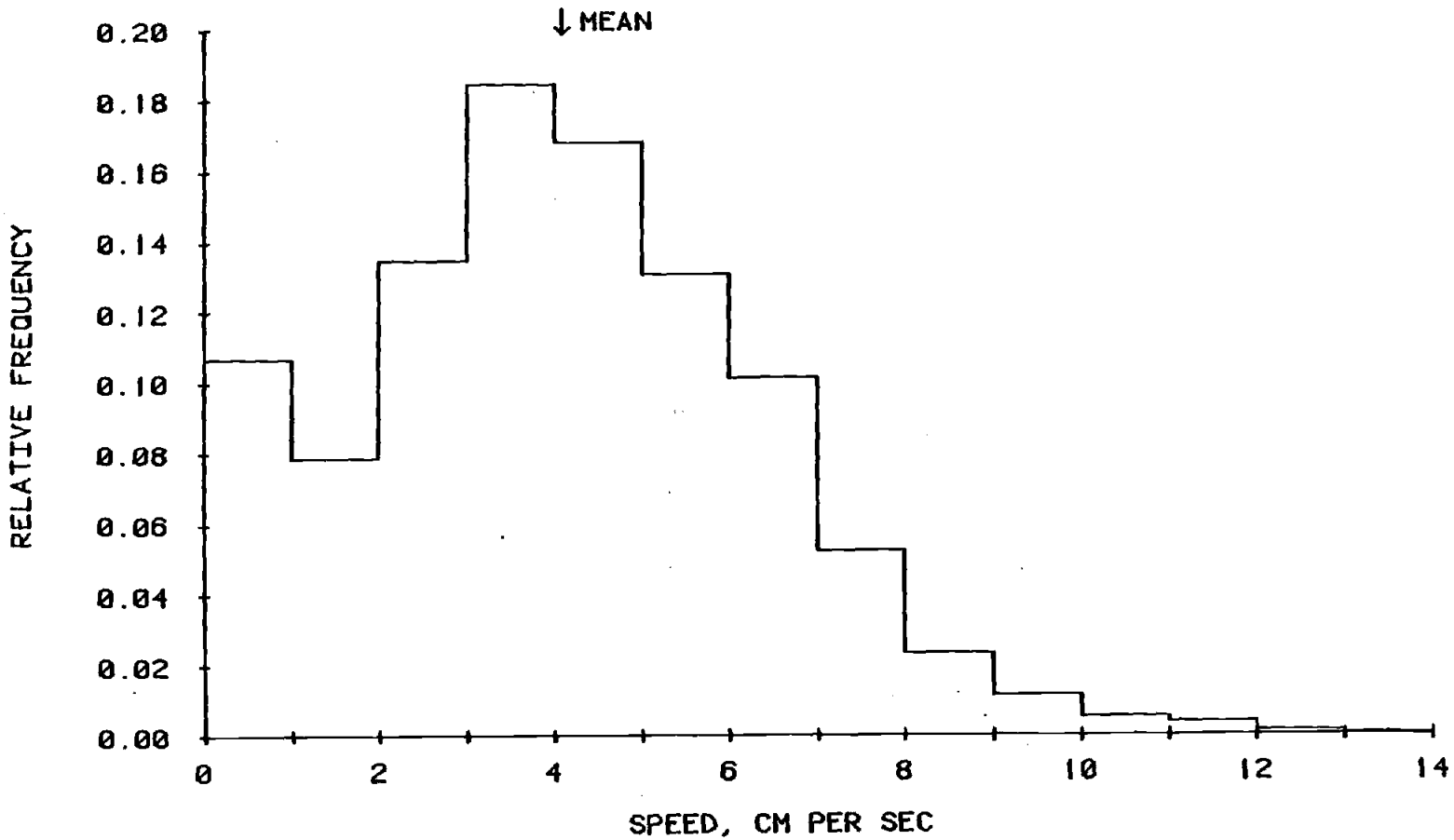

Figure AI-9. Current speed distribution for the 2900 m current meter at Site M.

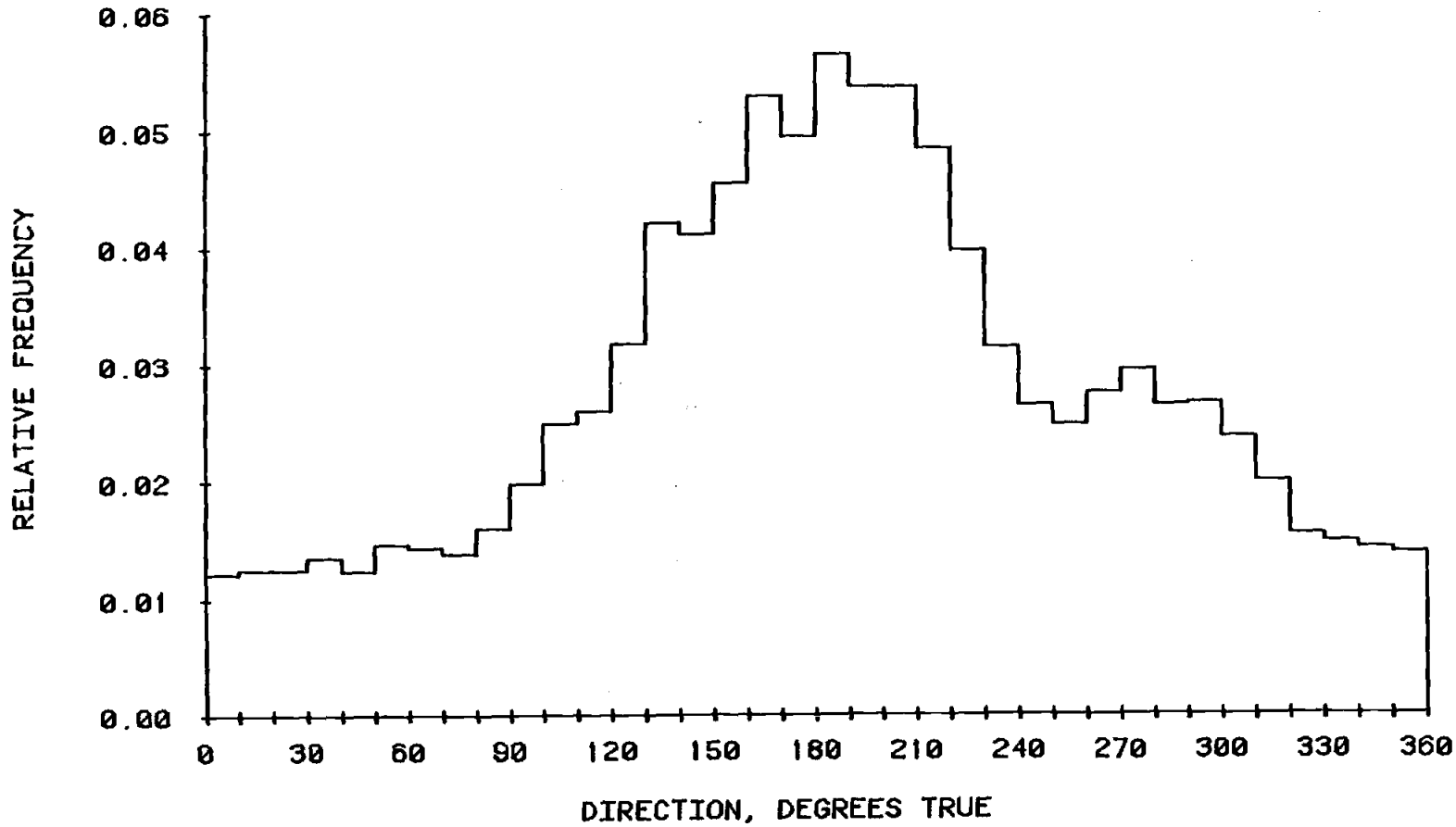

Figure AI-10. Current direction distribution for the 2900 m current meter at Site M.

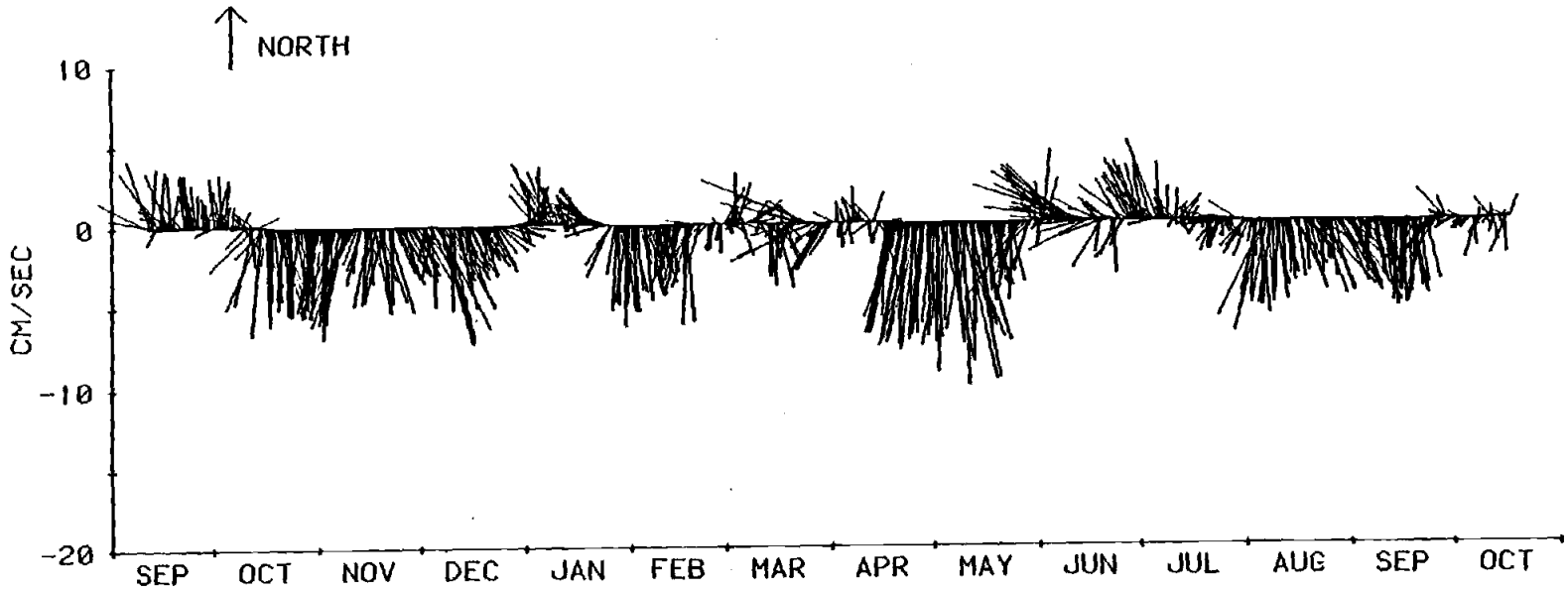

Figure AI-11. Plot of current speed and direction versus time for the 2900 m current meter at Site M.

Figure AI-12. Progressive vector diagram for the 2900 m current meter at Site M. Axes are in kilometers. See introductory comments to Appendix 1 for an explanation of this type of diagram.

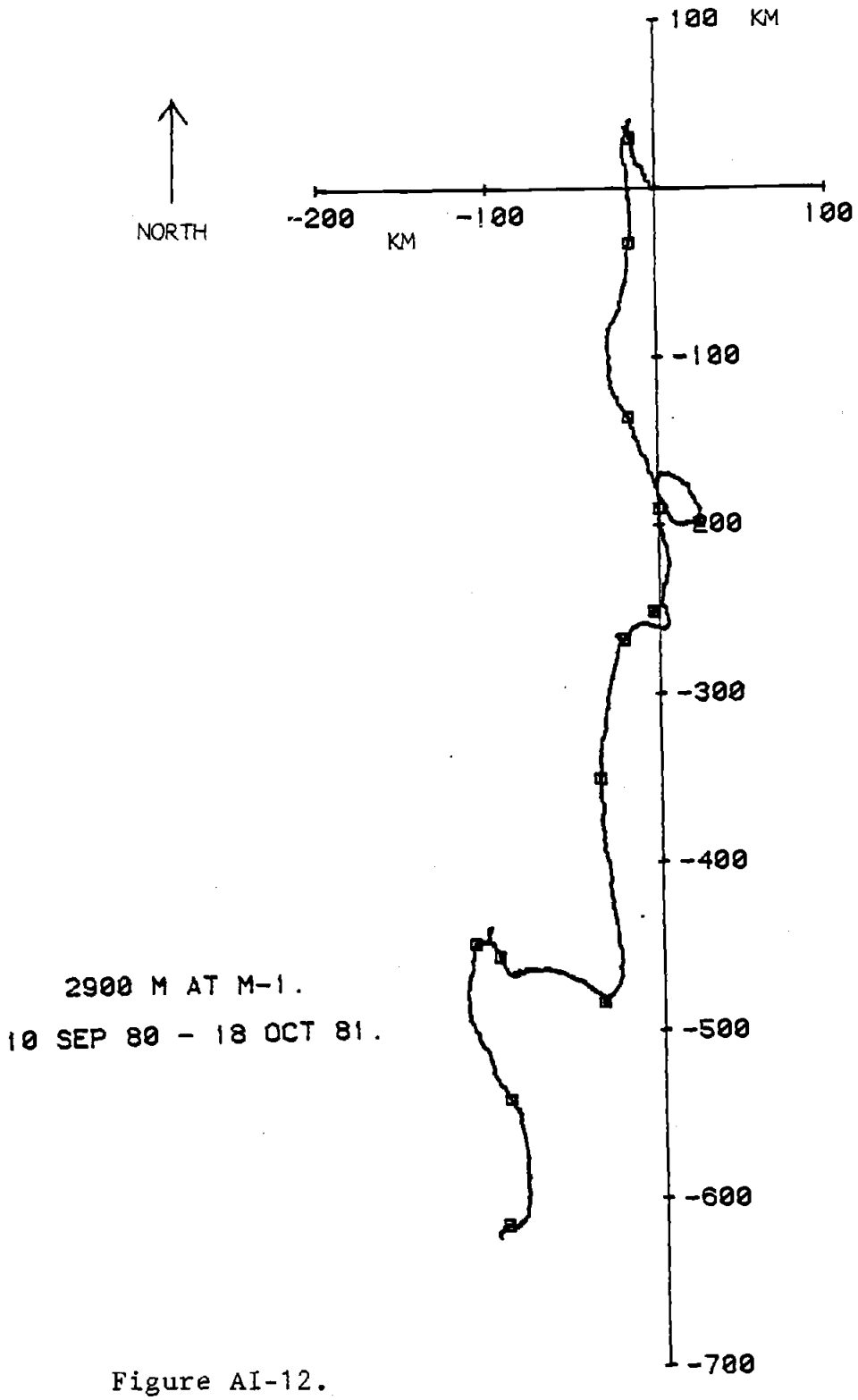
100 KM
NORTH
-200
KM
-100
100
-100
-200
-300
-400
-500
-600
-700
2900 M AT M-1.
10 SEP 80 - 18 OCT 81.

Figure AI-12.

Table AI-2. Current meter data for Site H. See introductory comments to Appendix 1 for explanations of symbols and parameters.

H-1

490 METERS

	MEAN	S.D.	SKEW	KURT	MIN	MAX	N
S(cm/sec)	7.16	3.72	0.51	2.81	0.70	21.70	7653
U(cm/sec)	0.47	5.62	0.05	2.93	-18.80	17.30	6813
V(cm/sec)	0.34	5.82	0.17	2.80	-18.80	18.50	6813
T(°C)	8.36	0.28	-0.09	2.38	7.57	9.15	7950
P(decibars)	497.92	3.83	1.47	6.61	489.60	522.30	7950

1450 METERS

S(cm/sec)	4.42	2.41	0.34	2.58	0.70	12.30	2455
U(cm/sec)	0.77	3.75	-0.13	2.82	-11.00	12.00	2455
V(cm/sec)	0.96	3.13	-0.05	2.94	-9.40	10.60	2455
T(°C)	3.24	0.08	-0.19	2.26	3.03	3.44	8056
P(decibars)	1468.42	3.77	0.44	3.81	1460.90	1491.10	8056

Table AI-2, continued. Current meter data for Site H. See introductory comments to Appendix 1 for explanations of symbols and parameters.

SITE H BOM DEPLOYMENT

3520 METERS

	MEAN	S.D.	SKEW	KURT	MIN	MAX	N
S(cm/sec)	3.05	1.93	0.40	2.21	0.80	10.00	9475
U(cm/sec)	-0.46	2.36	-0.05	2.94	-8.10	6.50	9475
V(cm/sec)	-0.21	2.68	0.07	3.09	-9.20	9.90	9475
T(°C)	1.86	0.01	0.27	4.03	1.80	1.87	9475
P(decibars)	3582.41	2.80	-1.40	3.76	3572.00	3590.00	9475

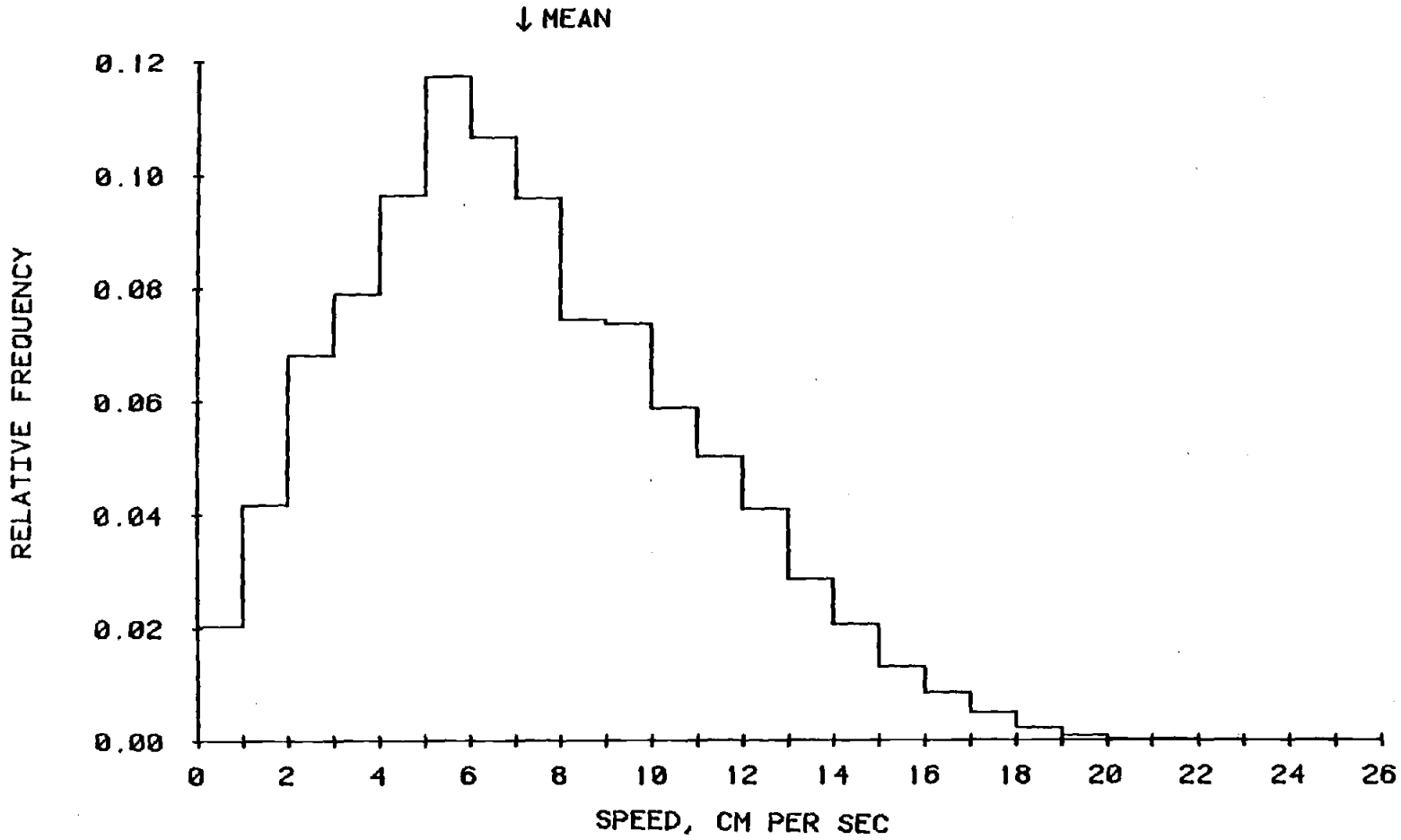

Figure AI-13. Current speed distribution for 490 m current meter at Site H.

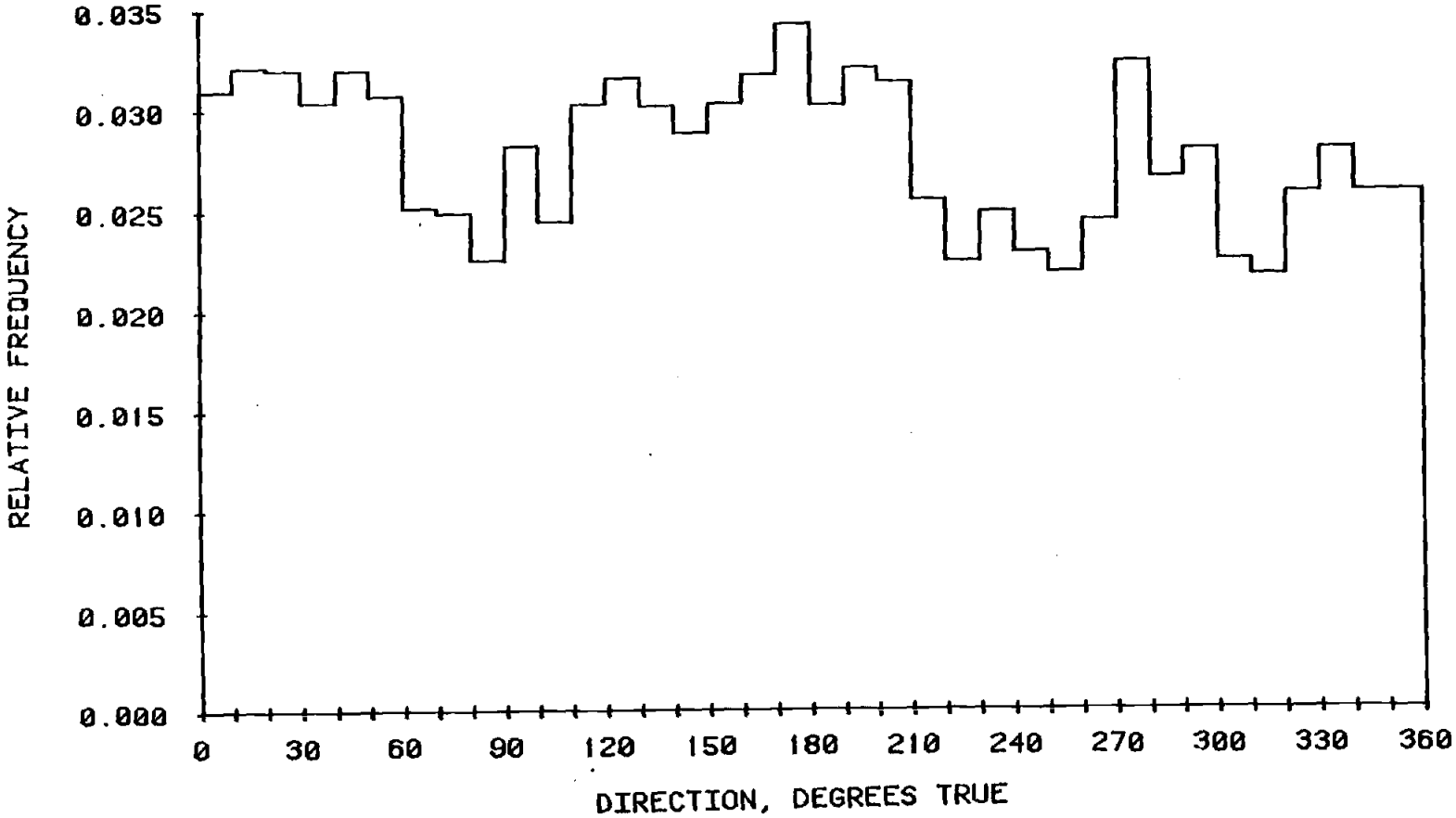

Figure AI-14. Current direction distribution for 490 m current meter at Site H.

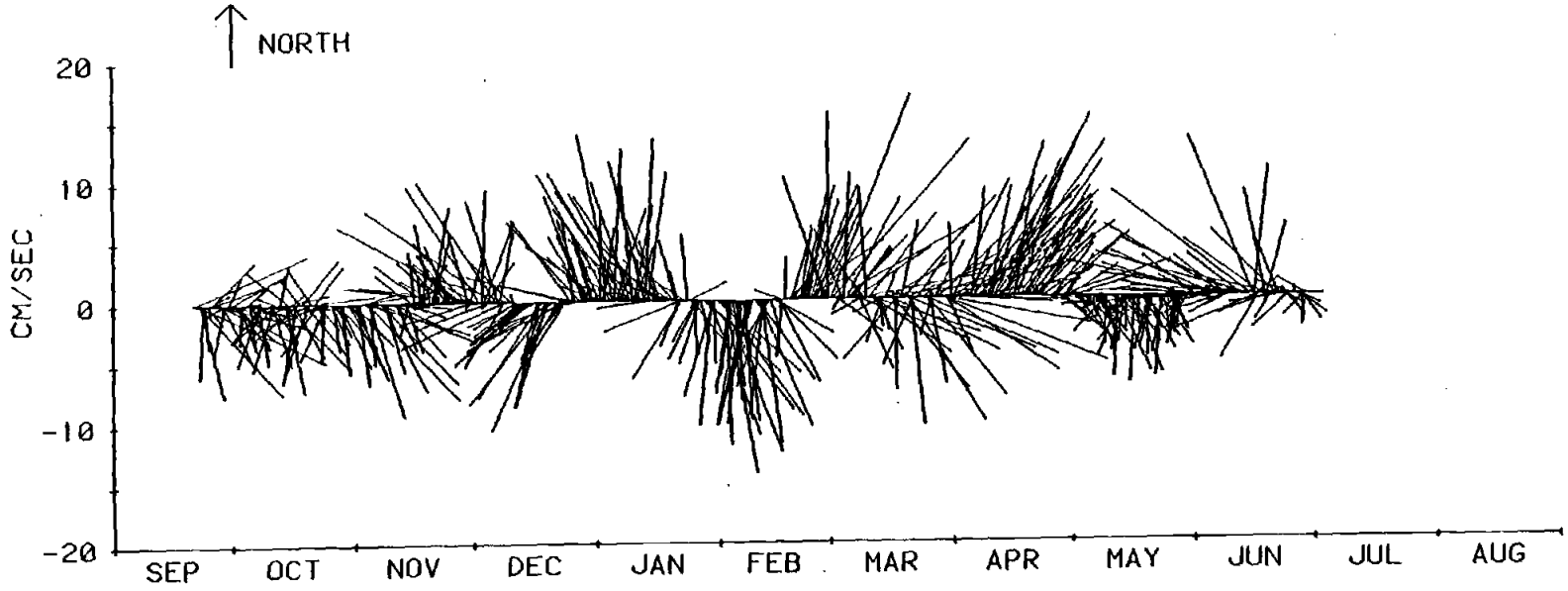

Figure AI-15. Plot of current speed and direction versus time at 490 m at Site H.

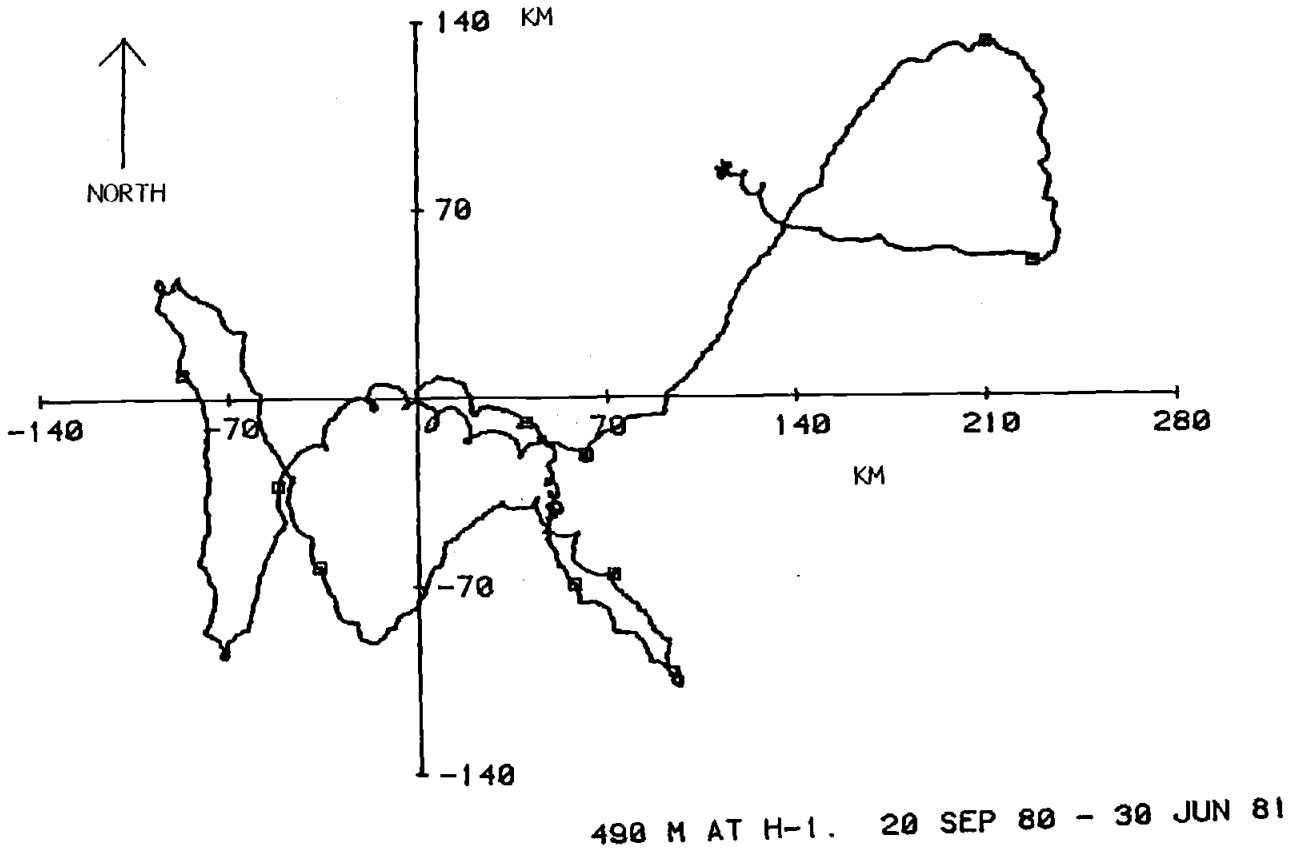

Figure AI-16. Progressive vector diagram for the 490 m current meter at Site H. Axes are in kilometers. See introductory comments to Appendix I for explanation of this type of diagram.

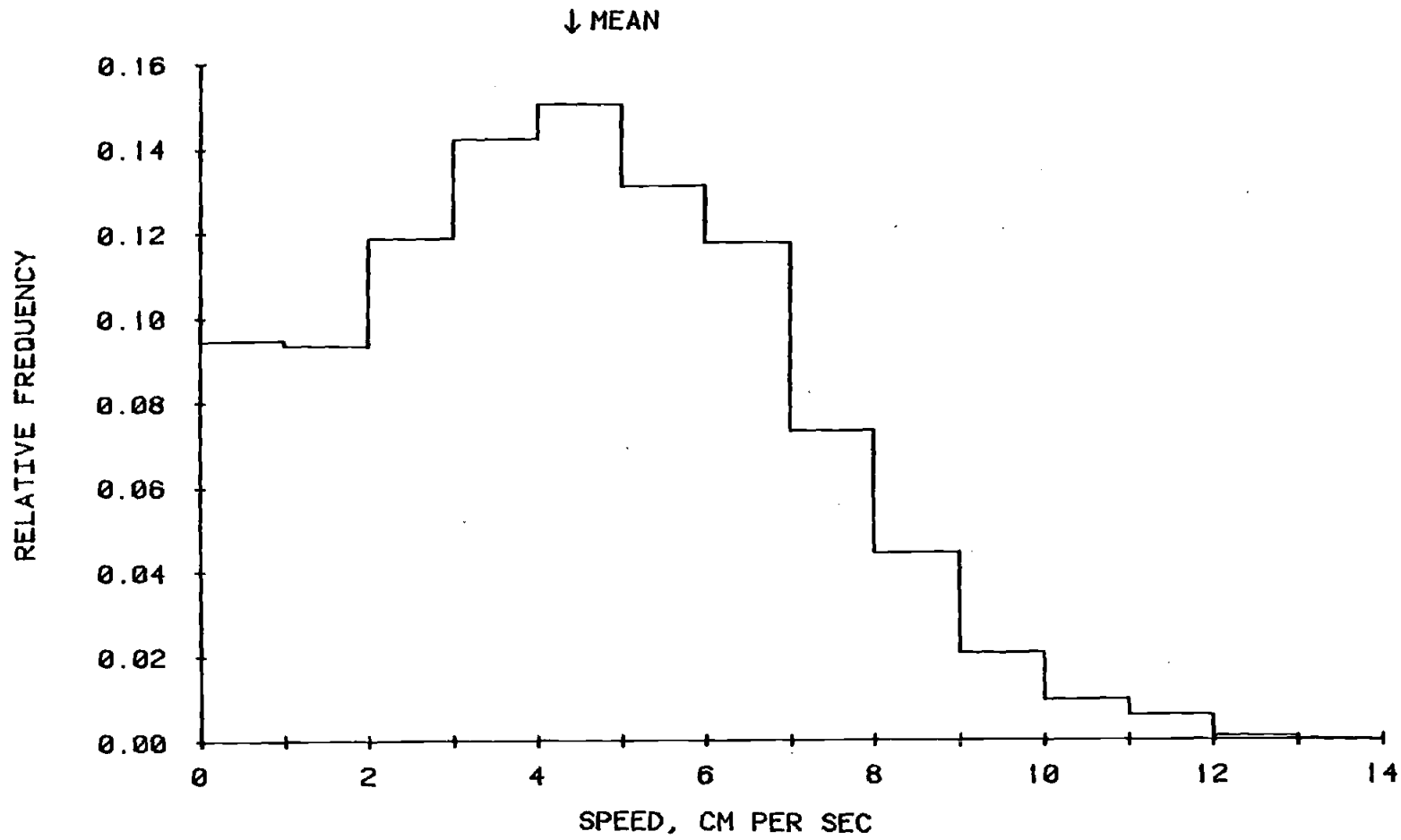

Figure AI-17a. Current speed distribution for the 1450 m current meter at Site H.

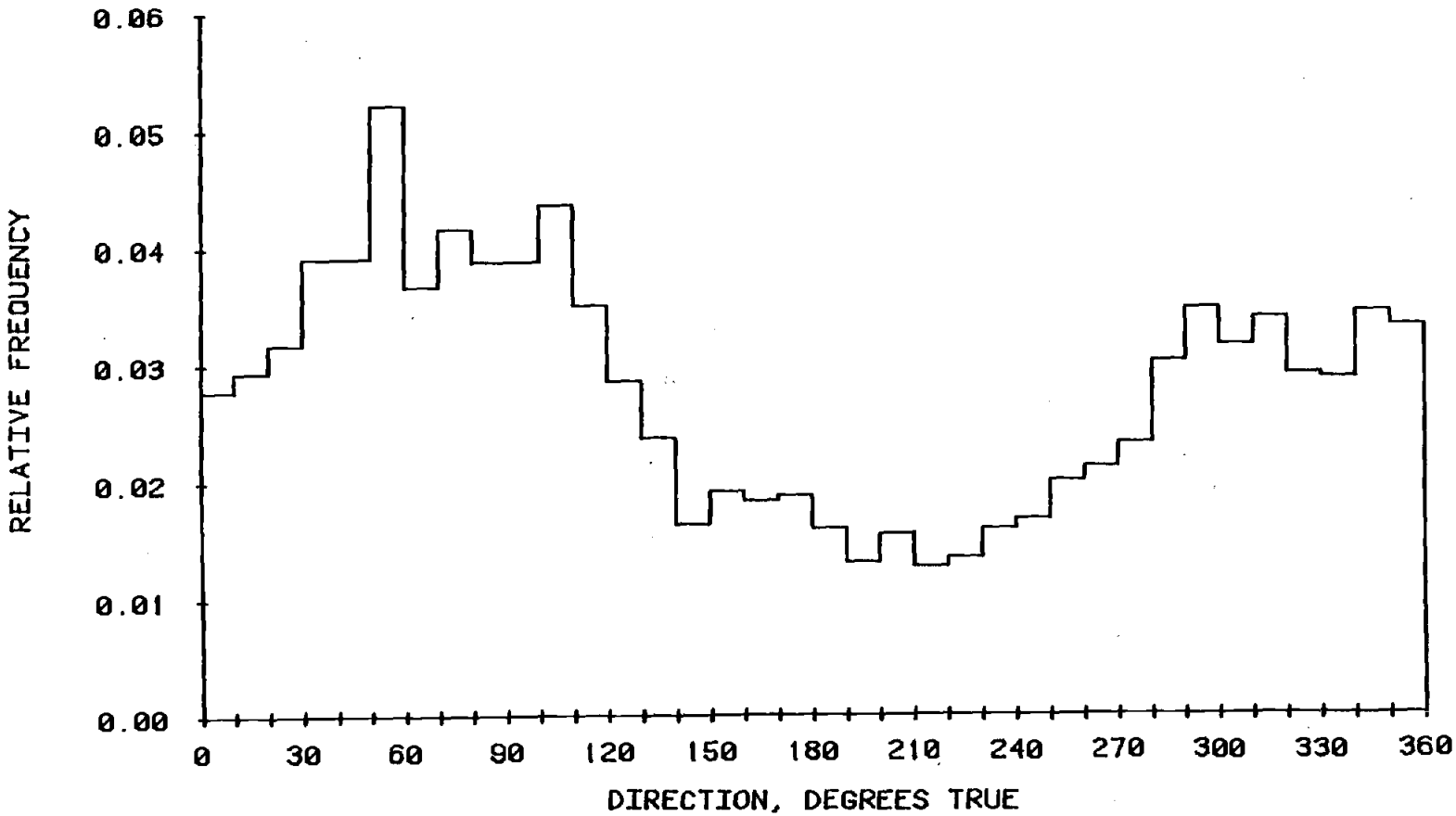

Figure AI-17b. Current direction distribution for the 1450 m current meter at Site H.

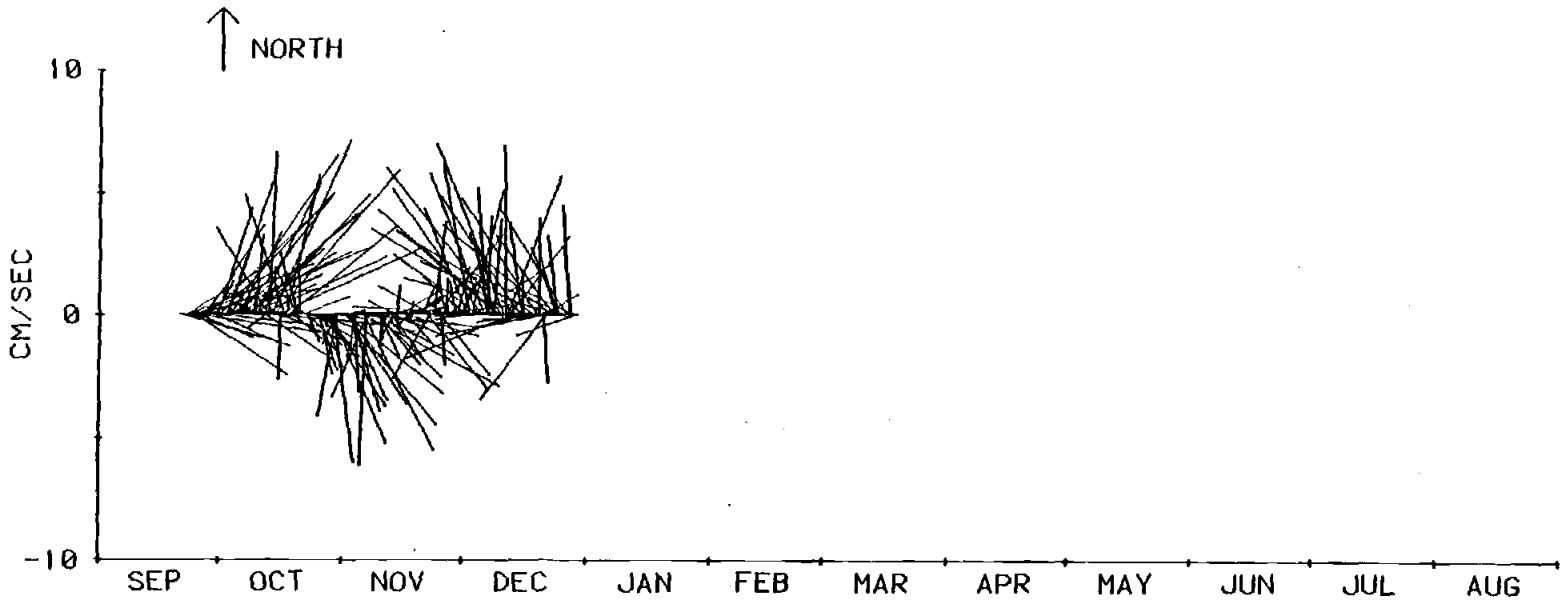

Figure AI-18. Plot of current speed and direction versus time at 1450 m at Site H.

Figure AI-19. Progressive vector diagram for the 1450 m current meter at Site H. Axes are in kilometers. See introductory comments to Appendix 1 for an explanation of this type of diagram.

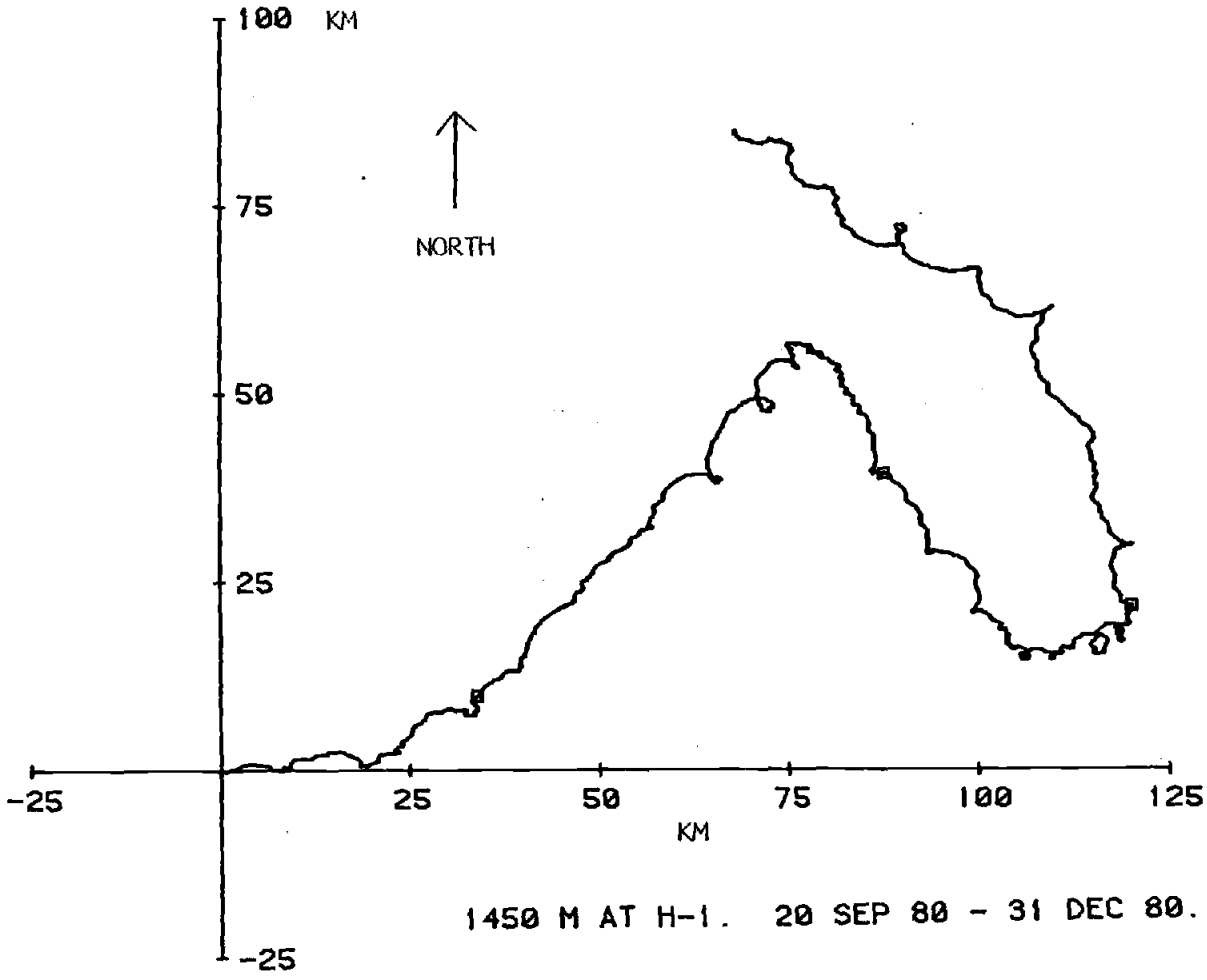
100 KM
75
50
25
-25
NORTH
-25
25
50
75
100
125
KM
1450 M AT H-1. 20 SEP 80 - 31 DEC 80.

Figure AI-19.

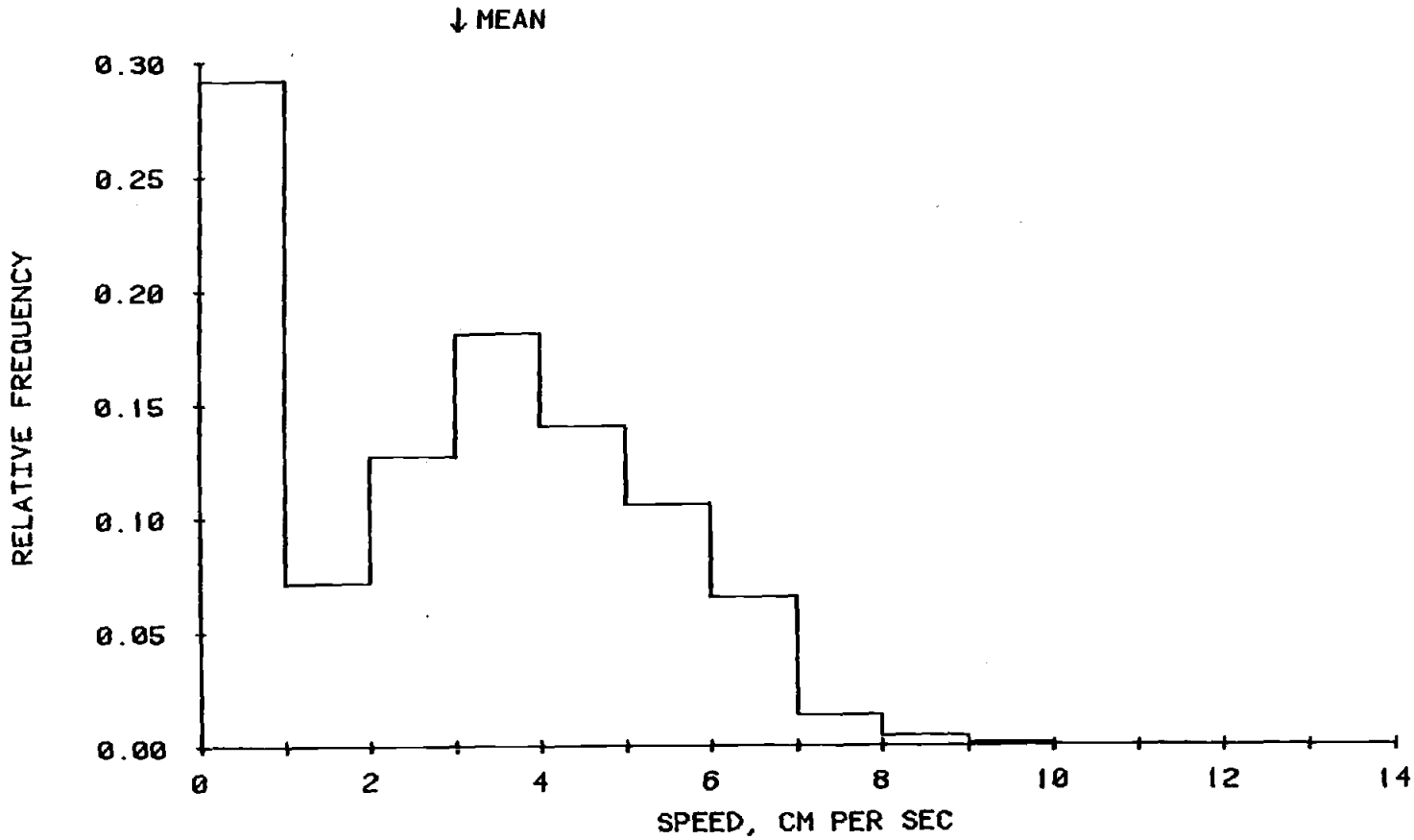

Figure AI-20. Current speed distribution for the 3520 m current meter at Site H. BOM refers to Bottom Ocean Monitor. (See introductory comments to Appendix I for a description.)

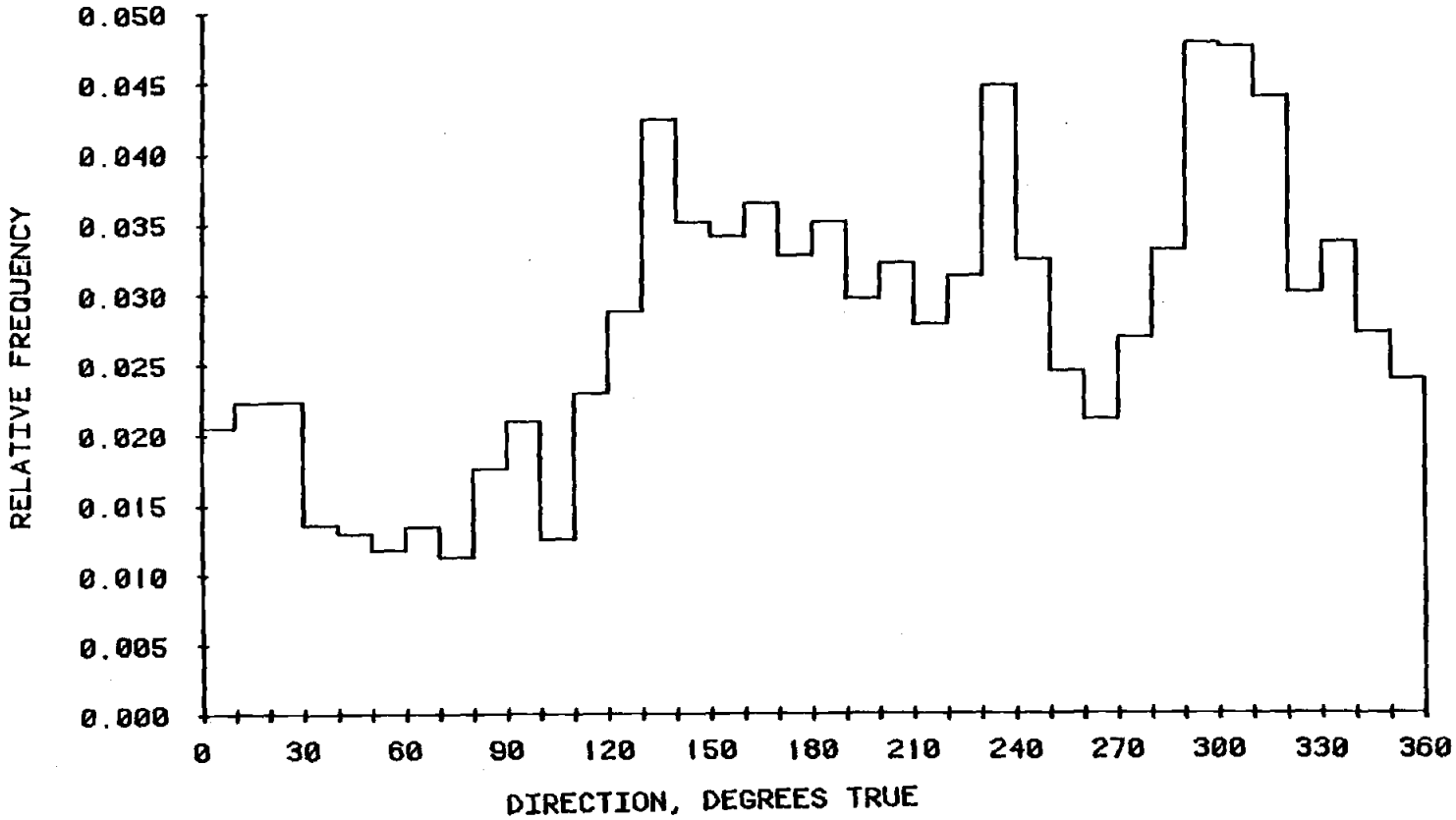

Figure AI-21. Current direction distribution for the 3520 m current meter at Site H. BOM refers to Bottom Ocean Monitor. (See introductory comments to Appendix I for a description.)

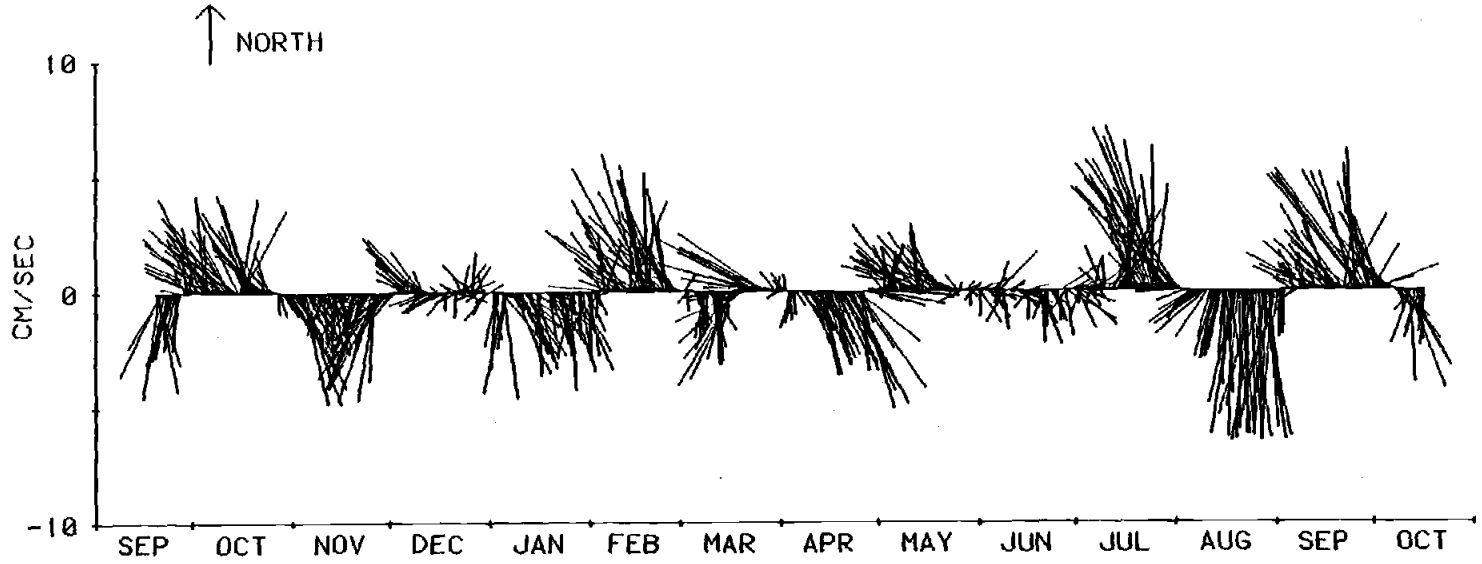

Figure AI-22. Current speed and direction plotted versus time for the 3520 m current meter at Site H. BOM refers to the Bottom Ocean Monitor. (See introductory comments to Appendix I for a description.)

Figure AI-23. Progressive vector diagram for the 3520 m current meter at Site H. Axes are in kilometers. See introductory comments to Appendix 1 for an explanation of this type of diagram and a description of the BOM (Bottom Ocean Monitor).

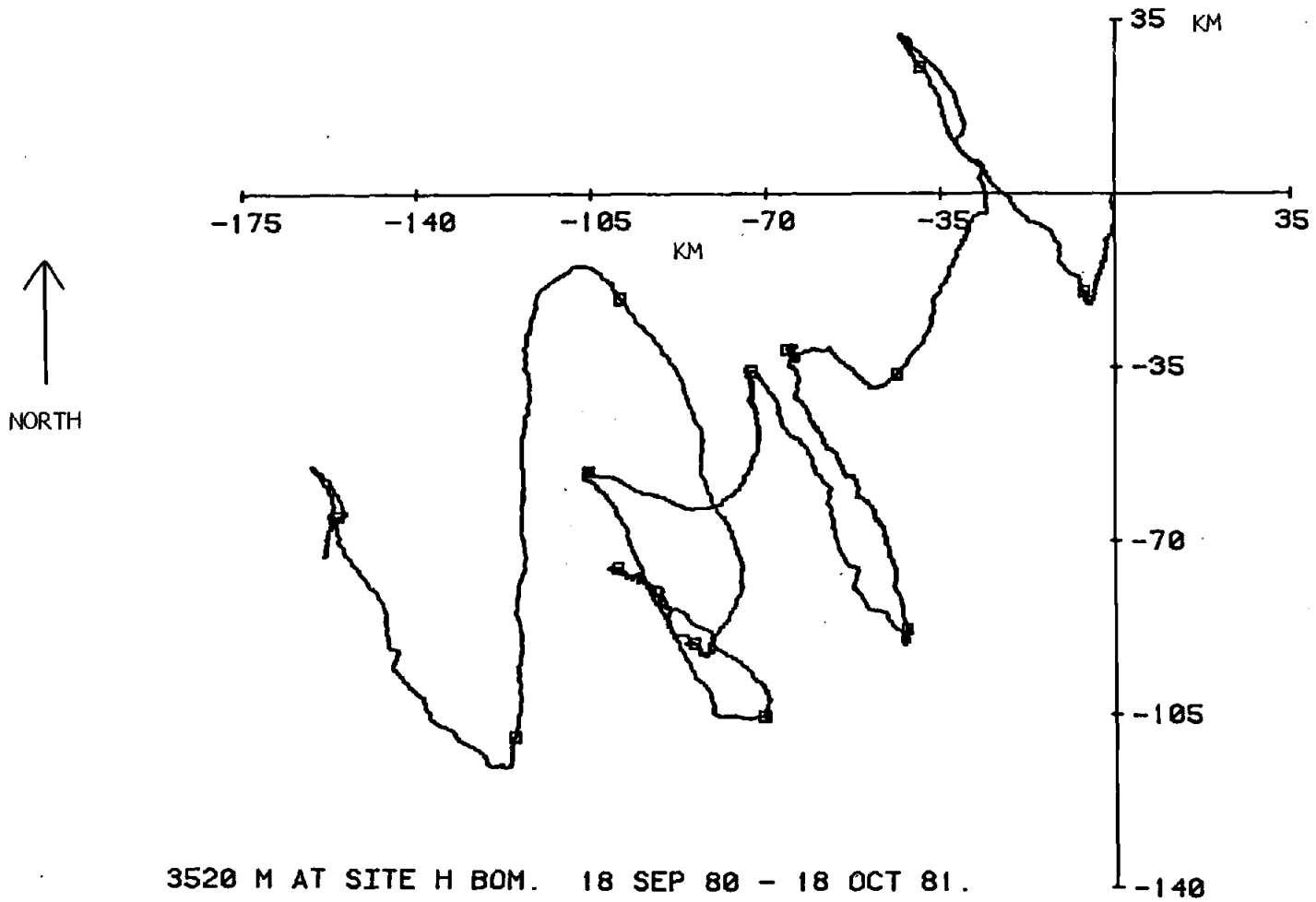
35 KM
-175
-140
-105
-70
-35
KM
35
NORTH
-35
-70
-105
-140
3520 M AT SITE H BOM. 18 SEP 80 - 18 OCT 81.

Figure AI-23.

APPENDIX II

CARBON, NITROGEN, AND PHOSPHORUS DATA

In the following tables, the results of the analyses for carbonate carbon, organic carbon, total nitrogen organic phosphorus, and inorganic phosphorus are listed as percent by weight. These have not been corrected for salt content, but do provide an indication of the precision of the analyses. In most cases, only the results of multiple determinations are listed. On many samples, single phosphorus measurements were made. The sampling periods are given in Chapter 2, Table II-2.

Table AII-1. Replicate measurements of organic and carbonate carbon in trap samples at Sites H and M. Values are uncorrected for salt content.

Trap	Period	Site-Depth, m	% C-CO3*	% C-org*
OSU	1	H-505	5.79	6.42
			5.71	6.62
OSU	2	H-505	4.18	9.37
			4.22	9.51
			4.49	9.73
OSU	3	H-505	3.65	5.29
			3.70	5.27
			3.95	
			3.91	
			3.86	5.36
			3.92	5.54
Soutar	avg.	H-1465	6.42	6.47
			6.43	6.55
			6.54	6.34
			6.45	6.36
Soutar	avg.	H-1465	6.17	6.01
			6.22	6.15
			6.62	6.89
			6.47	6.95
			6.16	6.34
			6.35	6.51
OSU	1	H-3075	7.24	4.09
			7.19	3.94
			7.34	4.26
			7.32	3.86
			7.13	3.86
OSU	2	H-3075	5.09	5.35
			5.06	5.37
			5.10	5.49
			5.11	5.39
			5.45	5.51
			5.41	5.41

* uncorrected for salt content

Table AII-1 - Continued.

Trap	Period	Site-Depth, m	% C-CO3*	% C-org*
OSU	3	H-3075	3.44	3.50
			3.70	3.28
OSU	avg.	H-3225	7.07	3.75
			7.11	3.75
			7.30	3.91
			7.29	3.91
Soutar	avg.	H-3415	6.52	5.11
			6.49	5.13
			6.82	5.08
			6.80	5.39
			6.75	5.30
Soutar	avg.	H-3415	6.22	4.73
			6.21	4.81
			6.29	4.71
			6.37	4.78
OSU	1	H-3545	6.96	4.00
			6.92	4.22
OSU	2	H-3545	5.15	
			5.47	5.28
			5.20	5.37
			5.23	5.42
			4.91	5.20
			4.92	5.29
OSU	3	H-3545	3.78	
			3.78	
			3.94	4.92
			3.95	4.84
OSU	1	M-635	3.94	11.51
			3.98	11.53
OSU	2	M-635	5.48	9.50
			5.45	9.43
OSU	3	M-635	6.16	4.99
			6.17	5.00

* uncorrected for salt content

Table AII-1 - Continued.

Trap	Period	Site-Depth, m	% C-CO3*	% C-org*
Soutar	avg.	M-1565	3.89	
			3.86	8.21
			4.12	8.63
			4.16	8.64
			4.13	8.62
			4.05	8.62
			4.41	8.44
			4.20	8.26
Soutar	avg.	M-1565	3.78	7.88
			3.76	7.92
			3.95	8.16
			3.93	8.36
OSU	1	M-2700	3.73	7.77
			3.76	7.72
OSU	2	M-2700	3.19	7.74
			3.16	7.92
OSU	3	M-2700	4.94	5.40
			4.97	5.66
			4.98	5.21
			4.96	5.24
Soutar	avg.	M-2883	3.23	6.04
			3.23	5.91
			3.40	5.76
			3.31	
			3.35	6.39
			3.44	6.38
Soutar	avg.	M-2883	3.32	5.43
			3.31	5.83
			3.26	5.80
OSU	avg.	M-3050	3.41	4.92
			3.58	5.35
			3.29	5.63
			3.24	5.28
			3.26	5.05
			3.30	5.12

* uncorrected for salt content

Table AII-2. Replicate analyses of total nitrogen on sediment traps samples at Sites H and M.

Traps	Period	Site-Depth,	ppm N-total*
OSU	1	H-505	11248
			9648
OSU	2	H-505	17538
			17137
			17163
OSU	3	H-505	9627
			9868
Soutar	avg.	H-1465	9229
			9123
Soutar	avg.	H-1465	9426
			9313
OSU	1	H-3075	6598
			6751
OSU	2	H-3075	9943
			9449
			9579
OSU	3	H-3075	6563
			6757
			6653
OSU	1**	H-3225	5765
			5741
			5899
OSU	2**	H-3225	8948
			8924
OSU	3**	H-3225	8458

* uncorrected for salt content

** The values from the three periods for this trap were combined since the timer did not perform as designed after recovery.

Table AII-2 - Continued.

Trap	Period	Site-Depth, m	ppm N-total*
Soutar	avg.	H-3415	6892 7322 7301 7134
Soutar	avg.	H-3415	6780 6810
OSU	1	H-3545	5600 5426
OSU	2	H-3545	8694 8854
OSU	3	H-3545	8820 9049
OSU	1	M-635	18237 17185
OSU	2	M-635	12143 12853
OSU	3	M-635	6924 6823
Soutar	avg.	M-1565	12584 12075
Soutar	avg.	M-1565	11864 11474
OSU	1	M-2700	11804 11474
OSU	2	M-2700	11667 11389
OSU	3	M-2700	9890

* uncorrected for salt content

Table AII-2 - Continued.

Trap	Period	Site-Depth, m	ppm N-total *
Soutar	avg.	M-2883	8586
			8232
Soutar	avg.	M-2883	7940
			8007
			8256
			8110
OSU	avg.	M-3050	7738
			7757

* uncorrected for salt

Table AII-3. Replicated determinations of total and inorganic phosphorus on sediment traps samples at Sites H and M. Values are uncorrected for salt content.

Trap	Period	Site-Depth, m	ppm P-inorg *	ppm P-total *
Soutar	avg.	H-1465	255	745
			274	778
OSU	1	M-635	767	
			749	
OSU	2	M-635	1781	2376
			1944	2376
Soutar	avg.	M-2883	436	952
			418	996

* uncorrected for salt content